`

PERFORMANCE STUDY OF INTERNAL COMBUSTION ENGINE USING NANO MATERIALS IN THE LUBRICANT

A Thesis submitted to the Delhi Technological University, Delhi in fulfilment of the requirements for the award of the degree of

DOCTOR OF PHILOSOPHY
in
Mechanical Engineering
by
SUMIT CHAUDHARY
(2K15/PhD/ME/03)

Under the Supervision of

Dr. R. C. SINGH   **Dr. RAJIV CHAUDHARY**
(Professor)   **(Professor)**

DEPARTMENT OF MECHANICAL ENGINEERING
DELHI TECHNOLOGICAL UNIVERSITY

Shahbad Daultpur Bawana Road

DELHI-110042, INDIA

October, 2019

`

DECLARATION

I hereby declare that the thesis work entitled **"Performance Study of Internal Combustion Engine using Nano Materials in the Lubricant"** is an original work carried out by me under the supervision of Dr. R.C. Singh, Professor, Department of Mechanical Enginnering, Delhi Technological University, Delhi, and Dr. Rajiv Chaudhary, Professor, Department of Mechanical Enginnering, Delhi Technological University, Delhi. This thesis has been prepared in conformity with the rules and regulations of the Delhi Technological University, Delhi. The research work presented and reported in the thesis have not been submitted either in part or full to aany other university or instiitute for thr award of any oher degree or diploma.

SUMIT CHAUDHARY

(Regd. No: 2K15/PhD/ME/03)

Deptt. of Mechaical Engineering

Delhi Technological University,

Delhi

Date: 14.10.2019

Place: Delhi

`

<u>CERTIFICATE</u>

This is to certify that the thesis entitled, "**Performance Study of Internal Combustion Engine using Nano Materials in the Lubricant**" submitted by **Mr. SUMIT CHAUDHARY** to the Delhi Technological University, Delhi for the award of the degree of **Doctor of Philosophy in Mechanical Engineering** is a bona fide record of original research work carried out by him under our supervision in accordance with the rules and regulations of the institute. The results presented in this thesis have not been submitted, in part or full, to any University or Institute for the award of any degree or diploma.

Dr. Ramesh Chandra Singh　　　　　**Dr. Rajiv Chaudhary**
Professor,　　　　　　　　　　　　　　Professor,
Department of Mechanical Engineering　　Department of Mechanical Engineering
Delhi Technological University,　　　　　Delhi Technological University,
Delhi, India　　　　　　　　　　　　　Delhi, India

ACKNOWLEDGMENTS

`

I am short of words to express my sincere gratitude to my parents. Whatever I have achieved in my professional life; it is because of them. I cannot express in words their efforts to nurture me.

I am unable to express my sincere gratitude in words for the affection, encouragement and support by my wife during the entire research work, without her support I could not have completed my work.

Last but not the least; I thank the Almighty for giving me strength to complete this work in all respects.

(Sumit Chaudhary)

Delhi

October, 2019

`

ABSTRACT

The lubricant is essential for the smooth working and desired performance of tribopairs. In the applications like internal combustion engine where the tribopairs have to operate in adverse tribological condition like high speed, high temperature, high range of operating temperature, long oil changing intervals etc., the use of proper lubricant becomes critical and essential. The improper lubrication in an I.C. engine may be hazardous for environment moreover it reduces the service life of the tribopairs.

The lubricant used for modern-day I.C. engine cannot be plain mineral oil or synthetic oil. A lot of performance booster additives have been used to enhance the physical and chemical stability along with tribological and thermal performance the lubricant. The lubricants nowadays are blended up to 25% with such lubricant additives. The nanoparticles have proved to be very promising lubricant additives as they possess unique physical, chemical, thermal and tribological properties. Such particles can be used as a lubricant additive to enhance overall the performance of the lubricant.

In the present work, attempts have been made to study the tribological performance of the 15W40 lubricating oil in the presence of various nanoparticles. The stable nanolubricant with various compositions of the nanoparticles have been prepared and investigated for stability by Zeta potential test. The zeta potential values for the nanolubricant ranges from 24 mV to 45 mV which indicate moderate to high stability

The tribological analysis of the nanolubricant was conducted on the pin on disc tribometer according to ASTM G-99. The coefficient of friction and specific wear rate in presence of nanolubricant has been compared with the fresh 15W40 lubricant for both fully flooded and starved lubrication conditions. The nanolubricant decreased the C.O.F. significantly moreover the S.W.R. in case of nanolubricant was negligible as compared to fresh 15W40.

The tribological and extreme pressure analysis of the nanolubricant had also been conducted on the four ball tester according to ASTM D4172 and ASTM Din 51350-02, the wear scar diameter was measured by the vision inspection system at 300 X magnification. The C.O.F. decreased upto 25% and WSD decreased upto 59% in case of nanolubricant. The weld load for the nanolubricant increased upto 29%.

`

The novel nanolubricants had been synthesized by combination of two nanoparticles and tested for the tribological performance on both pin on disc tribometer and four ball tester, performed better than the fresh 15W40. The novel nanolubricants were used in the internal combustion engine for the performance analysis and emission analysis. The BSFC decreased and BTE increased significantly in presence of nanolubricant. The engine emission also decreased in presence of nanolubricant.

List of Contents

`

`

`

`

`

List of Figures

`

`

`

List of Tables

`

List of Abbreviations

I C engine	Internal Combustion Engine
C.O.F.	Coefficient of friction
μ	Coefficient of friction
SFL	Specific Film Thickness
h_{min}	Distance between the tribopairs
R_{rmsa}	Distance between the consecutive peaks
R_{rmsb}	Distance between the consecutive volleys
Λ	Specific Film Thickness
Kg	Kilograms
SAE	Society of automotive engineers
C	Celsius
W	Watt
cSt	centi stoke
EP	Extreme Pressure
Nm	Newton Meter
MFR	maximum friction reduction
MWR	maximum wear reduction
ZnO	Zinc Oxide
SiO_2	Silicon dioxide
WS_2	Tungsten disulfide
H_2O	Water
CuO	Copper oxide
CTAB	Cetyl Trimethylammonium Bromide
DI	Deionized
kHz	Kilo hartz
NaHMP	Sodium hexametaphosphate
Al_2O_3	Aluminium oxide
ml	milli liter
w/w	Weight/Weight

pH	Power of Hydrogen
HCl	Hydro chloric acid
Wt	Weight
SEM	Scanning electron microscopy
TEM	Transmission electron microscopy
XRD	X-ray diffraction
TiO_2	Titanium dioxide
Fe_3O_4	Iron Oxide (Magnetite)
H_2SO_4	Sulfuric acid
PVP	Polyvinylpyrrolidone
α-Fe_2O_3	Alpha- hematite
AlN	Aluminium Nitride
Cu	Copper
SDBS	Sodium dodecylbenzenesulfonate
NaOH	Sodium hydroxide
SDS	Sodium dodecylsulfate
Au	Gold
Ag	Silver
AuCl4	Silver chloride
HAuCl4	Hydrogen tetrachloroaurate
ZrO_2	Zirconium oxide
M	Molarity
$CaCO_3$	Calcuim carbonate
$Mg(OH)_2$	Magnesium hydroxide
MoS_2	Molybdenum disulfide
ZDDP	Zinc dithiphosphate
CNTs	Carbon nano tubes
rpm	revolutions per minutes
mg/l	milligram per liter
mm	micro meter

UV	Ultraviolet
ANN	Artificial neural network
DND	Detonation nanodiamond
IF	Inorganic flurosat
Ni	Nickel
HV	Vickers hardness
hBN	Brinell hardness
PTFE	Polytetrafluroethylene
mV	Millivolt
LVDT	Linear variable differential transformer
ASTM	American society for testing and materials
Cr	Chromium
Mn	Manganese
Si	Silica
Fe	Iron
RTD	Resistance Temperature Detectors
PID	photoionization detector
WSD	Wear scar diameter
NL1	Nano lubricant 1
NL2	Nano lubricant 2
NL3	Nano lubricant 3
L	Load
R	Radius
N	Rotational speed in rpm
BP	Brake power
BMEP	Brake mean effective pressure
A	Area of piston head
n	Number of power stroke per cycle
BSFC	Brake specific fuel consumption
CO_2	Carbon dioxide

CO	Carbon monoxide
HC	Hydrocarbons

`

CHAPTER 1

INTRODUCTION

This chapter deals with the brief introduction to tribological parameters, lubricant, properties of lubricant, lubricant additives and grading of lubricant. The brief introduction of nanoparticles and their tribological impact has also been included in this chapter.

1.1 Motivation

The intrinsic international norms for engine emission made the researches to work on a highly efficient system with strict pollution norms. The frictional losses due to an improper lubricating system for the I C engine are around 20-30% [1,2], moreover the faulty lubrication results for the escape of harmful flue gasses and unburnt hydrocarbon to the environment. Therefore, the lubricant and lubricating system is an essential component of the I C engine for enhancing the performance. The lubrication requirements of modern automotive engines cannot be met by simple mineral oils alone, or even by synthetic fluids. Both require some additives for enhancing their physical and chemical properties according to the field of application. The typical constituents of lubricants for gasoline and diesel engines are to be selected in such a way that the frictional loss and wear of the cylinder liner and piston rings or piston and piston ring would be minimum. The major component of the lubricant is the base fluid that is high-quality solvent-refined mineral oil. For certain high-performance applications, e.g. high power output, long oil-change intervals, low starting temperatures, better efficiency etc., it may be necessary to use more highly processed mineral oils or synthetic chemical products. The base fluid is supplemented with additives, according to the required role in the field of application. In the formulation of lubricants, great care needs to be taken to obtain the correct balance of properties, some of which conflict with others, often more than one additive is used to obtain the desired result. The additives can be macroscopic or microscopic and with the recent development in nanotechnology, the nanoparticles added to the lubricant as additives enhance the performance by reducing friction and wear of the tribopair.

`

1.2 Tribology

Tribology 'the study of rubbing' has been coined in the Greek language, which is the combination of tribos and logy. Tribos means rubbing and logy means study. The knowledge of tribology and its effects are age-old still the term "Tribology" was coined in 1966 by "Committee of organization for economic cooperation and development". In other word tribology is the study of friction, wear, and lubrication of contacting surfaces subjected to some load and having relative motion.

1.2.1 Friction

Friction may be defined as the resistive force which opposes the motion occurred due to sliding or rolling of the solid body over another solid body. The direction of friction force is opposite to the direction of motion of the surface. Friction is a necessity for us for performing many days to day activities like walking, the weaving of clothes, driving automobiles, etc. at the same time it is important to study the power losses due to friction as around 30% of the power produced by the prime mover goes waste due to friction [2].

In 1519 Leonardo da Vinci was the first to postulate frictional laws. After that Amontons in 1699 and Coulomb in 1785 quantified friction. The differences between static and kinetic friction were given by Coulomb. The force which required to start the movement of one body over the other is termed as the static friction force. The force that maintains sliding along the surface is termed as the kinetic friction force. The magnitude of kinetic friction is generally lower as compared to static friction. The ratio of the force of friction to the normal applied load acting on the surface is termed as Coefficient of friction (C.O.F.).

$$F = \mu W \qquad \text{………………………. (1.1)}$$

where F = Force of friction, W = Normal applied load and μ = coefficient of friction (C.O.F.)

The coefficient of friction (C.O.F.) does not depend upon the normal load. It is the property of the materials of surfaces in contact. The theoretical calculation of C.O.F. was done by Bowden and Tabor's simple adhesion theory, modified adhesion theory and deformation theory [11], but this theoretical approach is very complicated than the experimental methods. Inclined plane

`

rig and pin-on-disc rig are two of the most widely used methods for determination of the C.O.F. of the tribopairs.

1.2.2 Wear

Wear may be termed as the gradual removal of material from one or both the surfaces in contact having a relative motion under a normal load. When the interaction occurs at the interface of the two surfaces having asperities, wear take place. It's not a characteristic of material but system feedback. Interface wear is mainly characterized by the operating conditions of the system. Wear may or may not be desired in a system depending upon the requirements. Wear is desired while performing the following tasks: shearing, machining, writing, and polishing, on the other hand, it is not desired in performing many machine applications such as gears, bearings and cams. Generally, it was observed that high frictional force caused accelerated wear rate in the surfaces, but this is not true always. The surface having solid lubricant shows lesser C.O.F. but higher wear as compared to the surface having liquid lubrication. The exceptionally low wear rate but average frictional values are shown by ceramics. Friction and wear can be associated with each other for some particular conditions. Mechanical or chemical action causes wear in the surfaces and the thermal action is the one which accelerates the wear rate.

A brief description of the different type of wear mechanism is given below:

1.2.2.1 Adhesion Wear

Adhesive wear could be experienced in material from one surface to another during the relative motion as shown in Figure 1.1. When the C.O.F. between the two surfaces becomes high it results in a high amount of heat generation between the surfaces which results in either solid phase welding at the contact point or localized bonding between the surfaces. An eradicated particle from one surface tends to be either completely or momentarily attached to another surface [3,4]. When this bond break it results in the removal of micro-particles from the surface. High friction coefficient was observed because of the adhesive wear of the sample [4]. One simply cannot observe the adhesion of two casually placed objects because of the oxides and oil film on the surface. Surface hardness is inversely proportional to the surface adhesion so it can be controlled with the increase of surface hardness. Adhesive wear of the coating can

`

be defined as plastic deformation of minor fragments within surfaces when two surfaces slide relatively [4].
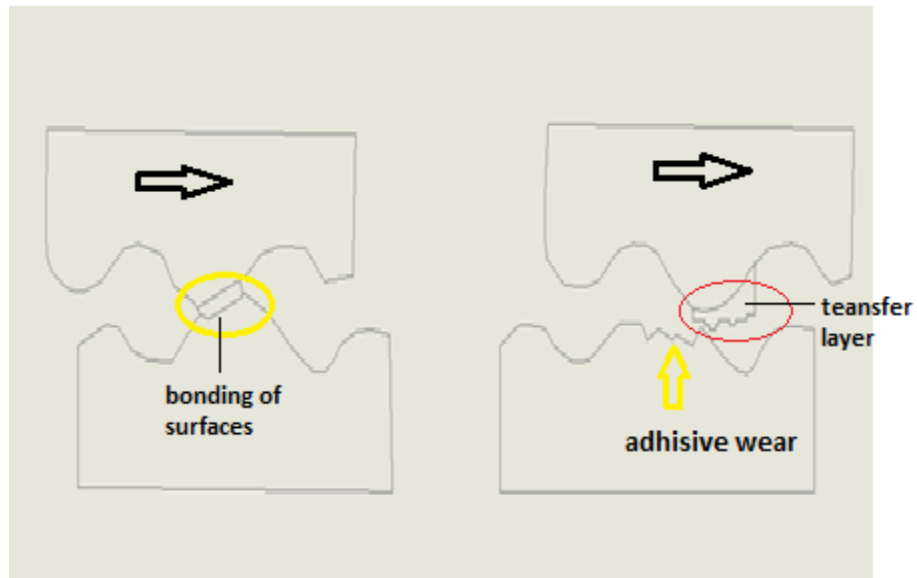
Figure 1.1 Mechanism of adhesion wear

1.2.2.2 Abrasive Wear

When a material with higher hardness is forced against the material having lower or equal hardness, abrasive wear occurs. The extent of abrasive wear is much more than realized. A soft material may also cause abrasive wear if there is any presence of a hard particle.
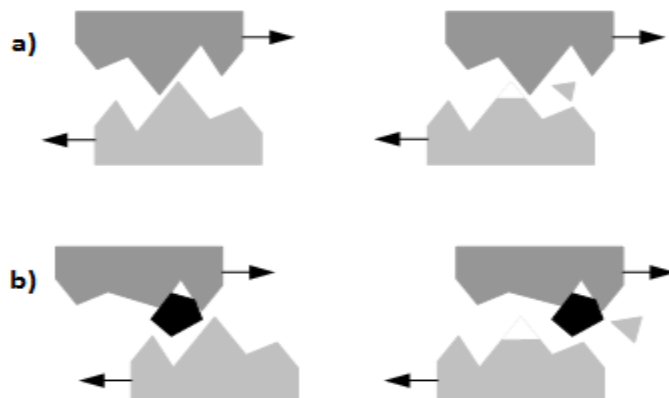
Figure 1.2 Abrasive wear mechanism a) Two-body abrasion, b) three body abrasion

There are two modes of abrasive wear mechanism: two-body wear mechanism and three body wear mechanism. The simplest example of two body wear mechanism is the rubbing of emery-paper on the surface. Rigidly held grit or hard asperities pass over the cutting tool. In the three-body mechanism, grits may roll and slide over the surface because of loose bonding [5]. Schematic of the two bodies and three body mechanism are given in Figure 1.2.

1.2.2.3 Fatigue Wear

When the two or more surfaces have asperities contacts and high-stress concentration, the asperities of one surface deforms the asperities of another surface. Due to multiple cycles the crack initiate as shown in Figure 1.3 (a). As the number of cycles increases the crack propagates (Figure 1.3 (c)) ultimately resulting in the release of wear particle (Figure 1.3 (d)) from the material. The wear particles are generated by fatigue propagated cracks, hence the term 'fatigue wear'. The strain on the worn surfaces are of very high magnitude and plastic in nature causes the modification of the microstructure of the material and effects the wear processes [6.7].
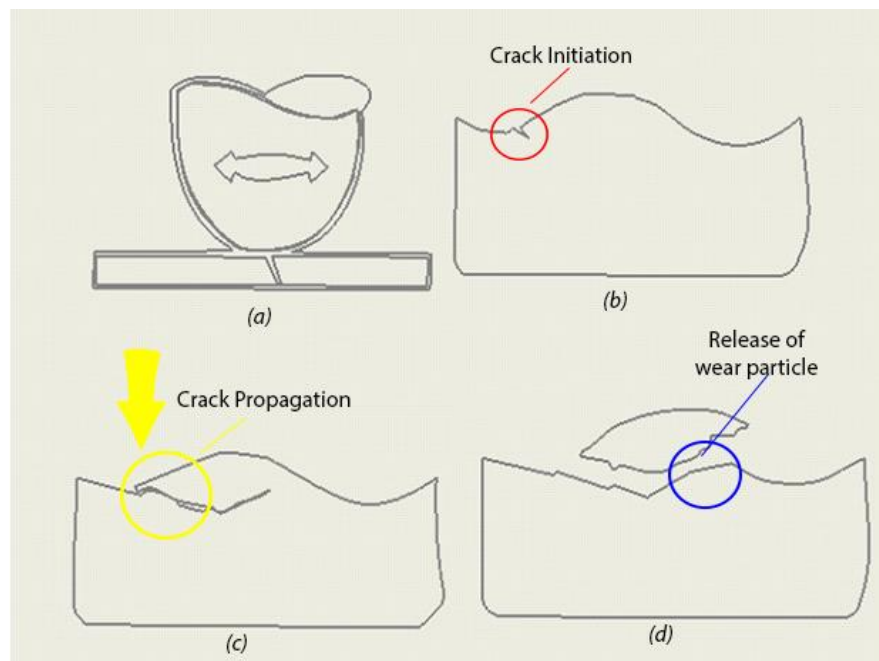
Figure 1.3 Mechanism of fatigue wear

1.2.2.4 Erosive Wear

The erosive wear caused due to the impact of solid or liquid particle against the surface of an object as shown in Figure 1.4. Erosive wear is very much present in the internal combustion engine where the wear debris or the dust or any other foreign material mixed in the lubricating oil strikes the surface and cause damage on the surface [8].

Erosive wear mechanism involved various mechanism which is controlled by a different parameter such as particle material, the angle of incidence, impact velocity, particle size, etc. If the erosive particle is hard, then there is the possibility of the abrasive type of wear process. Erosive wear refers to unspecified numbers of wear mechanism which occurs when relatively small particle impact against the mechanical components. The known mechanism of the erosive wear is abrasion, fatigue, plastic deformation, erosion by the brittle fracture, melting and melting and superplastic flow [9].
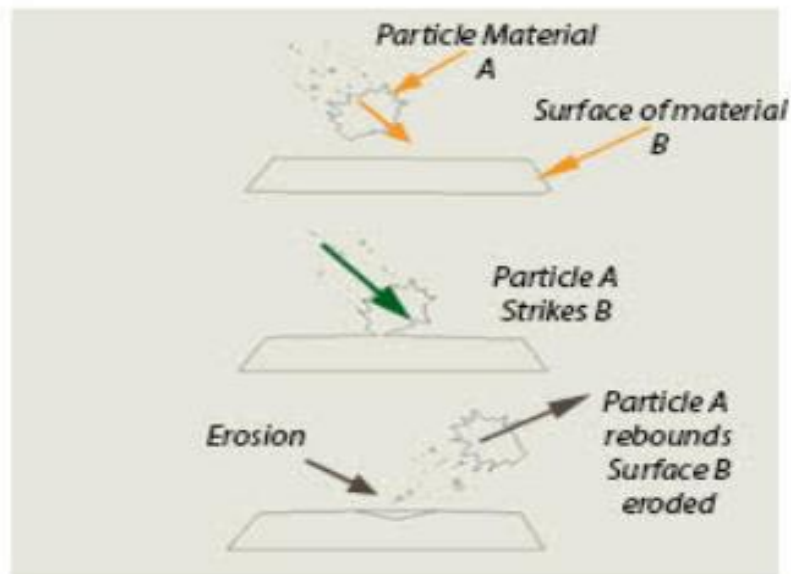
Figure 1.4 Mechanism of erosive wear

1.2.2.5 Corrosive wear

The wear due to the localized chemical reaction between the surface which is caused as elevated temperature and the tribofilm between the surfaces may act like an electrolyte. The

chemical reaction between the surfaces causes the wear of one surface due to anodic transfer as shown in Figure 1.5.
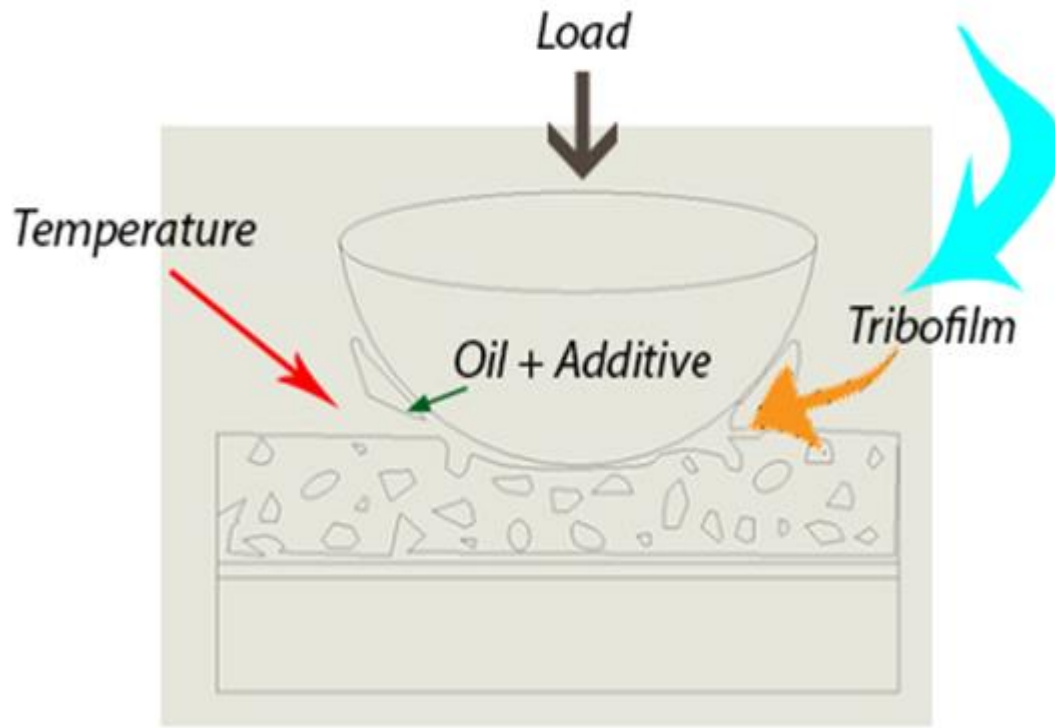
Figure 1.5 Mechanism of erosive wear

1.2.3 Lubrication

Lubrication is the process in which friction between the surfaces has close proximity and a relative motion is reduced using lubricants. i) It reduces the wear of one or both the surfaces. If there is adequate lubrication, then the rate of wear is considerably reduced preventing excessive stresses at tribopair. ii) Lubrication is also needed for smooth and continuous operations of equipment and different machine components. When the lubricants' layers break down, it causes the surfaces of the component to rub against each other which generates heat and further local welding occurs between the surfaces. By using different lubrication methods, the maintenance cost and power losses can be minimized too. Lubrication also minimizes the expansion of metal due to frictional heat. Lubrication Mechanism may be understood by Specific Film Thickness (SFL) [10].

`

$$\Lambda = \frac{h_{min}}{\sqrt{R_{rmsa}^2 + R_{rmsb}^2}} \quad \ldots\ldots\ldots\ldots\ldots\ldots\ldots\ldots (1.2)$$

h_{min} = Distance between the tribopairs

R_{rmsa} = Distance between the consecutive peaks

R_{rmsb} = Distance between the consecutive volleys

If

$\Lambda < 1$: Boundary Lubrication

$1 < \Lambda < 3$: Mixed Lubrication

$3 < \Lambda < 5$: Elastohydrodynamic Lubrication

$\Lambda > 5$: Hydrodynamic Lubrication

1.3 Lubrication Mechanisms

1.3.1 Thick Lubrication

In thick film lubrication as shown in Figure 1.6 (a) the tribosurface are separated from each other by a thick layer of lubricant. The C.O.F.(μ) ranges from 0.001 to 0.03 in this range. This type of lubrication regime is produced when the lubricant gets pumped between the tribopair, the speed of tribopair is high and the load on the tribopair is low. There is no asperity contact in this type of lubrication regime. The lubricant film thickness in the type of lubrication is in the category of elasto-hydrodynamic to hydrodynamic lubrication [11].

1.3.2 Boundary Lubrication

In boundary lubrication as shown in Figure 1.6 (b) the tribosurface are separated from each other by a thin layer of lubricant. The C.O.F.(μ) ranges from 0.05 to 0.15 in this range. This type of lubrication regime is produced when the lubricant has not been pumped between the tribopair, the speed of tribopair has been very slow and the load on the tribopair is high. There is very high asperity contact in this type of lubrication regime. This type of lubrication is

achieved by high adhesion between lubricant and tribopair. The film thickness in this type of lubrication regime ranges from 1-10 nm [11].

1.3.3 Mixed Lubrication

When the lubricant film thickness gets reduced due to the increase in load or decrease of speed or maybe some time due to inadequate pressure generated by the pump, the asperity contact starts to form. The asperity contact is not that high as in case of boundary lubrication still it is considerably high to increase the coefficient of friction, the C.O.F. values in mixed lubrication ranges from 0.035 to 0.05. The mixed lubrication regime can also be observed in the case of virgin surfaces where the surface roughness is considerably high [11].
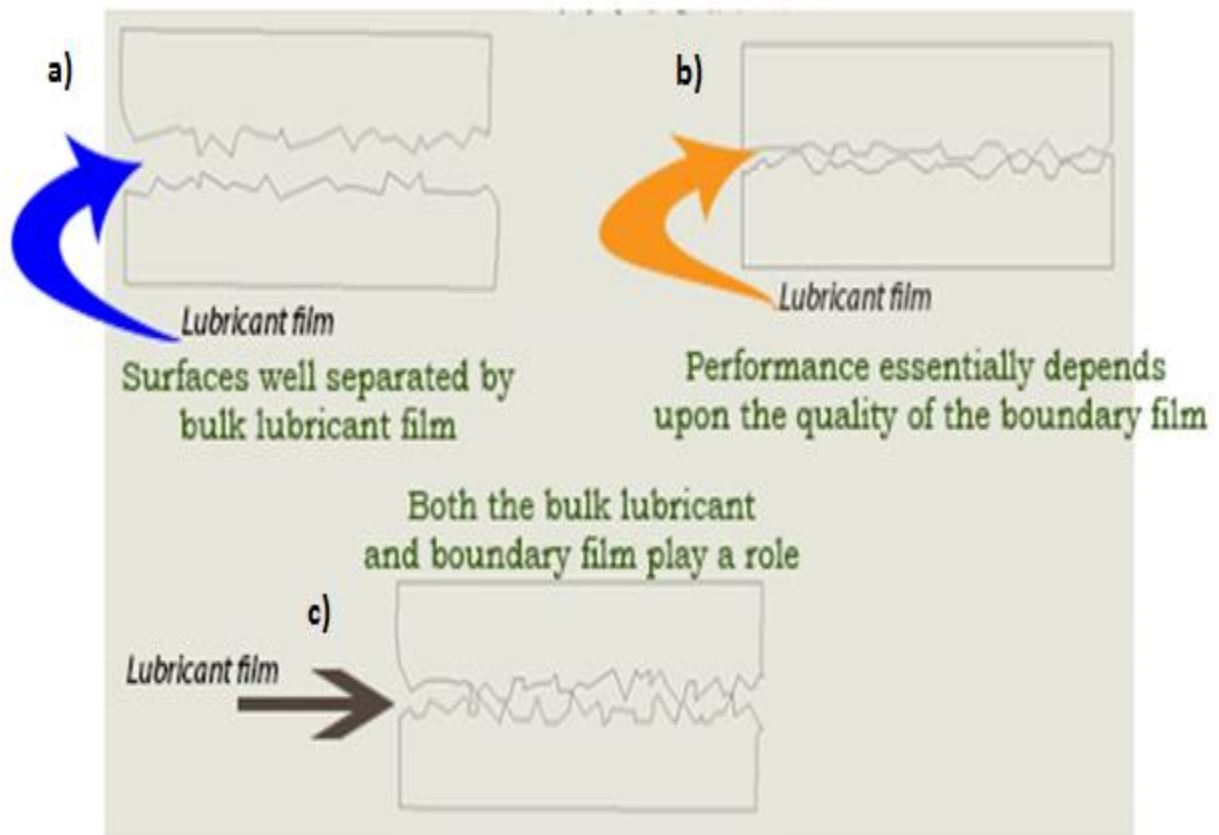
Figure 1.6: Lubrication Regimes, a) Fluid Film Lubrication, b) Boundary Lubrication, c) Mixed Film Lubrication

`

1.4 Lubricants

Lubricants are the substances used to i) reduce the wear, ii) reduce friction, iii) oxidation iv) corrosion, of the tribopairs. The basic function of the lubricants is to protect the surfaces from wear by providing slipping of one tribosurface over the other by developing a sharable layer over the tribopair. The researchers are continuously working on the development of advanced lubricants and oils to minimize the maintenance cost due to friction and wear. The properties of the lubricants like viscosity and surface tension enable the lubricant to maintain a stable layer between the tribopairs [12].

Table 1.1: Type of Lubricants

Type of Lubricant	Properties of Lubricant	Examples
SOLID - The coating of softer solid material in the tribopair Protecting the tribopair from the wear and reduces friction	High load bearing capacity Corrosion resistance High stability for changing temperature and pressure Easy to clean poor heat dissipation High C.O.F. and wear	Polymer Solid- Metal Cermet
LIQUID – The liquid lubricants are pumped to the interface of tribopair to resolve friction and wear.	Low viscosity oil High thermal conductivity Pressure is required to ensure proper lubrication Better adhesive property	Vegetable oils Animal Fat Mineral oil Synthetic oil

`

GAS – The pressurized gas used having ultra-low viscosity separating the tribopair to prevent wear and reduce friction.	High working temperature range Better cleaning Very low viscosity Highly Volatile	Air Nitrogen Helium Mist

The lubricant provides inertness to the atmosphere, protecting the surface from corrosion and oxidation. In the working conditions for the IC engine, the lubricant carries away extra heat generated and protects the surface from thermal cracking. The lubricant also prevents failure due to stress concentration and fatigue. Lubricants are selected according to the requirements for the reduction of wear and friction. Different types of lubricants are needed for different tribopairs as shown in Table 1.1.

1.4.1 Properties of lubricants

The study of physiochemical properties of the lubricant is very important as it gives an idea about the service life, service conditions and field of application of the lubricant.

1.4.1.1 Viscosity

The most important physical property of the lubricating oil is viscosity. Viscosity directly affects the thickness of oil film separating the two surfaces is directly proportional to viscosity. Hence more is the viscosity more will be the fluid film thickness but oil with higher viscosity are difficult to pump resulting in power loss more over such oil is not used for micro and nanochannels. The factors affecting oil viscosity are temperature, pressure and shear rate [13].

The viscosity of lubricating oil decreases rapidly as the temperature is increased. In case of I C engine during cold start, the film thickness at the interface of the cylinder liner and piston rings happens to be more as the temperature of the engine increases the viscosity of lubricant decreases resulting in thin film lubrication [14].

The viscosity of lubricant increases with the increase in pressure. The effect of pressure on lubricating oil is considerable for heavily loaded or concentrated contact such as ball bearing, in such contacts the lubricant at the interface of the tribopair behaves like a solid body separating the two surfaces so chances of failure/rupture of lubricating film increases [15,16].

`

The effect of pressure is not that much in case of engine lubrication as there is not any drastic change in the working pressure of the lubricant.

The lubricant behaves like a non-newtonion fluid. The viscosity of the lubricant decreases as the shear rate increases, such fluids are known as shear thinning fluids. The lubricants such as mineral oil show pseudoplastic behavior and the semi-solid lubricants show thixotropic behavior.

1.4.1.2 Specific Heat

Specific heat is another important parameter for lubricating oil as the lubricating oil also services as a cooling agent at the interface of the tribopair, i.e., it carries out excess heat generated due to friction at the interface of the tribopair [13]. Specific heat is the measure of heat carried out by the lubricating oil per kg, so more is the specific heat more will be the cooling performance of the lubricant.

1.4.1.3 Thermal Conductivity

Thermal conductivity is an important thermal property of the lubricating oil as it gives an idea about the amount of heat that the lubricant can conduct form the tribopair per unit temperature and protects the tribopair from damage due to thermal expansion.

1.4.1.4 Thermal Diffusivity

Thermal diffusivity enables the lubricant to eject the excess amount of heat conducted to the atmosphere and maintain its temperature at the safe working condition.

1.4.1.5 Pour Point

The pour point is the lowest temperature at which the lubricant would flow. The lubricant starts precipitating as it comes across the ultra-low temperature of the atmosphere, for such working conditions the pour point of the lubricant should be as low as possible [17].

1.4.1.6 Flash point and Fire Point

`

Flash point is the temperature at which the vapors of the lubricant will ignite and the temperature at which this ignition sustains is the fire point. The flash point and fire point should be as high as possible to avoid an accident.

1.4.1.7 Volatility

The lubricant working at higher operating temperature make come across the evaporation of the components due to higher volatility. This evaporation results in increased viscosity of the oil and the hydrocarbons evaporated mixes with the atmosphere which is hazardous.

1.4.1.8 Oxidation Stability

The lubricant working at a higher temperature may get molecular breakdown due to reaction with atmospheric oxygen. The resistance to such rearrangement at elevated temperature is termed as oxidation stability [18].

1.4.1.9 Surface Tension

The properties of the lubricant like wetting and spreading on the surfaces are governed by surface tension. The surface tension should have a higher value to get the desired wetting effect on the tribosurfaces.

1.4.2 Grading of Lubricants

The lubricants have different viscosity grades according to the field of application. The SAE grading of lubricants according to the viscosity at 100 C is as per Table 1.2.

The single grade oils are heaving constant viscosity at a different temperature at different environmental temperature. Such Oils cannot be used at the places where the temperature change is adverse. Moreover, these oils cannot be used for long oil change intervals as the effect of seasonal temperature change may affect the tribological performance of the lubricant.

The multi-grade oils having different viscosity at a different temperature, for example, 15W40, it will behave as SAE 15 in a colder environment and SAE 40 in a warmer environment. This

`

would help the long oil change intervals and smooth working during a change in environment temperature.

Table 1.2 SAE grading of lubricant [19]

SAE Viscosity Grade	Min. Viscosity at 100° C	Max. Viscosity at 100° C
0 W	3.8 cSt	-
10 W	4.1 cSt	-
15 W	5.6 cSt	-
20 W	5.6 cSt	< 9.3 cSt
25 W	9.3 cSt	-
30 W	9.3 cSt	<12.3 cSt
40 W	12.5 cSt	< 16.3 cSt
50 W	16.3 cSt	< 21.9 cSt
5 W	3.8 cSt	< 3.8 cSt
60 W	21.9 cSt	< 26.1 cSt

1.4.3 Lubricant additives

The tribological conditions in the modern machinery are very critical so mineral oil alone might not be enough for the effective lubrication as the working temperature, antiwear properties and chemical stability is very less for mineral oil or even for the synthetic lubricants. To improve the properties like antiwear ability, anti-corrosion, extreme pressure performance, chemical stability, antifriction characteristic, etc. the lubricant must be blended with some additives. Some of the lubricant additives have been discussed below given in Table 1.3.

`

1.5 Nanoparticles

The nanoparticles having at least one dimension less the less than 100 nm are considered as nanoparticles. These particles may be metal, metal oxide or non-metal [21]. The nanoparticles are having high surface are to volume ratio resulting in higher thermal conductivity, thermal diffusivity, and heat transfer coefficient. The mechanical properties like elastic modulus, strength, hardness, the toughness of the nanoparticles is multiple times better than the bulk material [22-28]. The nanoparticles are having better anti-friction and anti-wear characteristics it has been reported that by using the nanomaterials in the lubricant the friction and wear decreased hence improving the tribological performance [29-31].

The unique properties of the nanoparticles can be utilized by producing a nanofluid which is the colloidal solution of the base oil blended with the nanoparticles. The concentration of nanoparticles in the nanofluid is generally very low still the impact on the mechanical, chemical and physical properties is appreciable. The nanofluid is having wide application in the field of tribology, engine cooling, advanced air conditioning, and refrigeration systems, solar water heater, cutting fluid [32-35].

1.5.1 Tribological effect of nanoparticles

The properties of nanoparticles play a major role in influencing the tribological performance of lubricating oil. The different nanoparticles as lubricant additives had a different effect on the tribological properties. Nanoparticle provides the combined effects of rolling, sliding by the formation of a third body layer and tribofilms, as a result, improve the tribological properties when used as additives in the Lubricating Oil [36-40]. There are several parameters for quantifying the performance on Lubricating Oil. i) friction, the minimum friction coefficient approach (MFC) or maximum friction reduction (MFR) in order to determine the frictional losses. ii) wear performance, the maximum wear reduction percentage (MWR) may be selected to exhibit antiwear capability, regardless of the working conditions. iii) the statistical analysis, in this approach the experimented data can be analyzed by using software which will allow combining the major factors such as chemical composition, particle size, the morphology of nanoparticles along with the tribological performance together. Nanoparticles

`

having different chemical properties possess different chemical and physical properties, which will affect the performance of the Lubricating oil having the nanoparticles.

The nanoparticles as lubricant additive enhance the tribological performance by the following mechanism:

1.5.1.1 Rolling effect

The nanoparticles possess better mechanical properties than the bulk material. Due to these properties, the nanoparticles act like small bearings at the interphase of the tribopairs and assist the rolling as shown in Figure 1.7. The metallic nanoparticles of spherical, blub and oval shape blended with the lubricating oil assist the smooth guiding of the tribopair over one another and produce a ball bearing type of effect. The C.O.F. reduced due to this rolling action.

1.5.1.2 Mending effect

The continuous motion of the tribopair over each other result in wearing of the surfaces. The micro/nano cracks might be produced on the surface due to the rubbing. The small size nanoparticles of harder materials get settled in the micro and nano cracks present on the surface of the tribopair. The cracks present on the surface not only gets repaired by the mending effect but the propagation of the crack also gets controlled.
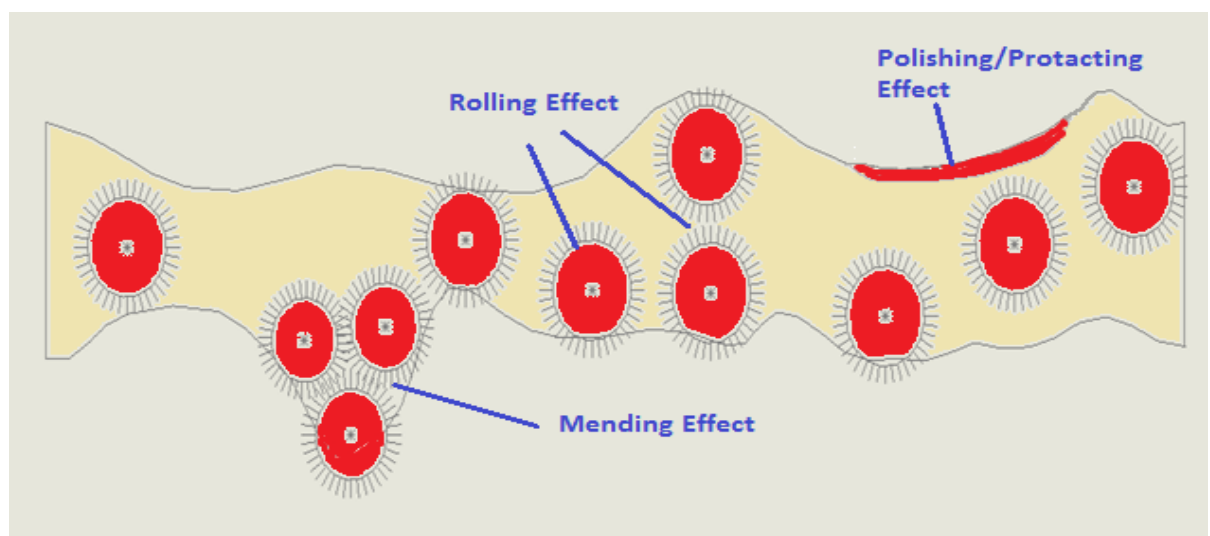
Figure 1.7: Tribological effect of the nanoparticles

`

1.5.1.3 Polishing effect

The softer nanoparticles of sheet shape when blended with the lubricating oil comes under high pressure between the tribopair gets deposited on the tribopair producing thin nanocoating over the surface. This coating prevents the direct contact of the tribopair resulting in a huge reduction in wear.

The nanoparticles played an important role in reducing the coefficient of friction, the rate of wear hence improving the tribological properties of the base lubricant. The nanoparticles enhanced the extreme pressure performance of the base lubricant. The nanoparticles present in the lubricant gave the healing effect to the tribopair. There is a need to explore the effect of blending of the nanoparticles in the field of IC engine.

`

CHAPTER 2

LITERATURE REVIEW

Literature review for the present work has been broadly divided into two parts. The first part contains the comprehensive review of for the preparation of nanofluid. In the second part, the study has been carried out for the tribological impact of the nanomaterial blended with lubricating oil.

2.1 Mechanism of Preparation of Nanofluid

The selection of the preparation method for nanolubricant is highly dependent on the stability of nanofluid. The nanoparticles have a small size and their shape may be considered as spherical so the particle's sedimentation velocity can be calculated by Stoke's Law [41].

It is observed that to reduce the particle's sedimentation velocity following measures may be taken: i) decrease the radius of the nanoparticles to be mixed in the solvent; if the radius of the nanoparticles is below the critical radius then no sedimentation takes place [42]. ii) Reduce the density gap between the nanoparticles and the Solvent. iii) Increase the flow velocity of the solvent.

2.1.1 Different techniques for producing the Nanofluid based on the physical method

2.1.1.2 Single Step Technique

In the single step technique, there is a simultaneous synthesis of nanoparticles and preparation of nanofluid. The nanofluid is directly prepared by synthesis of nanoparticles in the solvent by a chemical method or physical vapor deposition technique. The pH value of the prepared nanofluid is kept constant during the synthesis [43]. Due to the simulation synthesis of nanoparticles and nanofluid, there is very less chance of aggregation and sedimentation. So the nanofluid prepared is homogenous in nature and remain homogenous for a long time. The main disadvantage of this method is that the solvent should have low vapor pressure and the size of the nanoparticles can't be controlled precisely.

`

2.1.1.2. Two Step Technique

In this technique, the previously synthesized nanoparticles are blended into the solvent to produce a nanofluid. Due to the high surface energy of nanoparticles, there is always a chance of aggregation and clustering of nanoparticles. Later on, these aggregated nanoparticles may sediment at the bottom. So it is very challenging to make a homogenous solution using the two-step method [44]. There are some techniques like ultrasonic homogenizing which may be applied to get a homogenous nanofluid. The method is most suited for the nonmetallic nanoparticles. To increase the repulsion between the nanoparticles some surfactants may also be used [45]. The advantage of this technique is that the nanoparticles used for nanofluid may be purchased having standard size and shape, but the aggregation and sedimentation free blending is to be done to prepare a homogenous solution.

2.1.2. Preparation of non-metallic nanofluids

Zafarin et al. got dried out ZnO nanoparticles by warming them at 110^0C for 24 hr. The nanoparticles then added with polyethylene glycol and sonicated. The aggregation of particles was seen in the nanofluid bringing about more noteworthy size nanoparticles [46].

Moosavi et al. synthesized the ZnO and ethylene glycol Nanofluid by using magnetic stirrer for homogenous mixing and stability of nanofluid. Ammonium Citrate was included as a dispersant in the proportion 1:1 with the nanoparticles. The nanofluid watched was free from sedimentation and agglomeration [47].

Raykar et al. added acetylacetone in water-soluble ZnO the solution was ultrasonically homogenized and due to the presence of acetylacetone the size of nanoparticles reduced by chemical reaction and the nanoparticles remains homogenously suspended in the nanofluid [48].

Wei et al. proposed ethylene glycol as a base fluid for ZnO nanoparticles. The ultrasonic homogenization was utilized to homogenize the nanoparticles in solute yet the molecule collection couldn't be controlled and the measure of nanoparticles in the nanofluid expanded 10-20 times [49].

Chung et al. prepared the nanofluid by scattering ZnO powder in deionized water. The colloidal solution was kept at 25^0 C and stirred for 30 min, and afterward, it was ultra-sonicated using various sonicators for comparison systems such as a single piezo-actuated bath, a solenoid-

`

actuated bath and a static bath with the immersed horn. Ammonium polymethacrylate was blended as a dispersant. It was concluded that the size reduction rate was maximum in sonication by ultrasonic horn and more over the sedimentation rates was least in case of ultrasonic horn [50].

Lee et al. dispersed ZnO and Ethylene glycol Nanofluid using pulsed wire evaporation. The nanoparticles got scattered directly into Ethylene glycol with no surface contamination [51].

Kole and Dey suspended the ZnO nanoparticles in water as a solvent and applied ultrasonication. The examination was directed to get the ideal time of sonification. As the sonication time increased the size of nanoparticles decreased but after optimum value increase in time increased the nanoparticle size [52].

Suganthi et al. used ZnO nanoparticles and sodium hexametaphosphate as a dispersant in 5:1. They were blended with water as a solvent by ultrasonic homogenization. The nanofluid observed after several days was found to be stable [53].

Yang and Liu thought about the dependability of nanofluid by utilizing of surfactant (trimethyoxysilane) and without the utilization of surfactants. The nanofluid which was set up without surfactant i.e. the blending of nanoparticles was just by utilizing ultrasonication, the sedimentation happened. The utilization trimethyoxysilane of with mass fraction of 0.115 felicitated the homogenous mixing of SiO_2 nanoparticles in H_2O and there was no sedimentation observed after 12 months of the sample preparation [54].

Timofeeva et al. added silica nanoparticles in the organic solvents using Benzalkonium chloride, Benzethonium chloride and cetyltrimethyl ammonium using bromide as surfactants for the stability of nanofluid. The preparation of nanofluid went through a stepwise procedure, initially, the solvent was enriched with the surfactants and then the nanoparticles in powder form were blended. The nanofluid was then homogenized using string and ultrasonic homogenization. Dynamic light scattering method and Scanned Electron Microscope both demonstrated that smallest particles size was obtained by Benzalkonium chloride followed by Benzethonium chloride and cetyltrimethyl ammonium bromide the nanofluid with no surfactant indicated biggest molecule measure [55].

Kulkarni et al. made a solvent of 60 % ethylene glycol ($C_2H_6O_2$) and 40 % water the silica nanoparticles were homogenized in the solvent by using ultrasonication. Dynamic light scattering shows that the dispersion of nanoparticles was uniform [56].

`

Kanjirakat et al. prepared the colloidal solution of silica nanoparticles in deionized water as a solvent and this colloidal suspension later homogenized by sonicator. For stability of the nanofluid, the pH was kept to 4.5 by using Nitric acid [57].

Darzi et al. dissolved SiO_2 a nanoparticle in added distilled water mixing were done by a magnetic stirrer for two hours [58].

Fazeli et al. blended the silica nanoparticles in distilled water and then ultrasonication for 90 min. There was no sedimentation observed after 72 hours of the preparation of the nanofluid. [59].

Byrne et al. blended CuO nanoparticles in water with and without the use of surfactant. CTAB was used as a surfactant in 1:1 by volume to the nanoparticles. The homogenization was done by ultrasonic vibrator. Dynamic light scattering results shows that when no surfactant was used and concentration of CuO was 0.1%, the average size of nanoparticle in the nanofluid decreases from 3000 nm to 300 nm after 4 h. with CuO concentration 0.1% nanofluid and CTAB was used as surfactant the average particle size of about 200 nm was observed. The outcome demonstrates that by using the surfactant, the average particle size of the nanoparticles decreased [60].

Lee et al. looked at the CuO nanofluid created by both sonication of CuO nanoparticles in DI water (two-step method) and preparation CuO nanofluid by a pulsed laser (one-step method). The nanofluid prepared by one step method was more steady having smaller nanoparticles [61].

Priya et al. prepared CuO nanofluid with water as a solvent. To avoid aggregation of nanoparticles in the nanofluids tironas was added as a surfactant. The optimum ratio of tironas and CuO was calculated as 1:2.5 [62].

Harikrishnan dispersed CuO nanoparticles in oleic acid to prepared the nanofluids. The homogenazition of the nanoparticles in nanofluid was done by ultrasonic vibrations. As the mass fraction of nanoparticles increased from 0.5 to 2.0% by weight, the sonication time increased from 30-45 minutes. The solution prepared was a colloidal mixing of CuO nanoparticles and oleic acid [63].

Suresh et al. sol-gel method was used for synthesizing copper oxide nanoparticles. The nanoparticles were dispersed in distilled water by sonicating it for six hours for the homogeneity. The pH of the nanofluid was reported around 4.83 for stability [64].

Kannadasan et al. synthesized CuO nanoparticles by the chemical precipitation method. These CuO nanoparticles were sonicated in water to get the nanofluid. As the sample was observed after 25 days, there was some sedimentation of nanoparticles observed [65].

Saeedinia et al. blended CuO nanoparticles in oil by using an ultrasonic homogenizer (400Wand 24 kHz) to stay away from the aggregation of the particles in the nanofluid. There was sedimentation observed after a few days of preparation of nanofluid [66].

Chang et al. dispersed CuO nanoparticles into the water in the presence of NaHMP (CuO:NaHMP=1:3.12 by wt) as a dispersant. The homogenization of the solution was done by ultrasonic vibrator. It was observed that as the volume fraction of CuO was more than 0.40 vol.%, the sedimentation of the CuO nanoparticles was evident in the nanofluid which indicates that the nanofluid was highly unstable. [67].

Lui et al. blended CuO nanoparticles in deionized water. The colloidal solution was homogenized for ten hours in an ultrasonic water bath. The pH of the nanofluid was kept at 7 [68].

Sonawane et al. dispersed Al_2O_3 nanoparticles into aviation turbine fuel (ATF). The experiment was conducted to find the correct amount of surfactant to be added to the nanofluid for stability. At first, the Al_2O_3 nanoparticles were dispersed in ATF by ultrasonic sonication and no surfactant was used, the time of sonication was different for different samples but sedimentation was observed in all the samples within few minutes of the sonication. Oleic acid and Polyoxyethylene Sorbitan Monolaurate ('Tween' 20 42CrMo4) was used as surfactant and after several trials it was concluded that for the stability of nanofluid of ATF (10 ml) with 0.1 ml Al_2O_3, 0.026 ml Oleic Acid and 'Tween' 20 LR should be added for the stability of the nanofluid. As the amount of nanofluid increased the amount of surfactant to be added increased proportionally, the sonication time doesn't affect the stability of nanofluid [69].

Gharagozloo diluted 20% w/w concentration of Al_2O_3-water nanofluid with deionized water. The stability of the solution was enhanced by keeping the pH of the nanofluid was kept at 5.5 by adding nitric acid. The nanofluid was homogenized using ultrasonic homogenizer and remained stable for several days [70].

Hung et al. prepared a solvent of water and chitosan 0.5% by weight. Chitosan acts as a catonic dispersant in distilled water. Then Al_2O_3 nanoparticles were ultrasonically homogenized in the solution [71].

Suresh et al. used the chemical vaporization process to synthesize the Al_2O_3 nanoparticles. The nanoparticles were used for preparing the nanofluid having water as the base fluid. The colloidal solution was treated with ultrasonic vibrations for six hours and afterward, the pH of the nanofluid was maintained at 4.9 for the stability of nanofluids [72].

Beck et al. blended the Al_2O_3 nanoparticles in ethylene glycol and the colloidal was subjected to ultrasonic homogenization. The solution remained stable without any surfactant due to the surface charge present on the surface of solute [73].

Soltani et al. prepared the solvent having distilled water added with carboxymethyl cellulose 0.5% by weight. The Al_2O_3 nanoparticles were added to the solvent and mixed first by the mechanical method and after that ultrasonically [74].

Jian et al. added HCl to water to make the pH at 4.9. The Al_2O_3 nanoparticles were added and ultrasonically homogenized, the resultant nanofluid was stable without any traces of aggregation [75].

Singh et al. dispersed Al_2O_3 nanoparticles in ethylene glycol and water. The nanofluid of Al_2O_3-water was stabilized through electro-static technique; the pH of the nanofluid was kept at 4 by adding hydrochloric acid for the stability of nanofluid. The Al_2O_3-water nanofluid was stable for a few days. Al_2O_3 nanoparticles were sonicated in ethylene glycol and Al_2O_3-ethylene glycol based nanofluid was observed homogenous and stable [76].

Ho et al. used Al_2O_3 nanoparticles and water to form a colloidal suspension. The primary suspension was done by magnetic stirring for two hours. The pH value of the nanofluid kept at pH 3. The nanofluid didn't show any sedimentation after two weeks of synthesis [77].

Teng et al. dispersed Al_2O_3 nanoparticles in water blended using sonicator and electromagnetic stirring. The chitosan (0.3 wt.%) was used as a surfactant for the stability of nanofluid. There was no sedimentation and aggregation observed in the nanofluid after numerous days [78].

Yousefi et al. observed that as the concentration of Al_2O_3 nanoparticles increased more the 4% vol., the stability of solution decreased. Triton was used as a dispersant and the ultrasonic vibrator was used for homogenizing the nanofluid [79].

Heyhat et al. dispersed Al_2O_3 nanoparticles in distilled water. To enhance the stability of the suspension, sonication was done consistently for one hour at 400Wand 24 kHz. The characterization was done by SEM and zeta potential shows that the nanofluid was homogenous and physical stable [80].

`

Lee et al. dispersed Al_2O_3 nanoparticles in DI water and sonicated the suspension. The pH was kept constant at 6.04. The sonication time was variable and the zeta potential test shows that the optimum time for sonication was five hours [81].

Pandey and Nema blended Al_2O_3 nanoparticles in distilled water using ultrasonic sonication for 8-16 hours. The nanofluid was stable and no sedimentation was seen [82].

Hegde et al. dispersed Al_2O_3 nanoparticles in DI-water and sonicated the colloidal solution. Although the nanoparticles used were of very small size, there were no signs of any aggregation found initially [83].

Esmaeilzadeh et al. prepared their nanofluid by ultrasonic mixing of Al_2O_3 nanoparticles in DI- water for four hours and then by electromagnetic stirring. There were no signs of aggregation and sedimentation as observed by TEM and XRD [84].

Jacob et al. dispersed Al_2O_3 nanoparticles in Deionized water and the pH value of the suspensions was controlled. The colloidal solution was sonicated for homogeneity [85].

Mo et al. blended TiO_2 nanoparticles in deionized water in three different concentrations 0.3% wt., 0.5% wt., 0.7% wt. Ammonia was added to keep the pH value to 8 and sodium dodecyl sulfate was added as a surfactant. The colloidal suspension was magnetically stirred for 10 min and ultrasonically homogenized for 40 min. The nanofluid with a concentration of 0.3% w/w. and 0.7% w/w. was stable for several days but nanofluid with a concentration of 0.5% w/w. demonstrated sedimentation [86].

Fedele et al. dispersed TiO_2 nanoparticles in distilled water; the mixing was done by an ultrasonic homogenizer. The pH of the nanofluid was controlled to avoid sedimentation of the nanoparticles. The characterization was done by dynamic light scattering method. It was watched that following a few days the extent of nanoparticles in the nanofluid diminished because of halfway precipitation; however, after sonication, the nanoparticles procured a similar size starting size [87].

Kayhani et al. added TiO_2 nanoparticles and hexamethyldisilazane by mass ratio 2:1 the mixing was done by ultrasonic means for getting homogeneity. The resultant mixture was mixed with distilled water and again ultrasonic homogeneity of the nanofluid was done for 3-5 hours. The nanofluid showed no sedimentation [88].

Duanthongsuk and Wongwises prepared the water-based nanofluid having TiO_2 nanoparticles. To prevent the sedimentation and aggregation of the nanoparticles in the nanofluid surfactants

were used and ultrasonic homogenization was used for uniform distribution of nanoparticles in the nanofluid [89].

He et al. prepared TiO_2 – DI water Nanofluid by using ultrasonic homogenization. The nanofluid then processed in a medium mill to reduce aggregation of nanoparticles. The pH of the nanofluid was kept consistent to control the aggregation of nanoparticles [90].

Murshed et al. blended TiO_2 nanoparticles in DI water and it was observed that the size of nanoparticles in the nanofluid incremented due to accumulation. To enhance the stability of the nanofluid cetyltrimethyl ammonium bromide surfactants were added to the nanofluid [91].

Sajadi and Kazemi mixed TiO_2 nanoparticles in DI water by stirring process and then the ultrasonic homogenization was used for uniform distribution and stability of nanoparticles in the nanofluid [92].

Arani and Amani mixed TiO_2 nanoparticles in distilled water. The solution was homogenized by ultrasonic vibrator and magnetic stirrer. The pH of the nanofluid was kept 5.67-7 to avoid sedimentation. CTAB was used as the surfactant. The nanofluid was observed stable after several days [93].

Chen et al. prepared TiO_2 nanotube and ethylene glycol nanofluid using dry titanate nanotubes which were integrated based on the alkali hydrothermal transformation. The TiO_2 nanotube and ethylene glycol mixed by gentle stirring, preceded by ultrasonic homogenization. The nanofluid was stable over a period of two months [94].

Abareshi et al. used deionized water as a solvent and dispersed Fe_3O_4 nanoparticles in it through sonication. Tetramethyl ammonium hydroxide was used as a dispersant to enhance stability. The pH estimation of the nanofluid was kept consistent to enhance the crystallinity of Fe3O4 nanoparticles. The zeta potential test indicates nanofluids have great scattering and soundness [95].

Li et al. prepared Fe_3O_4-water nanofluid by two methods, in the first nanofluid Fe_3O_4 nanoparticles prepared by the chemical precipitation oleic acid were added as a dispersant. The distinctive volume fraction of the sample was obtained by adding more water to the original sample of the nanofluid. In the second technique, the nanoparticles were blended directly using an ultrasonic vibrator in deionized water. Sodium dodecylbenzenesulfonate was added for stability of the nanofluid [96].

`

Yu et al. Fe_3O_4 nanoparticles synthesized by coprecipitation were added to kerosene to prepare the nanofluid. The nanoparticles were dispersed in Oleic acid first then after one hour, kerosene was added as a solvent. The suspension was blended slowly by stirring. The Fe_3O_4-kerosene nanofluid was obtained having volume concentration 1% was obtained by the phase-transfer process [97].

Sundar et al. added Fe_3O_4 nanoparticles in water and balanced the pH value to 3, using H_2SO_4. The colloidal suspension was ultrasonicated for 2h. The nanofluid was having a uniform dispersion of the nanoparticles [98].

Sheikhbahai et al. prepared Fe_3O_4 –DI water nanofluid. To avoid sedimentation ethylene glycol was used as a surfactant and Fe_3O_4 nanoparticles were first sonicated in ethylene glycol and the DI water was added under vigorous agitation. No sedimentation was seen in the nanofluid [99].

Sundar et al. added Fe_3O_4 nanoparticles in the solvent having diverse concentrations of ethylene glycol and water mixture. The colloidal solution ultrasonically homogenized and was observed stable after several days. [100].

Asadzadeh et al. added Fe_3O_4 nanoparticles in ethylene glycol; the suspension was stirred and then sonicated. There was no sedimentation evident in the nanofluid [101].

Phuoc and Massoudi added Fe_2O_3 nanoparticles in deionized water. Polyvinyl pyrrolidone (PVP) or Poly (ethylene oxide) (PEO) were used as a dispersant. The blending was carried out using a magnetic blender and ultrasonic sonication. It was discovered that the nanofluids were stable for several days when the concentration of nanoparticles in the base fluid was less than 2% and the stability of the nanofluid decreased at higher concentration [102].

Abareshi et al. added α-Fe_2O_3 in glycerol. The homogenization of the colloidal suspension was done using ultrasonic vibrator [103].

Guo et al. added Fe_2O_3 nanoparticles in the blend of ethylene glycol and deionized water. Sodium oleate was used as the dispersant. The nanoparticles were mixed to the solvent with continuous stirring. Then the suspension was stirred using disperse mill and ultrasonication [104].

Yu et al. dispersed AlN nanoparticles in ethylene glycol and propylene glycol by stirring and ultrasonic homogenization. Due to aggregation, the average particles size of nanofluids increased as observed by Scanning Electron Microscope (SEM) [105].

`

Woznik et.al.dispersed AlN nanoparticles in polypropylene glycol (PPG 425 & PPG 2000) in powder form. The colloidal suspension was stirred the magnetically homogenous mixture. It was observed that the sedimentation of nanoparticles was more in PPG 425 as compared to PPG 2000 and after 30 hours sedimentation rate of nanoparticles was more than 90% and remained constant after that. The Zeta potential of both PPG 425 and PPG 2000 reported as negative [106].

Hu et al. dispersed AlN nanoparticles in the gaseous phase produced by plasma arc in ethanol, and castor oil was used as the surfactant. The mixing was done by magnetic stirrer at high speed after this the ultrasonic homogenization was done for 10 min. The nanofluid was characterized under Transmission Electron Microscopy (TEM) and it was observed that it remained stable for more than two weeks [107].

2.1.3. Preparation of metallic Nanofluids

Xuan and li dispersed copper nanoparticles in transformer oil oleic acid was added 22 % by weight of Cu nanoparticles as dispersant the homogenization of the nanofluids was done by ultrasonic homogenizer [108].

Li et al. CTAB and SDBS were used as surfactants for preparing Cu-water nanofluid. The pH control was used to enhance the stability of the nanofluid, HCl and NaOH were used for that purpose. The nanofluid prepared without surfactant reported 6770 nm particle size which indicates agglomeration but in the presence of SDBS as a surfactant and pH= 8.5-9.5 was 207 nm. The suspension with CTAB as a dispersant was found stable without sedimentation after a week [109,110].

Peng et al. synthesized the nano refrigerant by adding Cu nanoparticles in R113 using plasma evaporation techniques. SDBS, CTAB, and sorbitam monooleate were used as surfactants. The colloidal mixture was homogenized results [111].

Kathiravan et al. synthesized Cu nanoparticles by the sputtering method and dispersed them in water with 9.0% SDS anionic surfactant. The suspension was sonicated for ten hours. The nanoparticles were evenly dispersed in water; still some agglomeration was observed [112].

Kole and Dey dispersed Cu nanoparticles in distilled water the colloidal solution was homogenized by using magnetic stirrer there was no sedimentation observed, but due to aggregation the average particles sized increased [113].

`

Patel et al. synthesized Au and Ag nanoparticles by citrate reaction. The two-phase reduction of AuC14- by sodium borohydride was used for the synthesis of Au nanoparticles; the reduction took place in presence of an alkane thiol were present with thiolate covering in a medium of water and toluene. The nanofluid was stable after several months [114].

Asirvatham et al. added Ag nanoparticles in DI-water using ultrasonication. The pH values were measured differently for different volume concentration, of 0.3%, 0.6%, and 0.9%, were observed at 7.4, 7.1 and 6.8 respectively. The agglomeration of the nanoparticles was observed in the nanofluids [115].

Paranetthanuwat et al. dispersed Ag nanoparticles in water and sonication was done; the nanofluids was stable up to 48 h [116].

Tamjid and Guenther used a colloidal solution of Ag nanoparticles produced by sputtering on running liquid technique having a volumetric concentration of solid 4.37%. The colloidal solution was sonicated in diethylene glycol to make the homogenous nanofluids [117].

Sharma et al. prepared Ag nanofluids by single step technique using Ag nitrate as a precursor; the reducing agent was ethylene glycol, & polyacrylamide-co-acrylic acid as a dispersant. The concentration of polyacrylamide-co-acrylic acid and the reaction conditions played a vital role in controlling the size of nanoparticles and stability of nanofluid [118].

Hajian et al. dispersed Ag in DI water by chemicals reduction of Ag ions. The nanofluids were sonicated afterward [119].

Parametthanuwat et al. dispersed Ag nanoparticles in DI-water. The suspension was sonicated to get the stable nanofluid [120].

Paul et al. synthesized nano-Au and Ag nanoparticles dispersed water by a wet chemical bottom-up approach. The nanofluid was found stable without agglomeration and sedimentation as observed after 48 h [121.122].

Chaudhary et al. synthesized the Au nanoparticles in aqueous medium from HAuCl4 by chemical reduction and continuous stirring. The size of nanoparticles in the nanofluid can be controlled by controlling the rate of reaction and stirring. The nanofluid was stable after many days [123].

2.1.4. Mixture of Nanoparticles

Cho et al. a mixed combination of Al_2O_3 and AlN nanoparticles in n-hexane and oleic acid was used for pH controller to enhance stability. The mixture was subjected to ZrO_2 bead-milling and ultrasonication. The excess of oleic acid was removed by ultra-filtration membrane. The nanoparticles then mixed with transformer oil and n-hexane were removed using a rotary vacuum evaporator [124].

Kim et al. prepared the nanofluid having ZnO, TiO_2, Al_2O_3 as nanoparticles and water and ethylene glycol as solvent. The mixing was done by ultrasonic homogenization and .05 M Sodium dodecyl sulfate was the surfactant used for enhancing the stability of nanofluid [125].

Utomo et al. dispersed 30-40 wt.% of TiO_2 and Al_2O_3 in distilled water; the colloidal solution was ultrasonic homogenization keeping pH constant, Large aggregation was observed even after sonication [126].

Longo and Zilio prepared Al_2O_3-water (15 wt.%, 30 nm) and TiO_2-water (25 wt.%) nanofluids. The colloidal solution of nanofluid was first subjected to mechanical stirring, and then it was sonicated at 25 kHz for 48 h. The characterization of the nanofluid by Malvern nano-sizer shows that Al_2O_3-water and TiO2-water nanofluid show less aggregation and better stability when homogenized using sonication. The nanofluid remained stable for more than a month [127].

Qu and Wu dispersed Al_2O_3 and SiO_2 in water. The nanofluids were obtained in a stepwise procedure. At first, the pH value of the nanofluids was adjusted to 9.7 and 4.9 for the SiO_2 and Al_2O_3 nanofluids respectively. The colloidal solution of nanoparticles and water was ultrasonically vibrated for four hours. The TEM characterization shows that the Al_2O_3 nanoparticles were dispersed homogenously as compared to SiO_2 nanoparticles [128].

`

2.2 Tribological impact of the nanomaterial mixed with lubricating oil

A comparative study of Zhang et al. on CuNiAl against 42CrMo4 under different lubricants investigated that fretting friction torque was found out to be higher on comparing with sliding friction torque due to strain hardening and wear debris formation. It was also investigated that sea water had lower friction torques on comparing with filtered water, due to deposition of $CaCO_3$ and $Mg(OH)_2$ in seawater on wear trace. The wear morphologies showed that abrasive wear along with cracks and delamination was also observed, due to frequent shear stress and poor lubrication [129].

Alawi et al. investigated that nanoregrigerants can be used to reduce energy consumption. HFC134a refrigerant mixed with nanoparticles and mineral oil can save up to 26.1% energy when 0.1% TiO2 nanoparticles fraction of mass was mixed. It was also concluded that surfactant type could be used to eliminate long term use problems of nanoparticles [130].

Wu et al. observed that PIBS concentration can affect nano-MoS2-ZDDP tribological properties. Fig. 1 shows the mechanism of tribofilm formation of MoS2 with low PIBS concentration. It was also observed that C.O.F. of nano-MoS2-ZDDP without PIBS was 35.3% while when 3% PIBS concentration was used C.O.F. was 12.2% [131].

Xia et al. investigated that nano lubricant method shows good dispersibility and stability with TiO2 nanoparticle agglomerate size up to 420nm. Oil droplets and TiO2 nanoparticles can prevent agglomeration when used in the lubricants. It was also observed that 2% TiO2 nanoparticle addition in 1% O/W lubricant could reduce C.O.F. significantly up to 17.6% [132].

Salah et al. observed that CNTs of oil fly ash could be used as a good lubricant additive with the further addition of CuO nanosheets can significantly enhance the performance of lubricant oil. It was also noted that when 0.5% w/w concentration was used in the lubricant oil, C.O.F. can be reduced up to 43% due to the formation of a protective layer on the disk [133].

Asnida et al. experimental result shows that the addition of copper (II) oxide nanoparticle in SAE10W-30 can significantly reduce C.O.F. and wear rate. It was also discussed by using RSM as statistical software that for optimal parameters for lower the better wear rate and C.O.F. were 75.152N load, 0.0086 wt % concentration, and 291.3360 rpm speed [134].

Yazid et al. observed that for maintaining a long life, good stability, and good dispersion and for improved thermal properties, CNTs could be used as nanofluids. For better

`

functionalization of CNTs nanofluid, it was chemically treated via covalent functionalization [135].
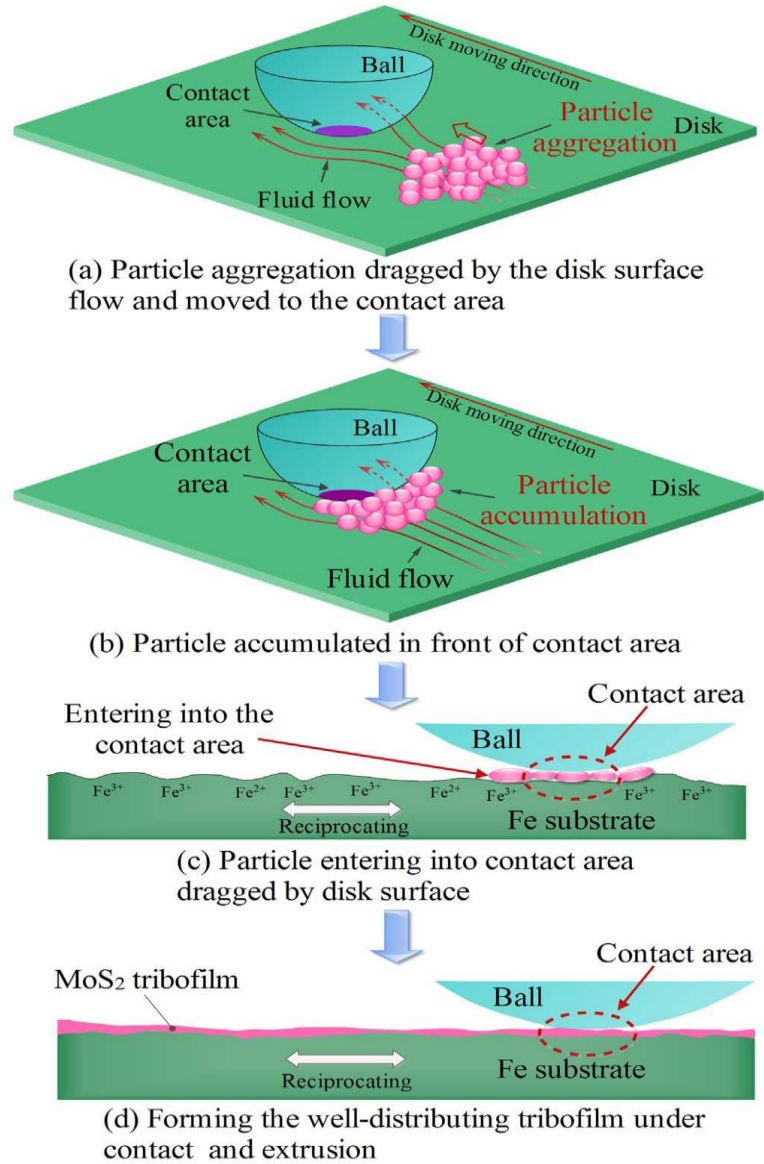
Figure 2.1 The tribofilm forming mechanism of MoS_2 nanosheet in the case of low PIBS concentration. [130]

Bena et al. investigated that RCA under different frequency and observed that as the frequency increases chatter marks decreases and was sufficient lubricant. It was also observed that due to re-lubrication, the oscillating forming process has mixed lubrication condition [136].

`

Hu et al. investigated new efficient continuity model for lubrication and also establish oil storage cross hatched texture. FBNS algorithm was adopted to solve the mass conserving model and to evaluate outlet and inlet boundaries accurately and efficiently [137].

Redhwan et al. examined the thermos-physical properties of PAG nanolubricants mixed SiO_2 nanoparticles and compared with Al2O3 nanolubricants. The experimental result shows that viscosity and thermal conductivity of SiO_2 nanolubricants decreases with increase in temperature while increases with increase in volume concentration [138].

Sidik et al. investigated that CNT nanofluids show long termed stability and homogeneous dispersion with high thermal properties. It was also noted that production cost and stability are major factors for CNT fluids and its application towards solar collectors needs to restructure [139].

Zhang et al. examined heterogeneous nucleation prepared Al2O3-coated h-BN powder and observed superior microstructure, relative density, and mechanical properties. It was also noted that STC ceramic cutting tool shows higher values and optimized cutting parameters obtained are f=0.102mm/rev, v=150m/min and ap= 0.2mm [140].

Dai et al. investigated the tribological performance of nanoparticle lubricants that possess different chemical and physical properties. Statistical comparison was used to study the morphological, physical and chemical properties of nanoparticle lubricants and results show that friction and wear were affected by all these parameters [141].

Zawawi investigated viscosity and thermal conductivity of composite nanolubricants for the refrigeration system. The experimental result shows that Al_2O_3 and SiO_2 and PAG 46 based nanolubricant are homogeneously dispersed and behaves like Newtonian fluids. It was also noted that viscosity of composite lubricants was lower than single component nanolubricant [142].

EL-Seesy et al. examined the engine performance of biodiesel-diesel fuel blend multi-walled carbon nanotubes (MWCNT). The experimental result shows that mechanical engine performance of blend diesel decreases while emission in engine increases during operating conditions. It was also noted that at 50mg/l nanodose level, best mechanical performance was obtained [143].

Darminesh et al. investigated biodegradable lubricants. The experimental result shows that biodegradable lubricant shows excellent properties on comparing with mineral oil. It was also

`

noted that there were some voids in biodegradable lubricants and additives were used to overcome these voids and result shows that excellent improvement was obtained. CuO, SiO$_2$, and TiO$_2$ are a common oxide of metals that were used as nano-additive, which shows excellent performance in nanolubricant [144].

Alasli et al. investigated sonicated MWCNTs blend with low viscous mineral oil. The experimental result shows that sonicated MWCNTs saturated, separated oil layer and lubricated. It had the ability to detach force with excellent viscosity and thermal conductivity of the nanolubricant [145].

Diabb et al. observed adhesion on the tool-tip. Experiments were conducted to study corn and sunflower oils with the addition of SiO$_2$ nanoparticle having 0.025 wt %. The frictional characteristics were described by the Stribeck curve and showed excellent lubrication properties on comparing with other vegeTable oils [146].

Kedzierski et al. investigated viscosity, density, and thermal conductivity of zinc along with aluminum oxides nanolubricants. It was noted with an increase in the mass fraction of nanoparticles, viscosity, thermal conductivity, and density also increases while other the other end when the temperature increases thermal conductivity, density, and viscosity decreases [147].

Laad and Jatti investigated tribological properties of mineral oil with TiO2 as nanoparticle additives for engine oil applications. Experimental tests were conducted at different loads and a variable concentration of nanoparticles. It was noted that significant improvement in friction and wear was obtained when TiO$_2$ nanoparticles were used as an additive in mineral oils [148]. The inorganic fullerene IF-WS$_2$ nanoparticles were useful in reducing sliding friction by 50%, where physical interference occurred in between the nanoparticles and the mating surfaces. The associated friction reduction was not appreciable in a hydrodynamic lubrication regime due to the lack of physical interaction between the IF particles in between the mating surfaces. The IF-WS$_2$ nanoparticles were ineffective under intensive contact pressures [149,150]. WS$_2$ nanoparticles used with PAO (polyalphaolefin) resulted in a decrease in friction and wear up to 70% at a temperature of 100^{0}C. The size of nanoparticles ranged from 50 nm to 130 nm [151. 152]. IF-MoS$_2$ nanoparticles exhibited ultra-low friction coefficients (close to 0.04). The performance of the IF nanoparticles depends strongly on their crystalline size [153.154]. MoS$_2$ nanoparticles form a solid complex adsorption film on the steel surface which reduced friction

`

and wear [155]. Metallic nanoparticles showed mainly two types of tribological properties, first was the formation of tribofilm which could result in good surface properties and separation of contacting surfaces and second was a reduction of wear and friction through tribo sintering as the nanoparticles compacted on the wear track due to heat and pressure [156]. The Copper nanoparticles as an oil additive displayed better anti-wearing ability, load-carrying capacity and friction-reduction properties than ZDDP (Zinc Dialkyl Dithiophosphate) due to the formation of the third body layer, formed by mechanical compaction [157]. With the increased composition of Cu nanoparticles in friction and wear resistance increased up to 0.2% and then decreased as the composition was increased further [158]. Nanoparticles of Au and Ag mixed with the lubricating oil formed soft and low shear strength tribofilms and consequently the friction and wear reduced. These nanoparticles could be preferred for heavy load conditions [159,160]. By adding 2% Ag nanoparticles to multi alkylated cyclopentane, the C.O.F. reduced resulting in increased load carrying capacity of the lubricant [161]. Ni nanoparticles, when added up to 0.5% in the Lubricating oil, reduced friction up to 30% but as the concentration of Ni nanoparticles increased, the reduction in C.O.F. decreased. The minimum reduction of the C.O.F. was 7% at Ni 1% [160]. The suspensions with 0.5% of ZnO and ZrO_2 had excellent tribological behavior, exhibiting a reduction in friction and wear. The tribological properties deteriorated as the concentration of ZnO and ZrO_2 increased beyond 0.5% [162]. The C.O.F. decreased by 14-23% as the concentration of CuO nanoparticle increased from 1%-2% [163,164]. The wear scar diameter reduced in presence in CuO nanolubricant had a concentration of CuO nanoparticles up to 2%. the concentration of CuO was up to 2% in the Lubricating oil [165,166]. The suspended Al_2O_3 nanoparticles decreased the C.O.F.by 40–50% and reduced the metal wear rate. Also, the wear accelerated corrosion rate decreased in the presence of nanolubricant. Moreover, the stability of the colloidal solution was very high [167,168]. 0.1-0.2% TiO_2 nanolubricant decreased the wear scar diameter due to the rolling effect of the nanoparticles on the surface. It also gave the surface repairing effect. Beyond 0.2% TiO_2 in the lubrication wear scar diameter increased due to the scratching effect of TiO_2 [169]. The nano-diamond particle in lubricant improved the anti-scuffing performance in the oil. The surface failure, attributed to the scuffing, was reduced due to the nano-diamond particles in the lubricant [170]. The expansion of graphite nanoparticles to the ointment upgraded the oil qualities. The nearness of nanoparticles between the rubbing surfaces

`

decreased contact between the plates going about as metal roller spacers. The morphological examination demonstrated that the expansion of nanoparticles diminished wear and brought about a generally smooth surface with fewer scars. The nearness of the graphite nanoparticles essentially diminished metal to metal contact at the tribopair [171,172]. The HV 1500 base oil with the expansion of WSe2 (Tungsten diselenide) nanorods indicated great tribological properties. Tribological tests demonstrated that the impact of WSe2 nanorods as oil added substance credited to the atom bearing component of moving a contact and the sliding grating between the scouring surfaces. Besides, a steady movie on the scouring surface not just endure the heap of the steel ball yet, also kept any immediate contact between the two scouring surfaces [173,174]. SiO_2 nanoparticles in the paraffin improved the load-bearing capacity of the lubricant by separating the tribopair, preventing the direct contact and promoting rolling effect. It also prevented the expansion of the micro-cracks on the tribopair surface due to particle embedment [175,176]. hBN nanoparticles used as nano composite enhanced the mechanical properties like strength, modulus, hardness by 4%, 7%, and 16% respectively. It also enhanced thermal conductivity by 9% as compared to micro-composite [177]. PTFE nanoparticle increased load bearing properties due to large adhesion between lubricant and tribosurface. The mechanical energy adsorbed by PTFE nanoparticles under deformation. It reduced the friction and wear at extreme pressure [178,179]. The size of the nanoparticles influenced the tribological properties of the lubricating oil. The smaller the size of the nanoparticles entered easily at the interface of the tribopair [180]. The nanoparticles had a higher volume/area ratio were less preferred as lubricant additive [181]. The nanoparticles had mainly five types of morphology: granular, onion, sheet, spherical and tube. Majority of nanoparticles had spherical shape followed by granular, sheet, onion and tube respectively [182,183]. Onion morphology was considered best for tribology point of view. The stable onion morphology promoted the rolling motion of the nanoparticles at the tribopair. The unstable onion morphology promoted the easy penetration of nanoparticles between the tribopair [184].

`

2.3 Gaps in the Literature Review

- The tribological properties of nanoparticles according to their size and morphology is not studied in details.

- The combination of nanoparticles as additives in lubricating oil has not been discussed thoroughly.

- The mathematical relation for computation of the amount of Nanoparticles to be added in the lubricating oil has not been developed.

- The universal blending technique for mixing the nanoparticles in lubricating oil has not been developed.

- The exhaustive study required for the study of tribological properties of Nanoparticles.

- The exhaustive study required for the study of the performance of the I C Engine using lubrication with Nanolubricants.

2.4 Objective

The proposed research work will incorporate the following objectives:

1. Developing the blending technique for the nanoparticles in the Lubricating oil such that the mixture formed will be homogeneous.

2. Fully flooded tribological and thermal analysis of lubricated piston rings material without nanoparticles in the lubricating oil.

3. Fully flooded tribological and thermal analysis of lubricated Piston rings material with nanoparticles in the lubricant.

4. Fully flooded tribological and thermal analysis of lubricated Piston rings material for computation of frictional losses when lubricant aided with a combination of different nanoparticles.

5. Analysis of performance of I C Engine using Nano Lubricants and compare among them.

`

CHAPTER 3

PREPARATION AND STABILITY ANALYSIS

This chapter includes the various mechanisms used for the preparation of a stable blend of the selected nanoparticles with the lubricating oil. This chapter also includes the Zeta potential analysis of the prepared nanofluid.

3.1 Equipment Used

The equipment used for blending of nanoparticles were

Magnetic stirrer

Ultrasonicator

3.1.1 Magnetic stirrer

The magnetic stirrer shown in Figure 3.1 was used for the primary dispersion of the nanoparticles in the lubricating oil. The temperature range of the magnetic stirrer was 350^0C and the speed range was 2000 rpm.
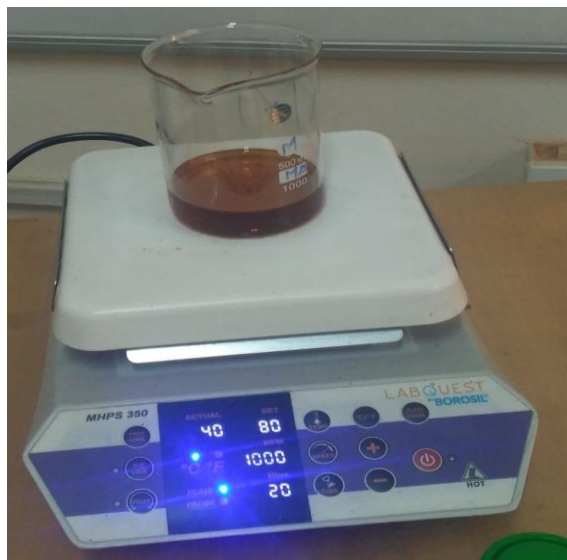
Figure 3.1 Magnetic Stirrer

`

The lubricating oil was measured and poured in a beaker and kept over the magnetic stirrer. The measured quantity of the nanoparticles was added to the lubricating oil with continuous stirring.

3.1.2 Ultrasonicator

The horn type ultrasonicator shown in Figure 3.2 was used for enhancing the dispersion quality of the lubricating oil. The rated power of the ultrasonicator was 500 W with a frequency range of 50 Hz. The pulse of the ultrasonicator was adjustable. This type of ultrasonicator has been used for the large quantity fluid. The ultrasonicator produced the ultrasonic vibrations which were transferred to the nanoparticles present in the lubricating oil, this resulted in the repulsion of the particles towards each other. The repulsion resulted in enhancing stability by reducing the sedimentation of nanoparticles in the lubricating oil.

Figure 3.2: Ultrasonicator

`

3.2 Preparation and stability of Nanofluid

The nanoparticles were selected based on the comprehensive literature review considering the tribological parameters and stability of the nanofluid. The selected nanoparticles of Graphite, SiO_2, WS_2, Cu and CuO were blended in 15W40 lubricating oil. The blending was done on w/w base from 0.2% to 1% in the succession of 0.2%. The blending started with the uniform dispersion of nanoparticles in the lubricating oil. The stability of the nanoparticles was enhanced by different means.

3.2.1 Preparation and stability of Graphite Nanofluid

The Graphite nanoparticles were dispersed in the lubricating oil by magnetic stirring at 70^0 C and 2000 rpm for 2 hours. The nanoparticles were uniformly dispersed in the lubricating oil. The lubricating oil having dispersed nanoparticles was ultrasonicated at 20 kHz, 400W full pulse for 60 minutes. The stability of the nanolubricant was analyzed by visual inspection and zeta potential test.
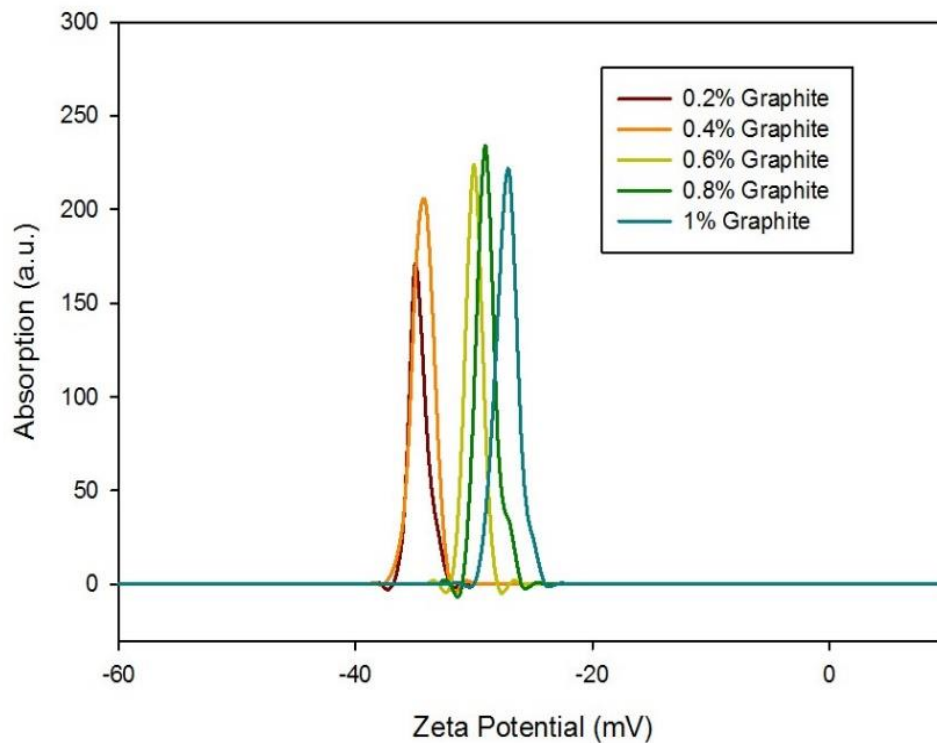
Figure 3.3: Effect of concentration of graphite nanoparticles on Zeta Potential

`

The zeta potential values shown in Figure 3.3 for graphite nanolubricants were found 25-36 mV, which reflect moderate to high stability. The zeta potential value for the nanofluid having lesser concentration nanoparticles showed more stability than the higher concentration nanofluid as shown in Figure 3.3.

3.2.2 Preparation and stability of SiO$_2$ Nanofluid

The SiO$_2$ nanoparticles were dispersed in the lubricating oil by magnetic stirring at 70^0 C and 2000 rpm for 2 hours. The nanoparticles were uniformly dispersed in the lubricating oil. The lubricating oil having dispersed nanoparticles was ultrasonicated at 20 kHz, 400W full pulse for 3 hours. The stability of the nanolubricant was analyzed by visual inspection and zeta potential test. The zeta potential values for SiO$_2$ nanolubricants were found 39-48 mV, which reflect high stability. The zeta potential value for the nanofluid having lesser concentration nanoparticles showed more stability than the higher concentration nanofluid.
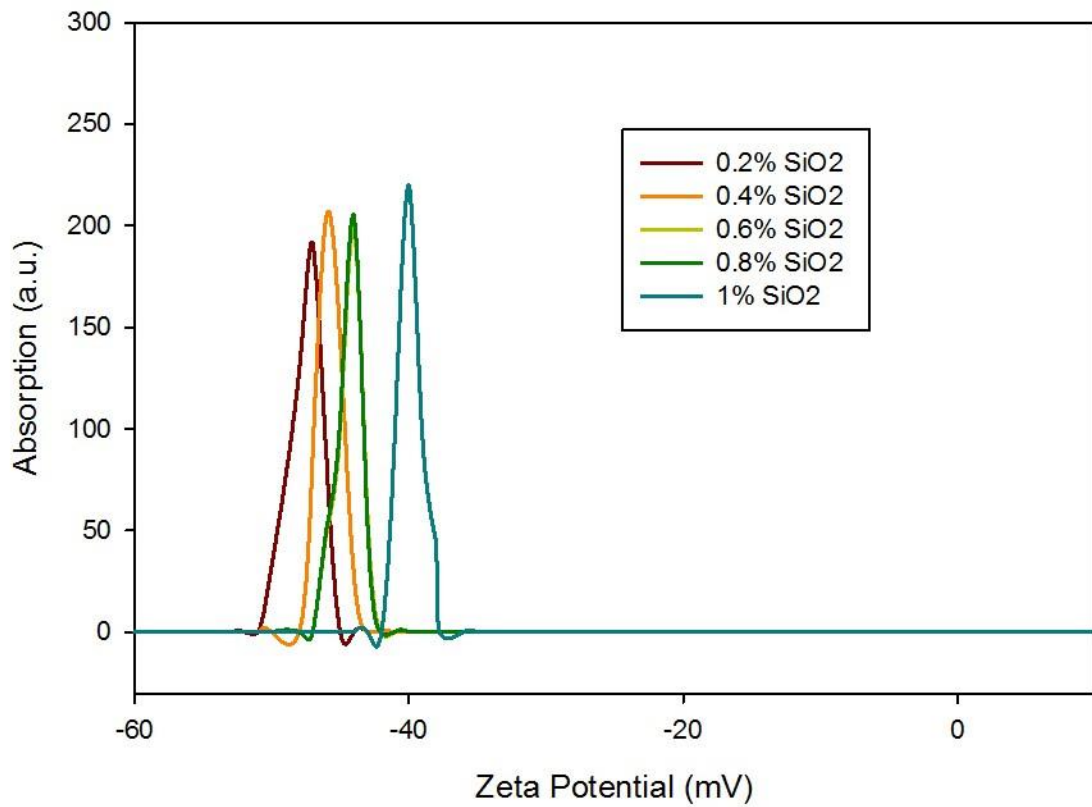
Figure 3.4: Effect of concentration of SiO$_2$ nanoparticles on Zeta Potential

41

`

3.2.3 Preparation and stability of Cu Nanofluid

The Cu nanoparticles were dispersed in the lubricating oil by magnetic stirring at 70^0 C and 2000 rpm for 2 hours. The nanoparticles were uniformly dispersed in the lubricating oil. The lubricating oil having dispersed nanoparticles was ultrasonicated at 20 kHz, 400W full pulse for 3 hours. The Cu nanoparticles showed sedimentation after 24 hours more over the zeta potential values for the 1% Cu nanolubricant was 9 mV. The stability of the nanolubricant was enhanced by using CTAB as a surfactant. CTAB was first blended in the lubricant by magnetic stirring at 70^0 C and 2000 rpm for 1 hour, the nanoparticles of Cu were then added while stirring. The nanolubricant was stirred for 2 hours and then ultrasonicated at 20 kHz, 400W full pulse for 6 hours. The sedimentation was not observed for 15 days and the zeta potential values for the Cu nanolubricant were found 17-24 mV, which reflect moderate stability shown in Figure 3.5,3.6. The zeta potential value for the nanofluid having lesser concentration nanoparticles showed more stability than the higher concentration nanofluid.
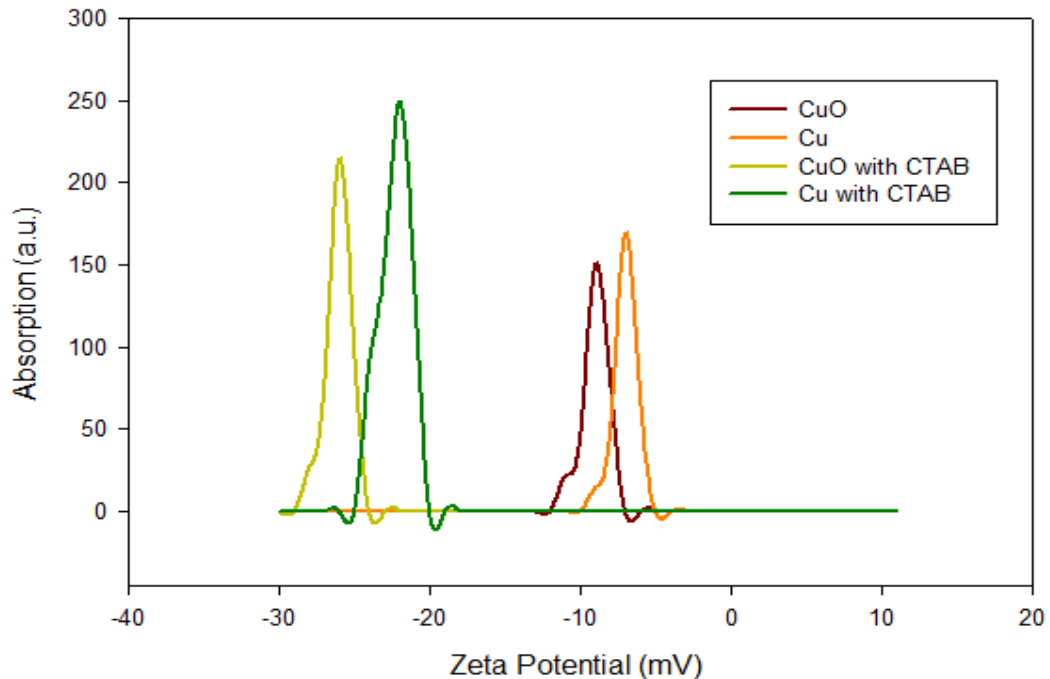
Figure 3.5: Effect of Surfactant on the Zeta Potential
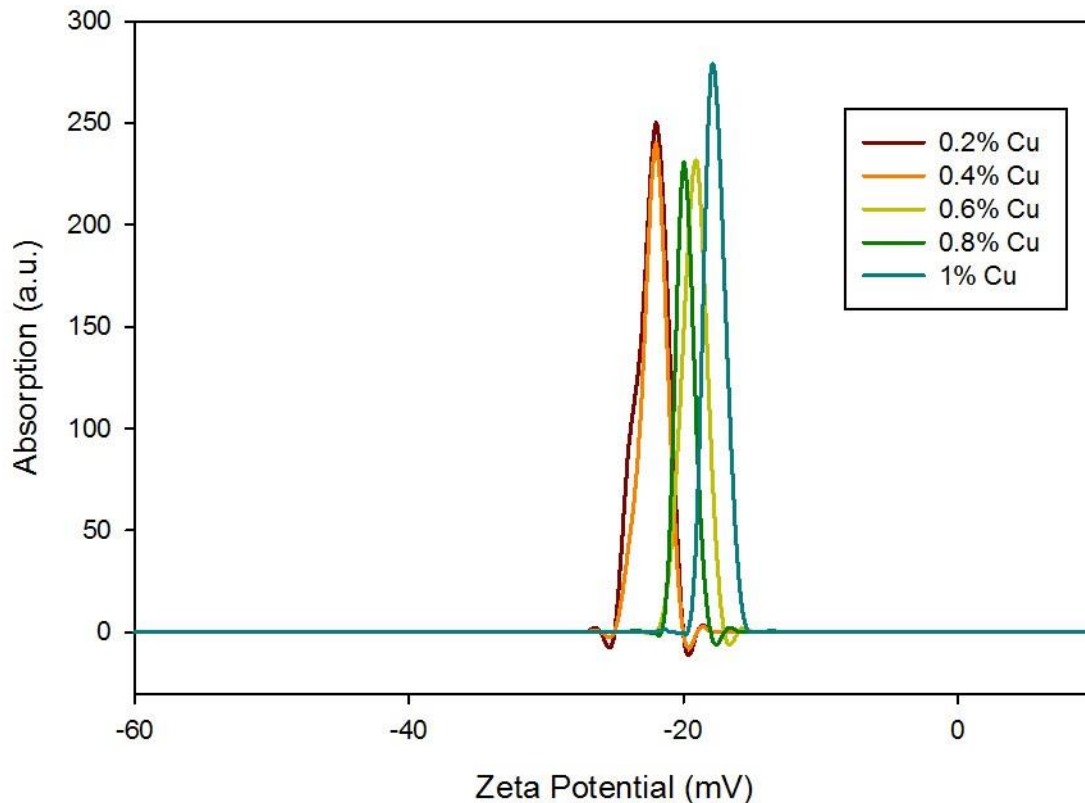
Figure 3.6: Effect of concentration of Cu nanoparticles on Zeta Potential

3.2.4 Preparation and stability of CuO Nanofluid

The CuO nanoparticles were dispersed in the lubricating oil by magnetic stirring at 70^0 C and 2000 rpm for 2 hours. The nanoparticles were uniformly dispersed in the lubricating oil. The lubricating oil having dispersed nanoparticles was ultrasonicated at 20 kHz, 400W full pulse for 3 hours. The CuO nanoparticles showed sedimentation after 48 hours more over the zeta potential values for the 1% CuO nanolubricant was 11 mV. The stability of the nanolubricant was enhanced by using CTAB as a surfactant. CTAB was first blended in the lubricant by magnetic stirring at 70^0 C and 2000 rpm for 1 hour, the nanoparticles of CuO were then added while stirring. The nanolubricant was stirred for 2 hours and then ultrasonicated at 20 kHz, 400W full pulse for 6 hours. The sedimentation was not observed for 19 days and the zeta potential values for the CuO nanolubricant were found 18-28 mV, which reflect moderate stability shown in Figure 3.5,3.7. The zeta potential value for the nanofluid having lesser concentration nanoparticles showed more stability than the higher concentration nanofluid.
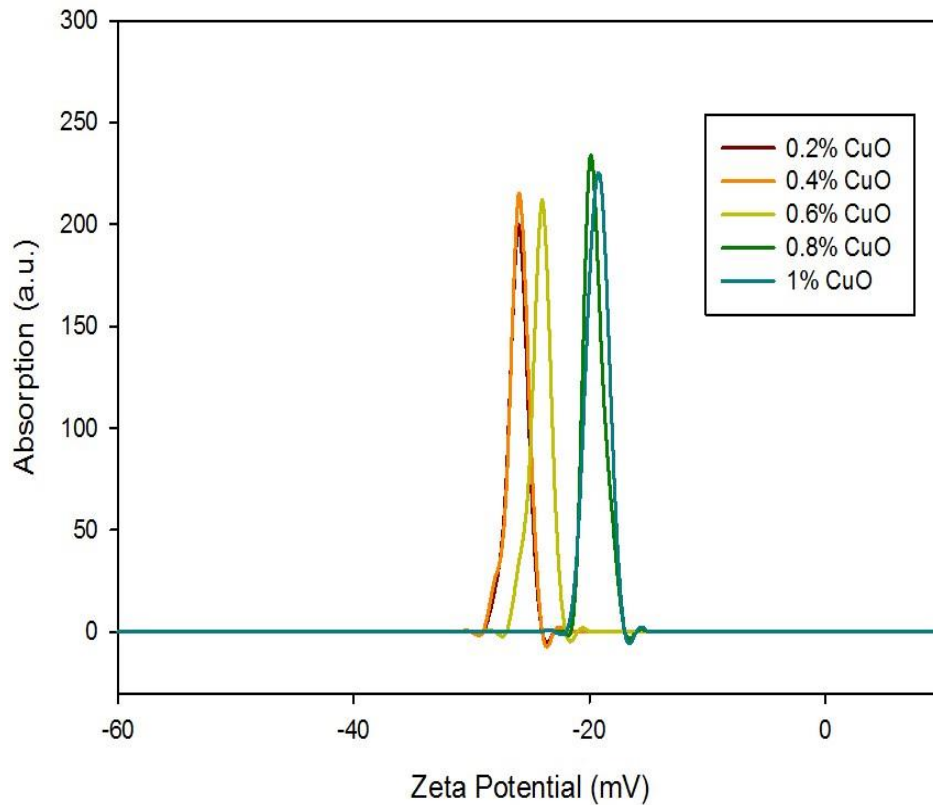
Figure 3.7: Effect of concentration of CuO nanoparticles on Zeta Potential

3.2.5 Preparation and stability of WS₂ Nanofluid

The WS$_2$ nanoparticles were dispersed in the lubricating oil by magnetic stirring at 70^0 C and 2000 rpm for 2 hours. The nanoparticles were uniformly dispersed in the lubricating oil. The lubricating oil having dispersed nanoparticles was ultrasonicated at 20 kHz, 400W full pulse for 8 hours. The stability of the nanolubricant was analyzed by visual inspection and zeta potential test. The zeta potential values for graphite nanolubricants were found 29-43 mV, which reflect moderate to high stability. The zeta potential value for the nanofluid having lesser concentration nanoparticles showed more stability than the higher concentration nanofluid as shown in Figure 3.8.
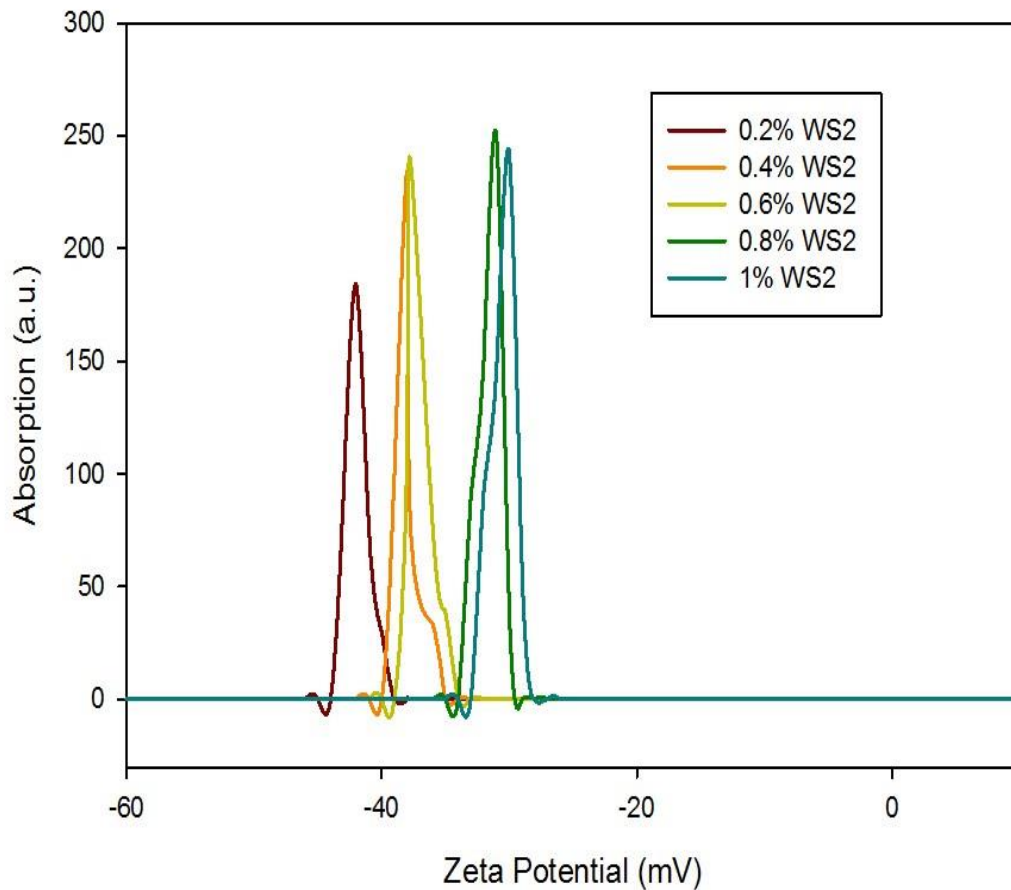
Figure 3.8: Effect of concentration of WS_2 nanoparticles on Zeta Potential

The blending technique and the stability of nanofluid have been discussed in Table 3.1. The nanolubricant of SiO_2 showed the highest value of zeta potential which means it is highly stable, followed by WS_2 and graphite nanolubricant as shown in Figure 3.9. Both graphite and WS_2 nanolubricant falls in the stable category as per zeta potential measurement. The nanolubricants of CuO and Cu using CTAB as surfactant showed moderate stability.

45

`

Table 3.1: Preparation and stability of nanolubricant

Nanoparticles	Base Fluid	Surfactant	Blending Technique	Stability of nanolubricant
Graphite Nanoparticles	15W40	-	Stirring for 2 hours at 70^0 C and 2000 rpm and then sonication at 20 kHz, 400W full pulse for 60 minutes.	The nanolubricant showed no sedimentation after 30 days of blending.
SiO$_2$ Nanoparticles	15W40	-	Stirring for 2 hours at 70^0 C and 2000 rpm and then sonication at 20 kHz, 400W full pulse for 3 hours.	The nanolubricant showed no sedimentation after 30 days of blending
Cu Nanoparticles	15W40	CTAB	Stirring for 2 hours at 70^0 C and 2000 rpm and then sonication at 20 kHz, 400W full pulse for 6 hours in succession of 1 hour.	The nanolubricant showed sedimentation after 15 days of blending
CuO Nanoparticles	15W40	CTAB	Stirring for 2 hours at 70^0 C and 2000 rpm and then sonication at 20 kHz, 400W full pulse for 6 hours in succession of 1 hour.	The nanolubricant showed sedimentation after 19 days of blending
WS$_2$ Nanoparticles	15W40	-	Stirring for 2 hours at 70^0 C and 2000 rpm and then sonication at 20 kHz, 400W full pulse for 8 hours in succession of 60 minutes.	The nanolubricant showed no sedimentation after 30 days of blending

`
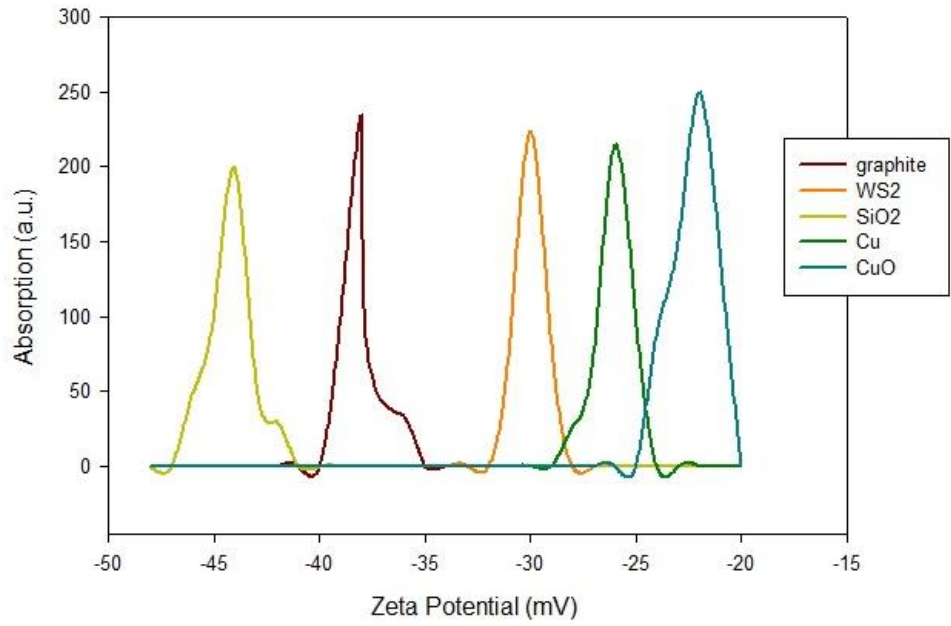
Figure 3.9: Zeta Potential of various nanolubricants

`

CHAPTER 4

TRIBOLOGICAL AND THERMAL ANALYSIS

This chapter contains the detailed tribological testing of the prepared nanolubricant using pin-on-disc tribometer and four ball tester.

4.1 Material and method

The TR-20-LE Pin on Disc tribometer had been used for friction and wear measurement of the tribopair in sliding contact in the presence of the nanolubricant in fully flooded and starved lubrication conditions according to ASTM G99. The change in temperature of the tribopair was measured by the thermal imaging camera. The weight loss due to wear was measured by the digital weight balance. The tribological and extreme pressure analysis was also conducted on the four ball tester according to ASTM - D4172 and ASTM - DIN 51350 respectively.

4.1.1 Pin on Disc tribometer

The TR-20-LE Pin on Disc tribometer had been used for friction and wear measurement of the tribopair in sliding contact in the presence of the nanolubricant in fully flooded and starved lubrication conditions according to ASTM G99. The tribopair used for the pin-on-disc tribometer has the cylindrical pin that remains stationary and the load is applied on it. The disc rotates at the desired speed. The variable parameters for tribological testing could be a normal load, sliding speed and the lubrication regime. The machine made up from several assemblies like spindle assembly, loading lever assembly, sliding plate assembly & environmental chamber which have been mounted on the base structure. The structure made up of steel tubes absorbs shocks and load during the test. The disc had been clamped on the spindle with the help of screw which had been driven by an AC motor through timer belt. The holding lever assembly made of a single bar with specimen holder and dead weight's. The dead weights had been suspended by wire rope to apply normal load on pin specimen. The fixed pivot point of the lever at center ensured that load applied at one end of pin get equally distributed. The frictional force produced between pin and disc was measured by the load cell. The lubrication chamber made up of two parts fixed around the disc to prevent oil spillage. The top part had

`

leak proof toughened glass and bottom part consisted of a cylindrical leak-proof chamber with a large outlet for draining oil during the test. At entry port to tank, a wire gauge mounted to collect debris and allows oil to flow through. The LVDT (Linear variable differential transducer) had been used to measure the wear between pin and disc. To achieve 1:1 leverage ratio this sensor is mounted at an exactly the same distance of specimen from the pivot point. The least count was 0.1 micrometer and the range of LVDT wear measurement was $\pm$ 2mm. Load Cell has been used to measure friction between pin and disc. It was mounted on a bracket at a distance equal to the distance between specimen and pivot. The frictional force measured by the load cell was up to 200N. The load cell with a bracket was mounted on a sliding plate and moved along with the sliding plate while setting wear track diameter.

Figure 4.1: Pin on disc Tribometer
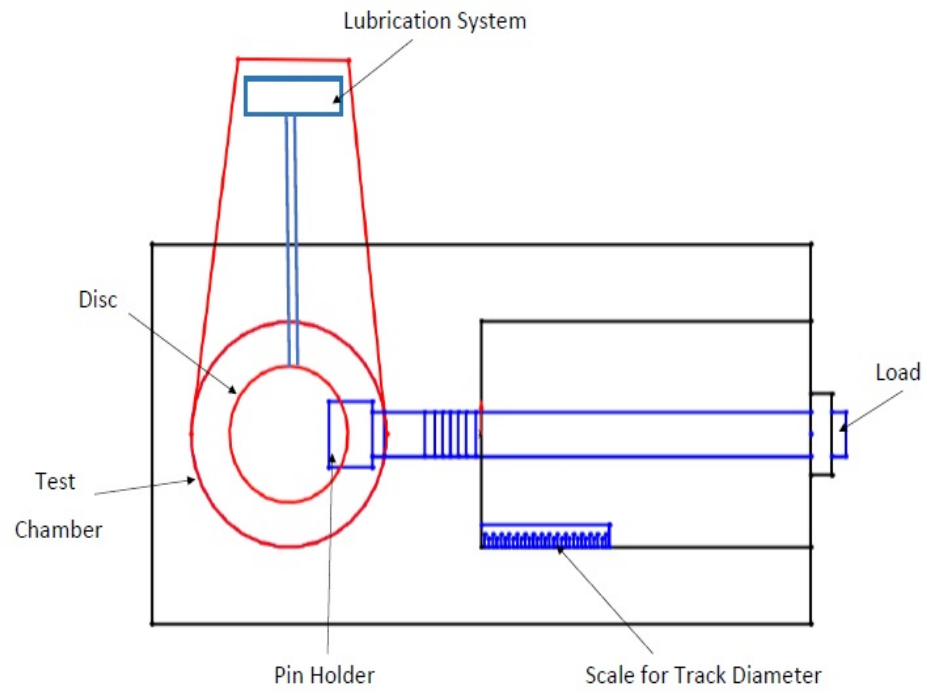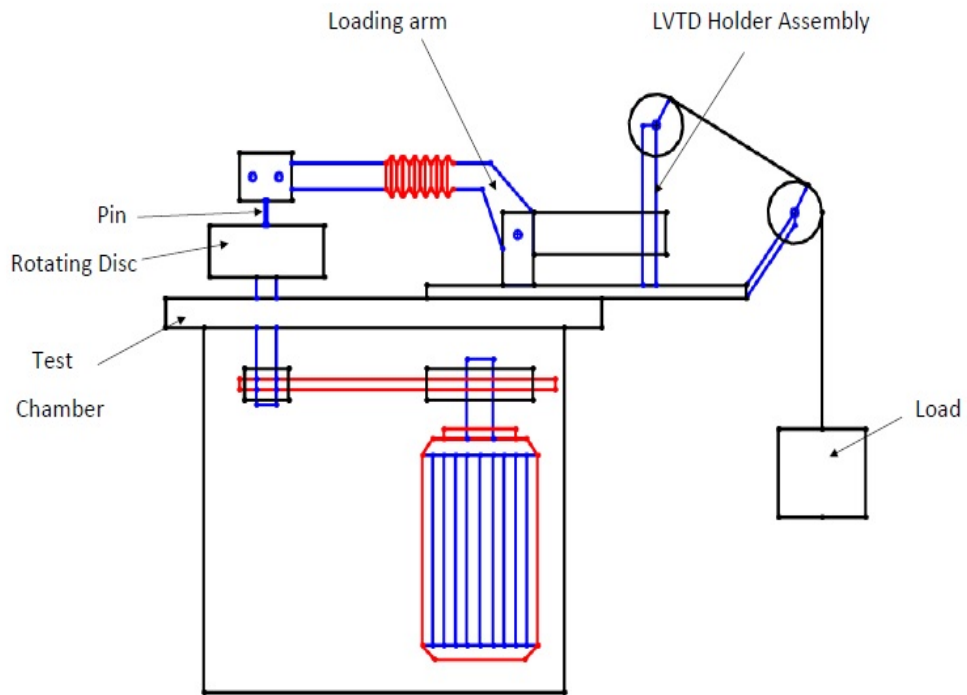
Figure 4.2: Pin on disc Tribometer

`

Table 4.1: Specifications Pin-On-Disc Tribometer

Detail		Description	Remarks
Tribopair	Pin	Dia 3,1,6,8,10 & 12	Material: according to field of application
	Disc	Dia 165mm x 8mm thick	Material: according to the field of application
Sensor specification			
Disk Speed	Range	200 rpm-2000 rpm	Can be controlled through software in the step of 1 rpm
	Least Count	1 rpm	
	Display accuracy	1 ± 1 % of the measured speed	
Normal Load	Range	1N-200N In succession of steps of 5N.	
Frictional forces	Range	0-200N	
	Least Count and accuracy	0.1 N; (0.1 ± 2% measured frictional forces) in N	
Wear	Range	±2 mm	
	Sensor spec	LVDT	
	Least Count and accuracy	0.1 micron; (0.1 ± 1% of measured wear) in micron	
Wear track diameter		50mm to 140mm	
Sliding speed		0.5m/s max 15m/s	
Timer		Max 99 hrs,59min, 59sec	

`
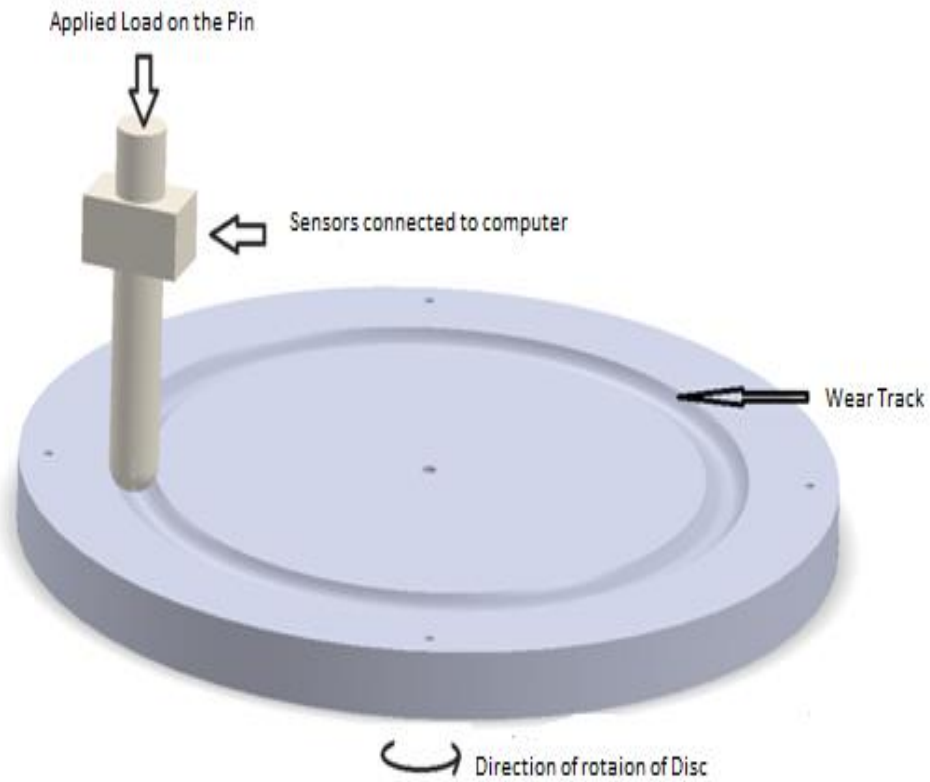
Figure 4.3: Pin on Disc Schematic

Table 4.2: Parameters for tribological investigation on pin on disc

Parameters	Value
Standard	ASTM-G99
Composition of Pin Specimen (%)	C-3.55, Cr-1.04, Mn-0.59, Si-2.92, Fe-91.9.
Composition of Disc Specimen (%)	C-0.102, Cr-0.045, Mn-0.459, Si-1.727, Fe-97.667.
Oil Specimen	15W40 and 15W40 blended with nanoparticles
Load (N)	40
Sliding speed (m/s)	3.663, 5.2631, 7.3260, 10.4712, 13.6054.
Temperature	Ambient
Sliding Distance (m)	8000

`

4.1.1.1 Tribopair

The mild steel disc had diameter 165 mm and thickness 10 mm was cast and then surface grinder was used for improving the surface finish of the disc, finally lapping was done on the disc to achieve a surface roughness less the 2 μm. The counter pin was a solid cylindrical pin made up of cast iron had 10 mm diameter 30 mm length. The parameters for the tribological investigation have been shown in Table 4.2.

4.1.2 Thermal imaging camera

The infrared radiation based thermal imaging camera having the temperature range up to 1200 ^{0}C and sensitivity 0.1^0C was used as shown in Figure 4.4. The thermal imaging camera has been used for measuring the temperature of the tribopair before and after the experiment so that the change in temperature can be measured. The camera has been placed in a fixture near the pin on disc tribometer to get the accurate results.

Figure 4.4: Thermal imaging camera

4.1.3 Four ball tester

TR-30L has been utilized for evaluating the wear and extreme pressure properties and coefficient of lubricants according to various ASTM standards. The equipment consists of four 12.7 mm diameter steel balls, out of which three balls have been clamped together and placed

`

in lubricating oil which has to evaluate. The fourth ball which is placed over three steel balls rotated with the help of a motor. These balls have been held in position by a clamping ring and force applied by tightening lock nut. The normal load has also been applied on the balls by loading lever and dead weight placed on loading pan. The frictional force has been measured by a frictional force load cell placed in the ball pot. The machine can work on various variable parameter i.e. load, speed, temperature and duration of the test. After the compilation of test wear scar measured on the stationary ball. The wear scare diameter can be measured with the help of a standalone microscope.

The machine may also be used for measuring the extreme pressure performance of the lubricant according to ASTM standards. The load during extreme pressure performance analysis have been increased in succession. The machine stops automatically as the weld has been achieved. Greater the value of the load at which the weld is achieved better is the performance of the lubricant.

The four ball tester mainly consists of three assemblies

4.1.3.1 Spindle assembly

The spindle has been connected to the motor by belt and pulley arrangement at a ratio 1:1. The idler pulley has been used to increase the tension. The spindle has been mounted on top of the body between two high precision ball bearing to form a self-containing unit.

4.1.3.2   Ball pot assembly

This assembly made of three parts ball pot, ball pot race, and lock nut. Ball pot has been used to filling sample oil and to tightened the steel balls by ball pot race. The ball race has been used to position the ball at the time of tightening the lock nut. The Resistance Temperature Detectors (RTD) sensor placed between the heater to measure the oil temperature. The Λ (PID) sensor has been used to control the heating and set the oil temperature. The ball pot has been placed using the ball pot handle under the spindle. The loading button fixed inside the ball pot pushes the frictional force load cell button and the results have been displayed on the controller.

`

4.1.3.3 Loading arrangement

The variable loading ratio up to 1:15, the loading arm has been pivoted and it exerts pressure when dead weight placed on the pan at the longer end. The load cell which measures the 1100 Kg mounted inside the shorter end of loading lever lifts plunger, anti-friction disc, and ball pot when weights have been placed in loading pan. to exert a force on plunger the roller arrangement is used. The plunger has been moved over the linear bush bearing and on its top, a thrust bearing is placed to seat anti-friction disc. The dead weights of 1 Kg to 5Kg can be used to provide load upto 9999N.

Table 4.3: Parameters of Four Ball Tester

Parameters	Wear Test	Extreme Pressure Test
Standard	ASTM- D4172	ASTM- DIN 51350
Ball Specimen	Steel Balls, Diameter 12.7 mm, Ra=0.04 microns, Hardness RC 65	Steel Balls, Diameter 12.7 mm, Ra=0.04 microns, Hardness RC 65
Oil Specimen	15W40 and 15W40 blended with graphite nanoparticles	15W40 and 15W40 blended with graphite nanoparticles
Load	196 N, 392 N, 588 N	Incremental Load Starting form 2000 N
Rotational speed of the top ball	1200 rpm	1450 rpm
Temperature	75 ºC	Ambient
Test Duration	60 minutes	60 s
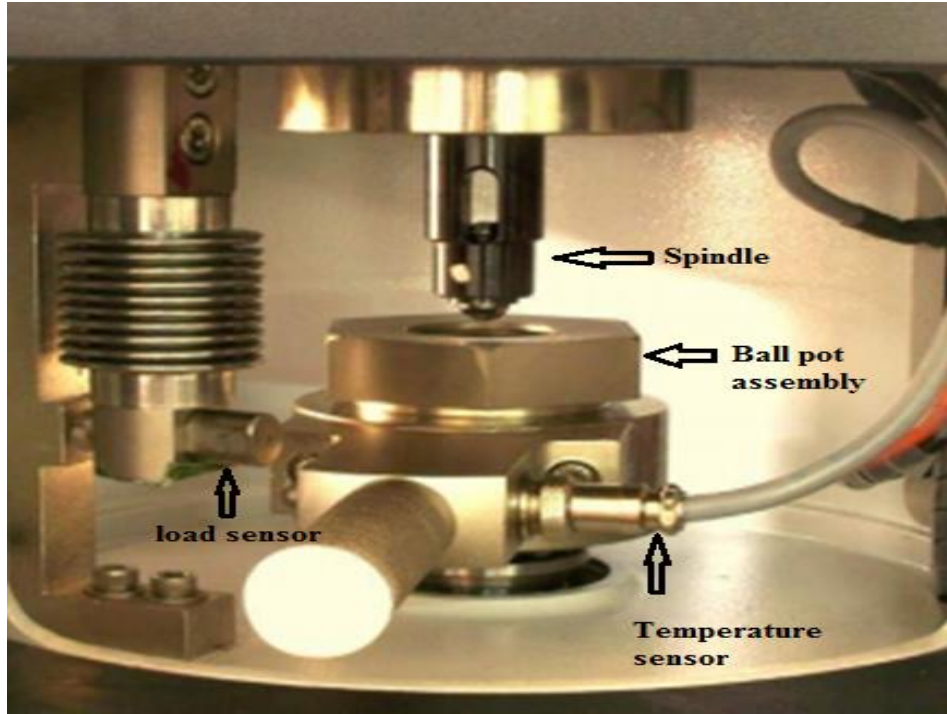
Figure 4.5: Four ball tester
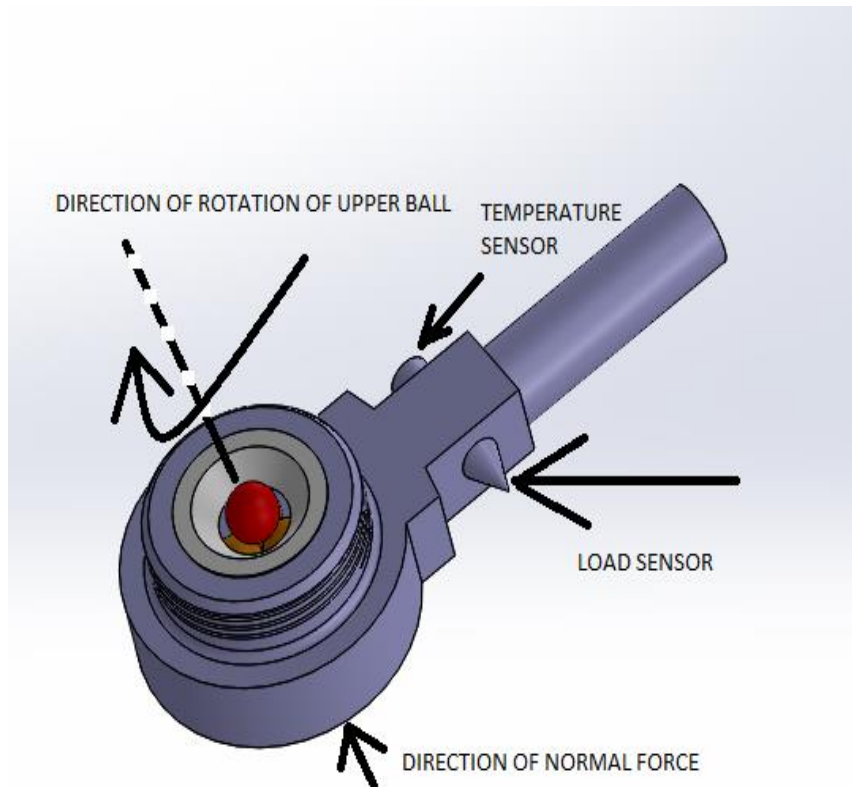
Figure 4.6: Four Ball Tester Schematic
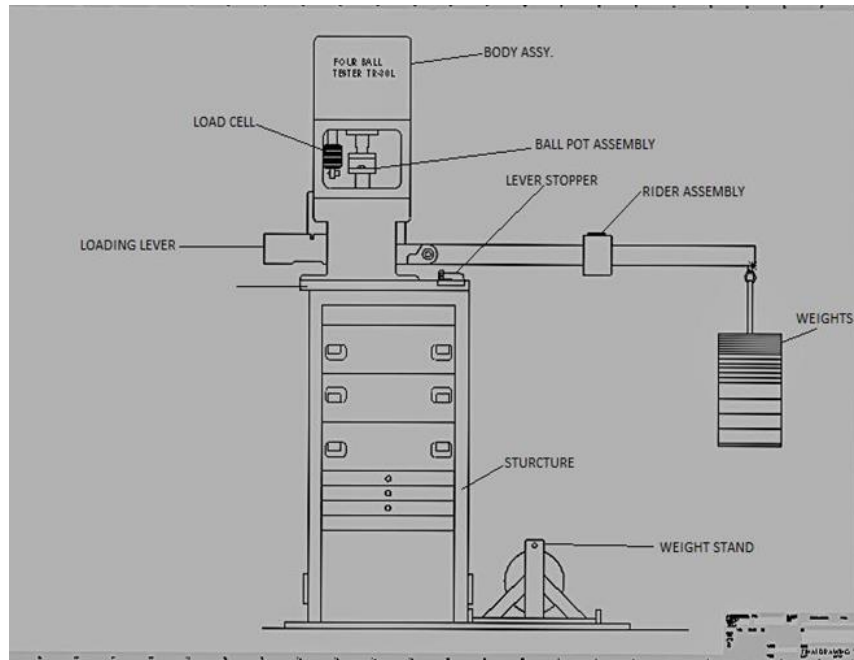
Figure 4.7: Schematic diagram of four ball tester

Figure 4.8: Four Ball Tester

`

4.1.4 Vision Inspection System

SVI IMG 5300 vision inspection system shown in Figure 4.9 has been used for measuring the wear scar diameter. The vision inspection system consists of a high magnification microscope have the magnification range of 35x to 225x. The picture of the sample can be captured by 1/3" high-resolution camera. The sample has been placed under the microscope and the focus can be adjusted by using the joystick. Once the focus has been adjusted the image of the sample appears on the computer screen attached to the sample. The diameter of the wear scare can be measured by the measuring tools given in the software.

Figure 4.9: Vision Inspection System

`

4.2 Tribological and thermal analysis on the Pin on disc tribometer

The experiment was conducted at a load of 40 N with variable sliding speed of 3.663m/s, 5.2631m/s 7.3260 m/s, 10.4712 m/s, 13.6054m/s. The atmospheric temperature at the time of testing was 28^0 C. The experiment was carried in fully flooded as well as starved lubrication condition.

4.2.1 Measurements

The values of the friction force were recorded from the friction sensor of the machine and wear of the pin was measured by weighing it before and after the experimental run. A weighing scale with 0.0001g accuracy was used for weighing of pin specimens. The collected data of the wear was then converted to volume loss (ΔV) and specific wear rate (W_{swr}) using the following relations, [(Equation (1) and (2)]:

$$\Delta V = \frac{(w_1 - w_2)}{\rho} \times 1000 \tag{1}$$

Where, ρ the = density of the pinned specimen, w_1=Weight of the pin before test, w_2 = Weight of the pin after the test

$$W_{swr} = \frac{\Delta V}{F_{nl} \times S_{sd}} \qquad (mm^3/Nm) \tag{2}$$

Where, F_{nl} = Normal load (N), S_{sd} = Sliding distance

4.2.1.1 Effect of Graphite nanoparticles on C.O.F.

Figure 4.10 shows the variation of C.O.F. with respect to speed at a constant load of 40 N for the different compositions of nanoparticles in the lubricant starting from 1%, 0.8%, 0.6%, 0.4%, 0.2% and Fresh 15W40 for fully flooded and starved lubrication.

For fully flooded lubrication condition the fresh 15W40 lubricant showed higher C.O.F. then the graphite nanolubricant. At 3.663 m/s sliding speed the average value of C.O.F.in case of fresh 15W40 lubricating oil was observed ≈ 0.0229 which decreased as the nanoparticles were added to the lubricating oil. The minimum C.O.F. was observed in case of 0.6% w/w of

`

graphite nanoparticles ≈0.0102. After 0.6% the C.O.F. again increased up to 1% w/w graphite nanoparticles ≈ 0.0184 but the value was less than the fresh 15W40. Similar trends were observed at 5.263, 7.326, 10.471 and 13.605 m/s sliding speed as shown in Figure 4.10.

Figure 4.10: Variation of C.O.F. with sliding speed for various compositions of Nanofluid in a) fully flooded Lubrication and b) Starved Lubrication c) Comparison of COF for fully flooded and Starved Lubrication.

For Starved lubrication condition, the fresh 15W40 lubricant showed higher C.O.F. then the graphite nanolubricant. At 3.663 m/s sliding speed the average value of C.O.F.in case of fresh 15W40 lubricating oil was observed ≈ 0.0651 which decreased as the nanoparticles were added to the lubricating oil. The minimum C.O.F. was observed in case of 0.8% w/w of graphite nanoparticles ≈0.0433. After 0.8% the C.O.F. again increased up to 1% w/w graphite nanoparticles ≈ 0.0536 but the value was less than the fresh 15W40. Similar trends were observed at 5.263, 7.326, 10.471 and 13.605 m/s sliding speed as shown in Figure 4.10.
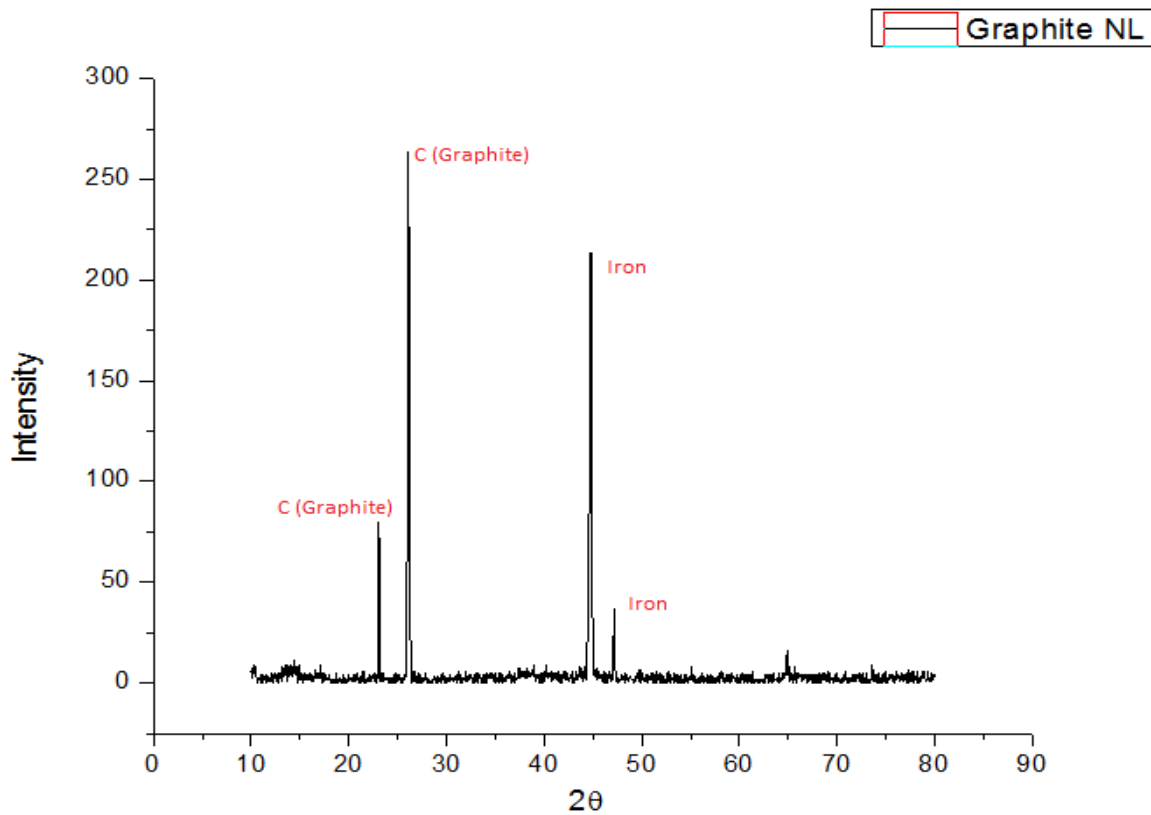
Figure 4.11: XRD analysis of tribopair in presence of Graphite NL

For both fully flooded and starved lubrication conditions the C.O.F.in case of the nanolubricant was less as compared to fresh 15W40. The 0.6% w/w of graphite nanoparticles blended in fresh 15W40 showed lowest C.O.F. for almost all the sliding speed values. The COF in case of graphite nanofluid first decreased but as the concentration was increased further the COF value again increased. The decrement in COF may be due to the coating action of nanoparticles on the surface of tribopair which can be observed by high intensity of nanoparticles in the XRD

`

analysis (Figure 4.11). The COF started increasing after an optimum concentration of nanoparticles in the nanofluid, this may be due the cluster of nanoparticles not allowing the smooth gliding of the tribopair i.e. the increased concentration of nanoparticles acted as obstacle in the gliding of one tribosurface over the other.

4.2.1.2 Effect of Graphite nanoparticles on Specific Wear Rate

Figure 4.12 shows the variation of Specific wear rate with respect to sliding speed at a constant load of 40 N for the different compositions of nanoparticles in the lubricant starting from 1%, 0.8%, 0.6%, 0.4%, 0.2% and Fresh 15W40 for fully flooded and starved lubrication.

The specific wear rate for the fully flooded condition has lower values as compared to starved lubrication due to the presence of stable lubricating film between the tribopairs. The value specific wear rate was almost negligible in case of nanolubricant due to the no wearing of the contact surfaces. However, some wear observed at a higher concentration of nanoparticles in the lubricant.

Figure 4.12: Variation of Specific wear rate with sliding speed for various compositions of nanofluid in a) Fully Flooded Lubrication and b) Starved Lubrication.

62

4.2.1.3 Thermal Analysis of graphite nanolubricant

The temperature of the tribopair was measured at the start and end of the experiment with the help of a thermal imaging camera. The change in average temperature or temperature rise of the tribopair was calculated and plotted against sliding speed.
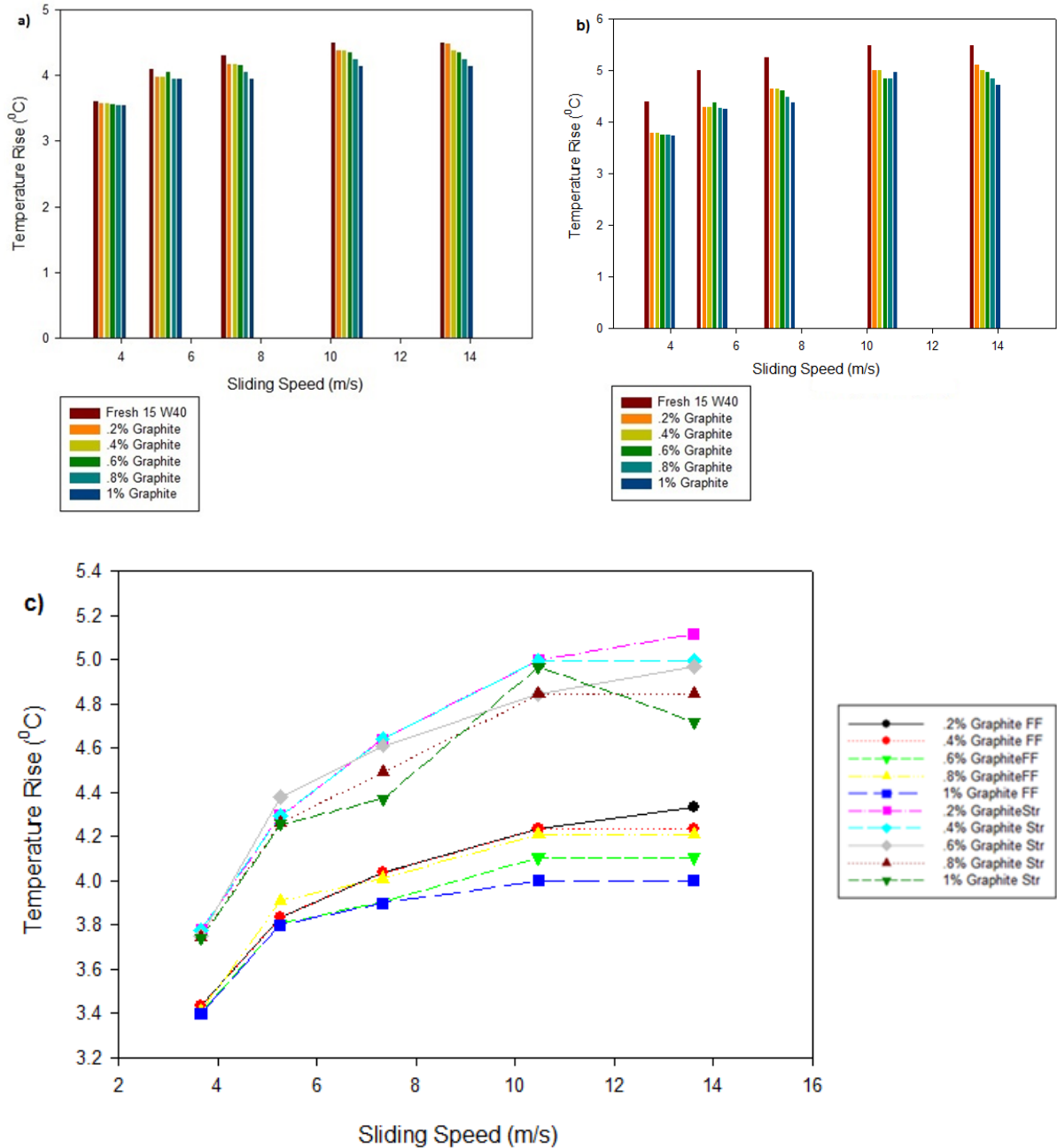
Figure 4.13: Temperature Rise with sliding speed a) fully flooded lubrication b) starved lubrication c) Comparison of Temperature Rise for fully flooded and Starved Lubrication.

`

Figure 4.13 shows the temperature rise at various speeds for fully-flooded and starved lubrication condition. The temperature rise of the tribopair was less in case of graphite nanolubricant as compared to the fresh 15W40 lubricating oil. The temperature rise was less for the higher concentrations of the nanoparticles in the lubricant.

The less temperature rise was an indicator of the increased thermal conductivity and specific heat of the lubricant due to the addition of nanoparticles. The theoretical change in thermal conductivity and specific heat was calculated with the help of ESS software as shown in Figure 4.14. The blending of nanoparticles enhanced the thermal conductivity and specific heat of the nanolubricant.
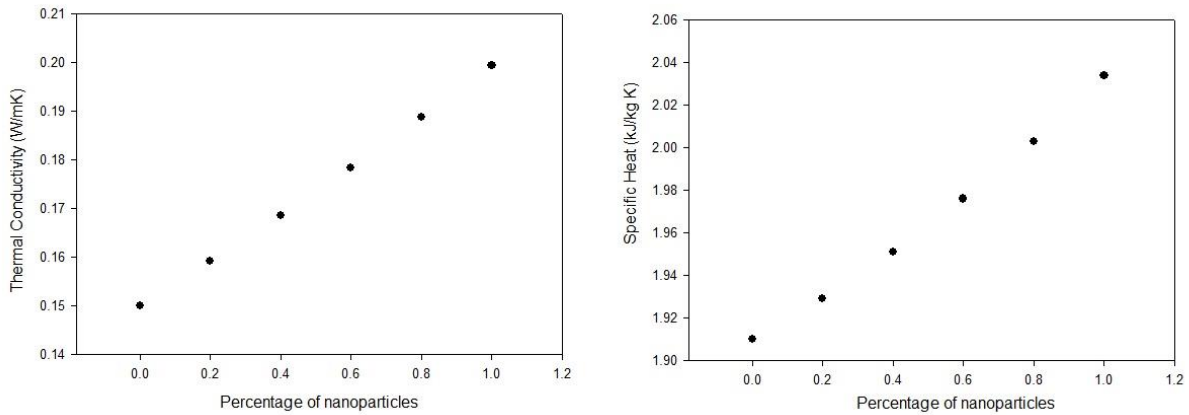
Figure 4.14: Variation in thermal conductivity and specific heat with the percentage of nanoparticles

4.2.2.1 Effect of SiO$_2$ nanoparticles on C.O.F.

Figure 4.15 shows the variation of C.O.F. with respect to speed at a constant load of 40 N for the different compositions of nanoparticles in the lubricant starting from 1%, 0.8%, 0.6%, 0.4%, 0.2% and Fresh 15W40 for fully flooded and starved lubrication.

For fully flooded lubrication condition the fresh 15W40 lubricant showed higher C.O.F. then the SiO$_2$ nanolubricant. At 3.663 m/s sliding speed the average value of C.O.F.in case of fresh 15W40 lubricating oil was observed ≈ 0.0229 which decreased as the nanoparticles were added to the lubricating oil. The minimum C.O.F. was observed in case of 0.6% w/w of SiO$_2$ nanoparticles ≈ 0.00765. After 0.6% the C.O.F. again increased up to 1% w/w SiO$_2$

`

nanoparticles ≈ 0.0127 but the value was less than the fresh 15W40. Similar trends were observed at 5.263, 7.326, 10.471 and 13.605 m/s sliding speed as shown in Figure 4.15.
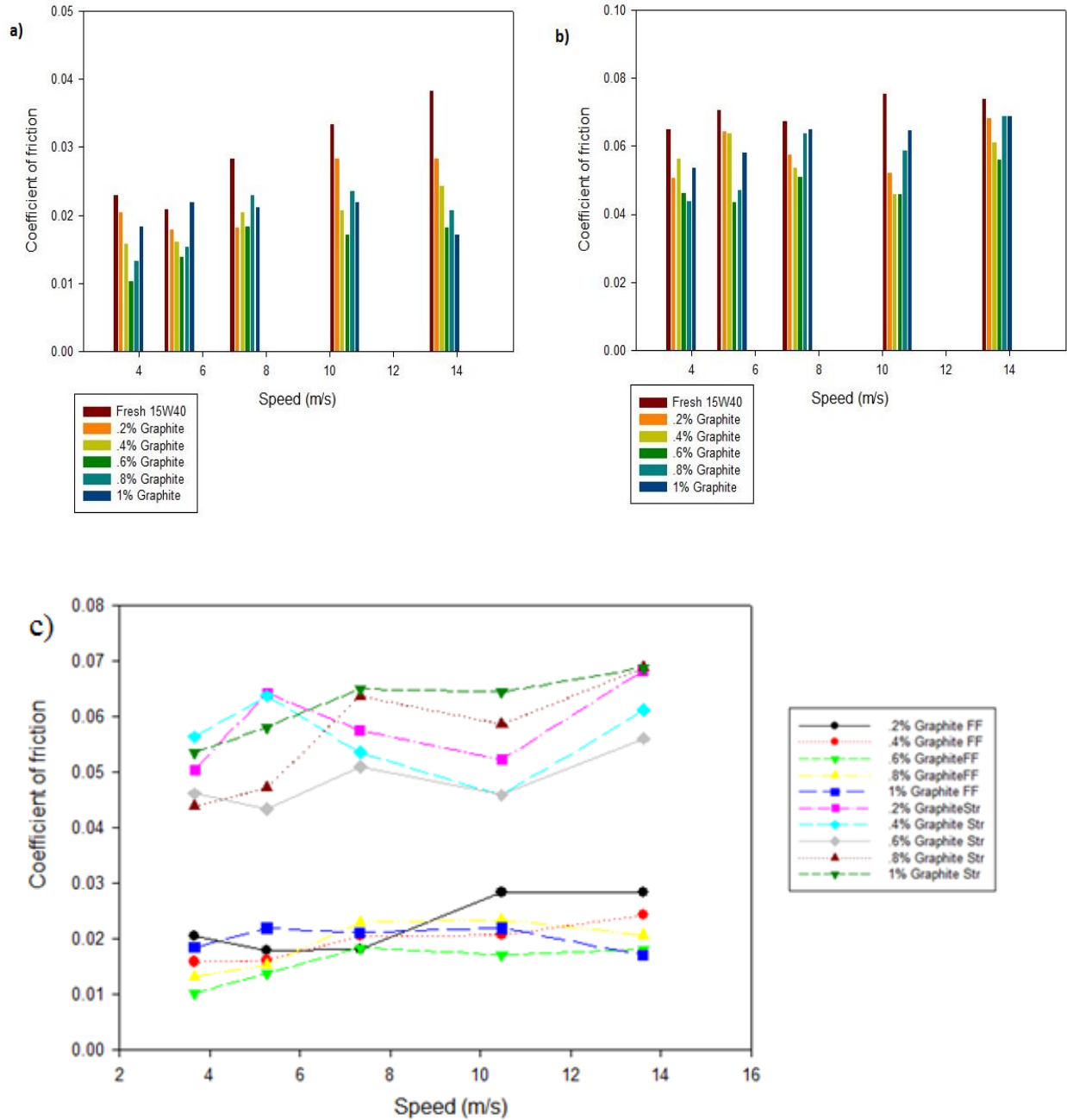

Figure 4.15: Variation of C.O.F. with sliding speed for various compositions of Nanofluid in a) fully flooded Lubrication and b) Starved Lubrication c) Comparison of COF for fully flooded and Starved Lubrication.

`

For Starved lubrication condition, the fresh 15W40 lubricant showed higher C.O.F. then the SiO$_2$ nanolubricant. At 3.663 m/s sliding speed the average value of C.O.F. in case of fresh 15W40 lubricating oil was observed ≈ 0.0651 which decreased as the nanoparticles were added to the lubricating oil. The minimum C.O.F. was observed in case of 0.6% w/w of SiO$_2$ nanoparticles ≈0.0331. After 0.6% the C.O.F. again increased up to 1% w/w of SiO$_2$ nanoparticles. The maximum value of C.O.F. was observed in case of 0.2% w/w of SiO$_2$ nanoparticles ≈ 0.0663 but the value was less than the fresh 15W40. Similar trends were observed at 5.263, 7.326, 10.471 and 13.605 m/s sliding speed as shown in Figure 4.15.
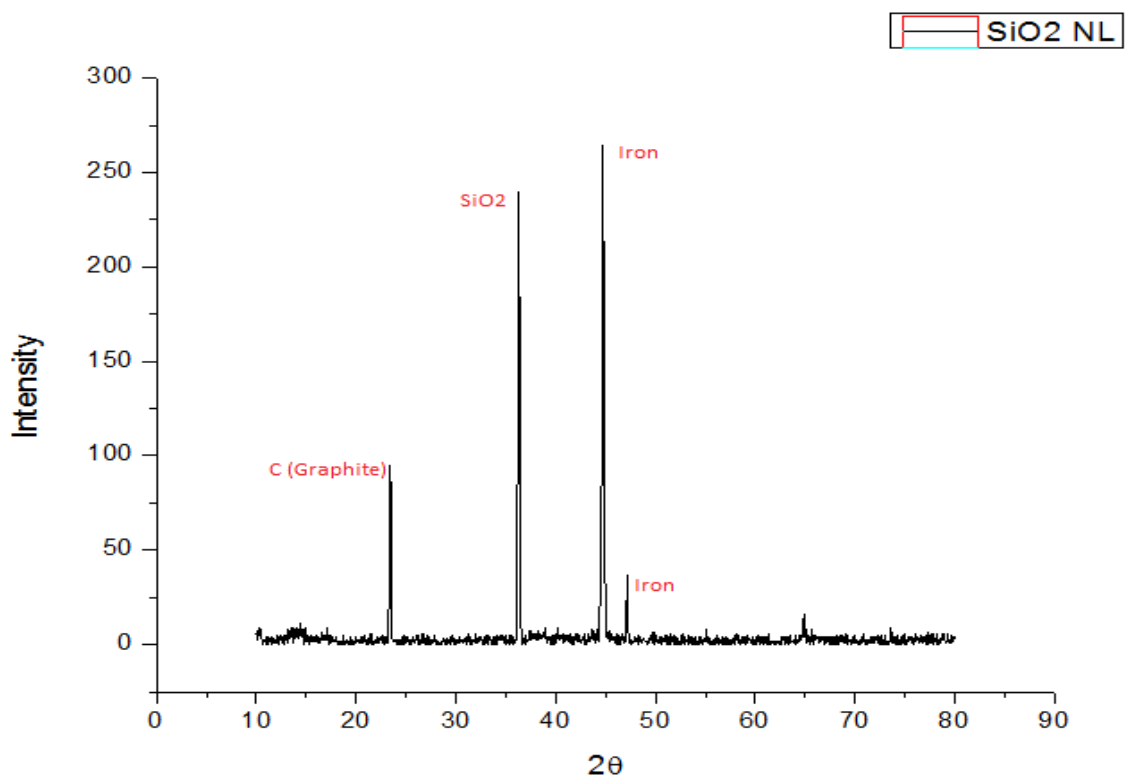
Figure 4.16: XRD analysis of tribopair in presence of SiO2 NL

For both fully flooded and starved lubrication conditions the C.O.F.in case of the nanolubricant was less as compared to fresh 15W40. The 0.6-0.8% w/w of SiO$_2$ nanoparticles blended in fresh 15W40 showed lowest C.O.F. for almost all the sliding speed values. The COF in case of SiO$_2$ nanofluid first decreased but as the concentration was increased further the COF value again increased. The decrement in COF may be due to the coating action of nanoparticles on the surface of tribopair which can be observed by high intensity of nanoparticles in the XRD

`

analysis (Figure 4.16). The COF started increasing after an optimum concentration of nanoparticles in the nanofluid, this may be due the cluster of nanoparticles not allowing the smooth gliding of the tribopair i.e. the increased concentration of nanoparticles acted as obstacle in the gliding of one tribosurface over the other.

4.2.2.2 Effect of SiO₂ nanoparticles on Specific Wear Rate

Figure 4.17 shows the variation of Specific Wear Rate with respect to sliding speed at a constant load of 40 N for the different compositions of nanoparticles in the lubricant starting from 1%, 0.8%, 0.6%, 0.4%, 0.2% and Fresh 15W40 for fully flooded and starved lubrication.

Figure 4.17: Variation of Specific wear rate with sliding speed for various compositions of nanofluid in a) Fully Flooded Lubrication and b) Starved Lubrication.

The specific wear rate for the fully flooded condition has lower values as compared to starved lubrication due to the presence of stable lubricating film between the tribopairs. The value specific wear rate was almost negligible in case of nanolubricant due to the no wearing of the contact surfaces in fully flooded lubrication condition but there was considerable wear in a starved condition still the specific wear rate in case of SiO₂ nanolubricant was very less as compared to fresh 15W40.

4.2.2.3 Thermal Analysis of SiO₂ nanolubricant

The temperature of the tribopair was measured at the start and end of the experiment with the help of a thermal imaging camera. The change in average temperature or temperature rise of the tribopair was calculated and plotted against sliding speed.

Figure 4.18: Temperature Rise with sliding speed a) fully flooded lubrication b) starved lubrication c) Comparison of Temperature Rise for fully flooded and Starved Lubrication.

`

Figure 4.18 shows the temperature rise at various speeds for fully-flooded and starved lubrication condition. The temperature rise of the tribopair was less in case of SiO_2 nanolubricant as compared to the fresh 15W40 lubricating oil. The temperature rise was less for the higher concentrations of the nanoparticles in the lubricant.

The less temperature rise was an indicator of the increased thermal conductivity and specific heat of the lubricant due to the addition of nanoparticles. The theoretical change in thermal conductivity and specific heat was calculated with the help of ESS software as shown in Figure 4.19. The blending of nanoparticles enhanced the thermal conductivity and specific heat of the nanolubricant.
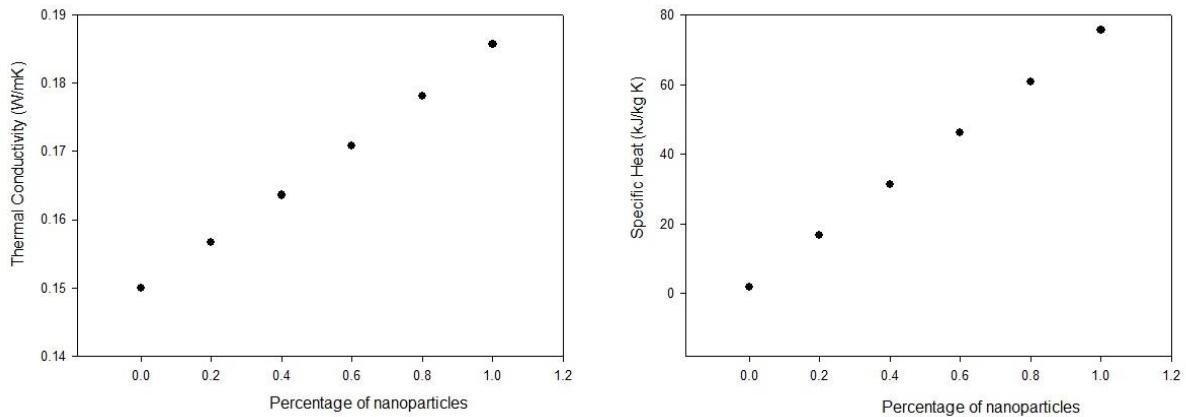
Figure 4.19: Variation in thermal conductivity and specific heat with the percentage of nanoparticles

4.2.3.1 Effect of Cu nanoparticles on C.O.F.

Figure 4.20 shows the variation of C.O.F. with respect to speed at a constant load of 40 N for the different compositions of nanoparticles in the lubricant starting from 1%, 0.8%, 0.6%, 0.4%, 0.2% and Fresh 15W40 for fully flooded and starved lubrication.

For fully flooded lubrication condition the fresh 15W40 lubricant showed higher C.O.F. then the Cu nanolubricant. At 3.663 m/s sliding speed, the average value of C.O.F.in case of fresh 15W40 lubricating oil was observed ≈ 0.0229. There was a slight increment in the C.O.F. was observed in case of 0.2% w/w Cu nanoparticles but with the increase in concentration, the C.O.F. decreased. The C.O.F. in case of Cu nanolubricant at higher speed was very less as compared to fresh 15 W40.
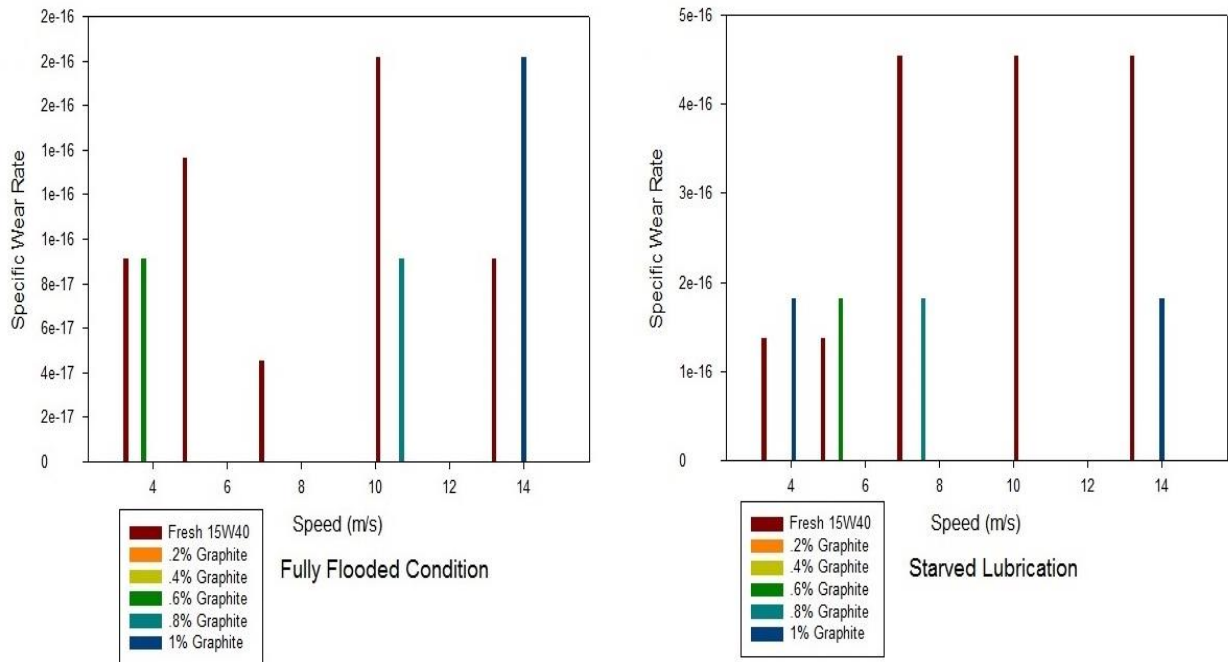
69

`

Figure 4.20: Variation of C.O.F. with sliding speed for various compositions of Nanofluid in a) fully flooded Lubrication and b) Starved Lubrication c) Comparison of COF for fully flooded and Starved Lubrication.

For Starved lubrication condition, the fresh 15W40 lubricant showed higher C.O.F. then the Cu nanolubricant. At 3.663 m/s sliding speed the average value of C.O.F.in case of fresh 15W40 lubricating oil was observed ≈ 0.0651 but in case of 0.4% w/w Cu nanolubricant, it

70

was slightly higher 0.0665. The minimum C.O.F. was observed in case of 0.8% w/w of Cu nanoparticles ≈0.0464. After 0.8% the C.O.F. again increased up to 1% w/w Cu nanoparticles ≈ 0.0546, but the value was less than the fresh 15W40. The C.O.F. in case of nanolubricant was less at sliding speeds of 5.263, 7.326, 10.471 and 13.605 m/s as shown in Figure 4.20.

For both fully flooded and starved lubrication conditions the C.O.F.in case of the nanolubricant was less as compared to fresh 15W40. The 0.6% w/w of Cu nanoparticles blended in fresh 15W40 showed lowest C.O.F. for almost all the sliding speed values. Figure 4.21 shows the presence of Cu nanoparticles on the surface of tribopair when investigated by XRD. These nanoparticles might be responsible for mending effect of the surface of the specimen.
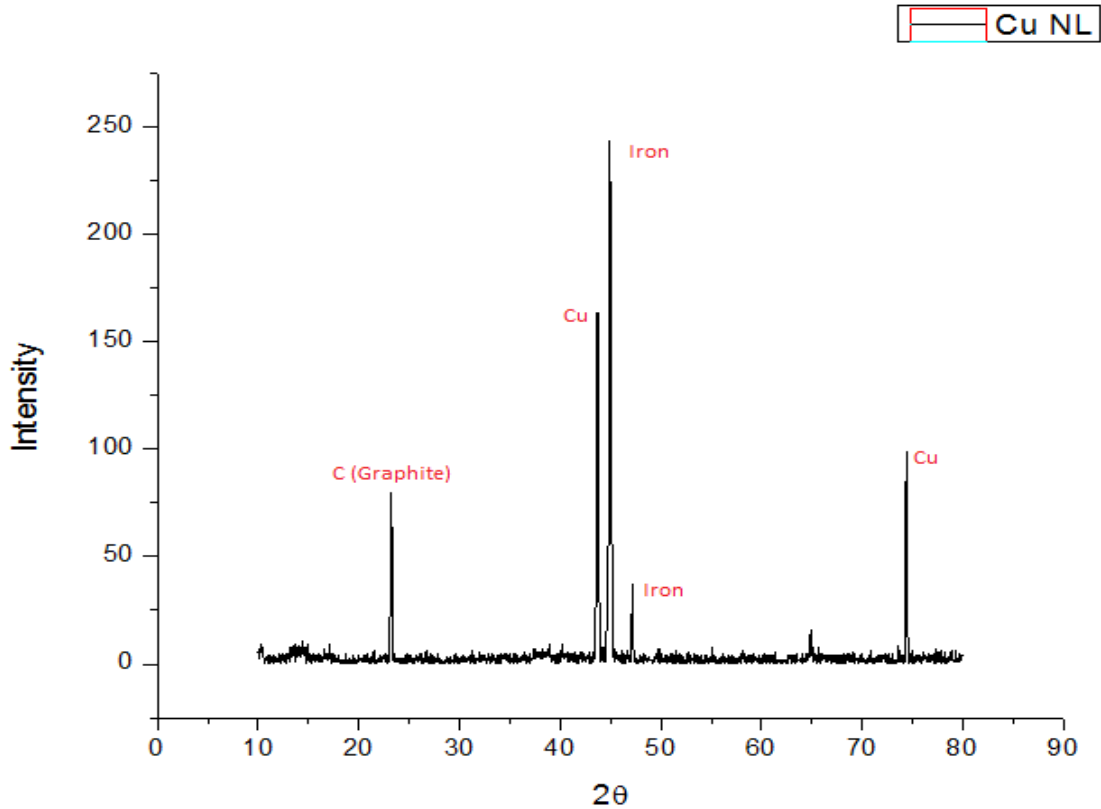
Figure 4.21: XRD analysis of tribopair in presence of Cu NL

4.2.3.2 Effect of Cu nanoparticles on Specific Wear Rate

Figure 4.22 shows the variation of Specific Wear Rate with respect to sliding speed at a constant load of 40 N for the different compositions of nanoparticles in the lubricant starting from 1%, 0.8%, 0.6%, 0.4%, 0.2% and Fresh 15W40 for fully flooded and starved lubrication.

`

The specific wear rate for the fully flooded condition has lower values as compared to starved lubrication due to the presence of a stable lubricating film between the tribopairs. The value specific wear rate increased with the increase in the concentration of the Cu nanoparticles in the lubricant in both fully flooded and starved condition.
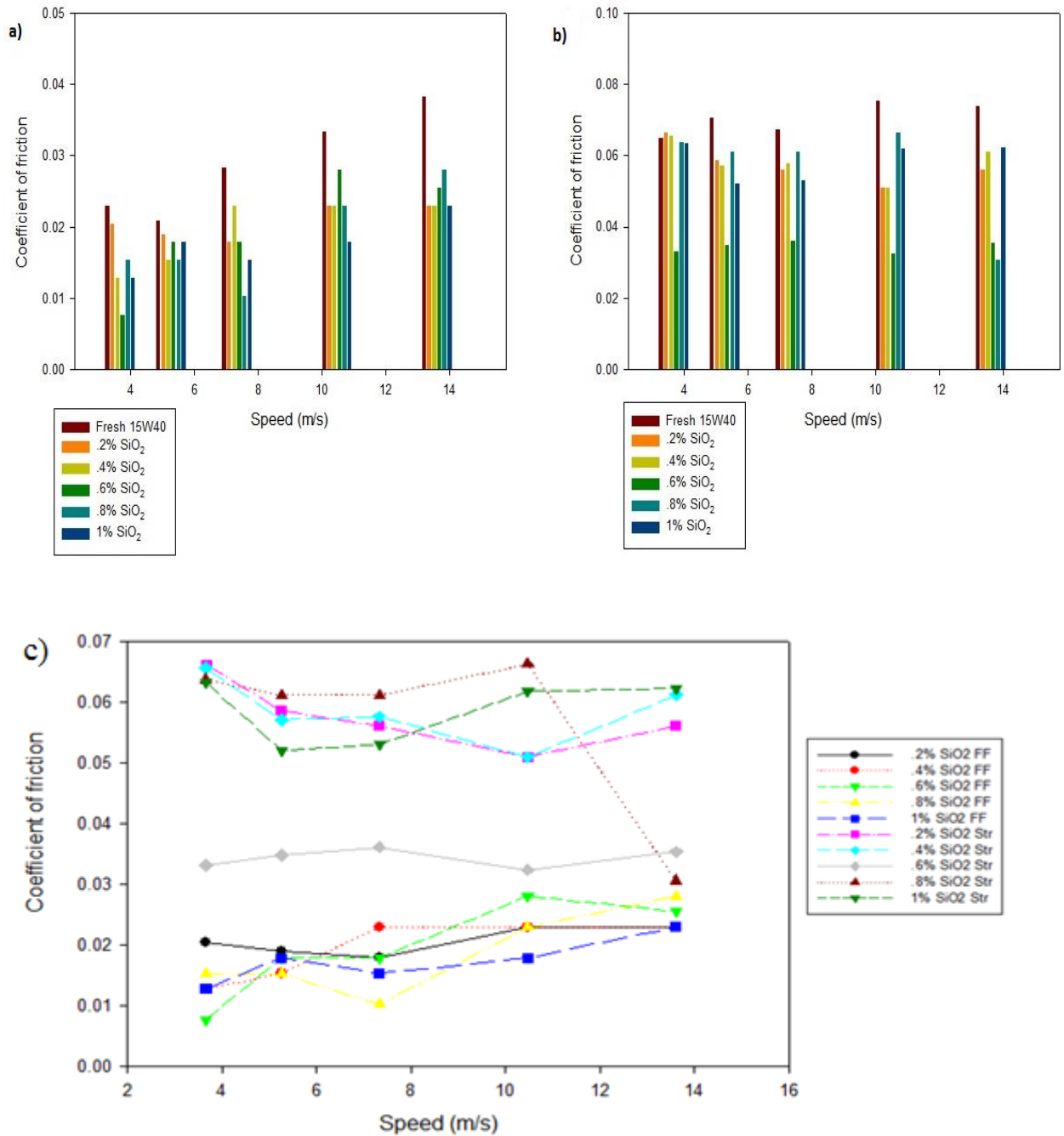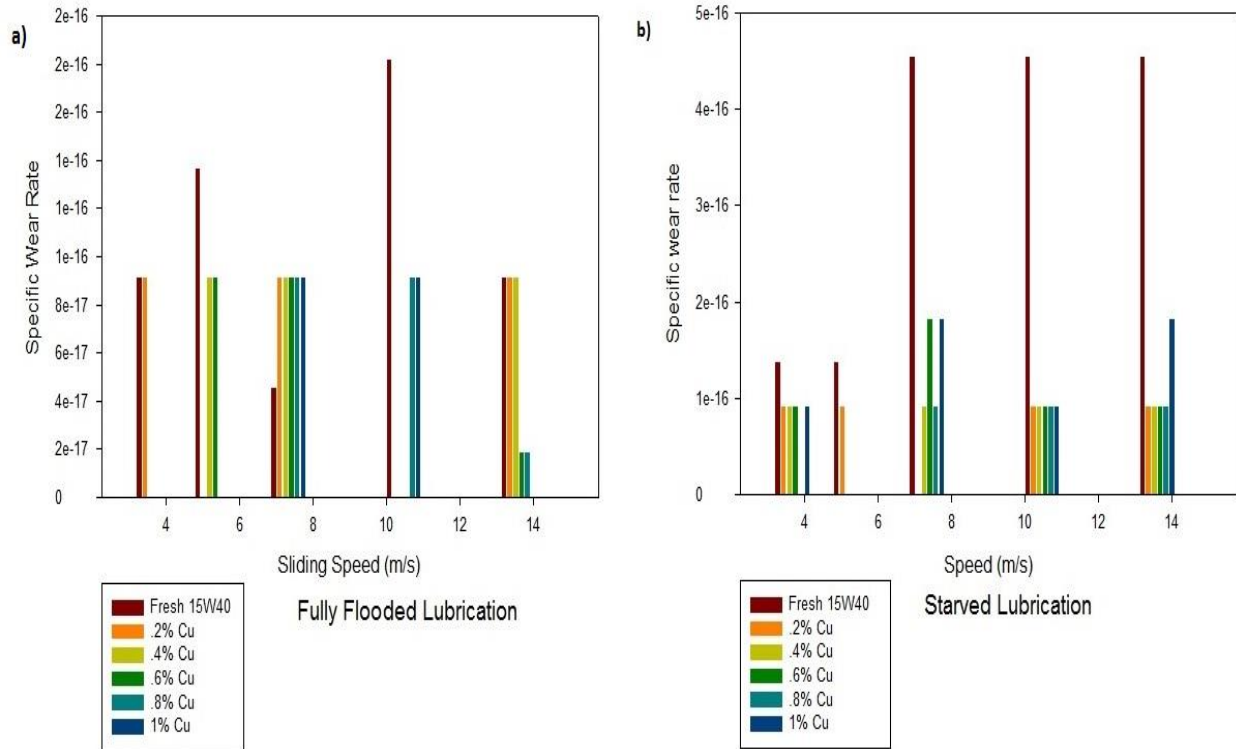

Figure 4.22: Variation of Specific wear rate with sliding speed for various compositions of nanofluid in a) Fully Flooded Lubrication and b) Starved Lubrication.

4.2.3.3 Thermal Analysis of Cu nanolubricant

The temperature of the tribopair was measured at the start and end of the experiment with the help of a thermal imaging camera. The change in average temperature or temperature rise of the tribopair was calculated and plotted against sliding speed.
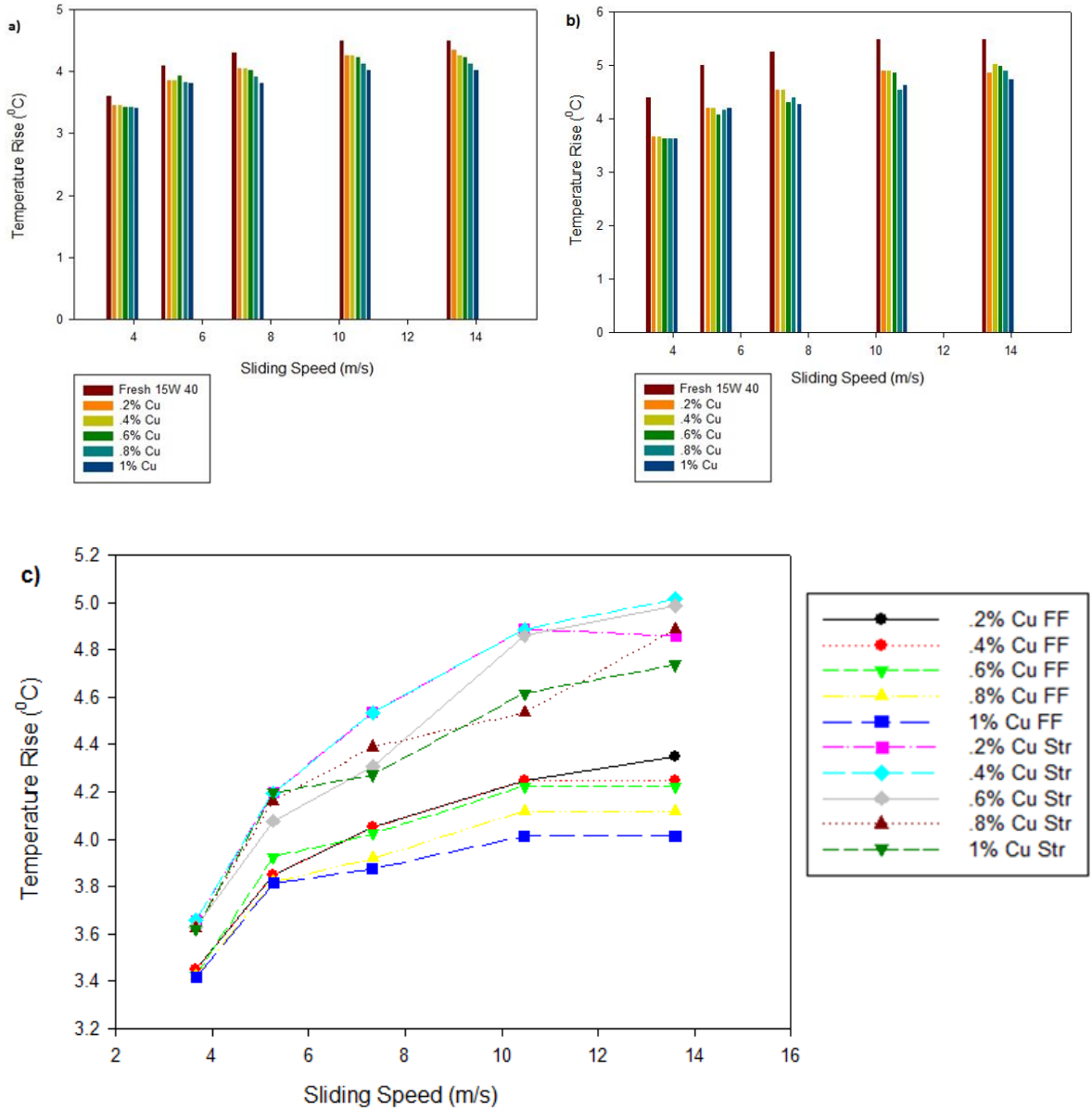
Figure 4.23: Temperature Rise with sliding speed a) fully flooded lubrication b) starved lubrication c) Comparison of Temperature Rise for fully flooded and Starved Lubrication.

Figure 4.23 shows the temperature rise at various speeds for fully-flooded and starved lubrication condition. The temperature rise of the tribopair was less in case of Cu nanolubricant as compared to the fresh 15W40 lubricating oil. The temperature rise was less for the higher concentrations of the nanoparticles in the lubricant.

`

Figure 4.24: Variation in thermal conductivity and specific heat with the percentage of nanoparticles

The less temperature rise was an indicator of the increased thermal conductivity and specific heat of the lubricant due to the addition of nanoparticles. The theoretical change in thermal conductivity and specific heat was calculated with the help of ESS software as shown in Figure 4.24. The blending of nanoparticles enhanced the thermal conductivity and specific heat of the nanolubricant.

4.2.4.1 Effect of CuO nanoparticles on C.O.F.

Figure 4.25 shows the variation of C.O.F. with respect to speed at a constant load of 40 N for the different compositions of nanoparticles in the lubricant starting from 1%, 0.8%, 0.6%, 0.4%, 0.2% and Fresh 15W40 for fully flooded and starved lubrication.
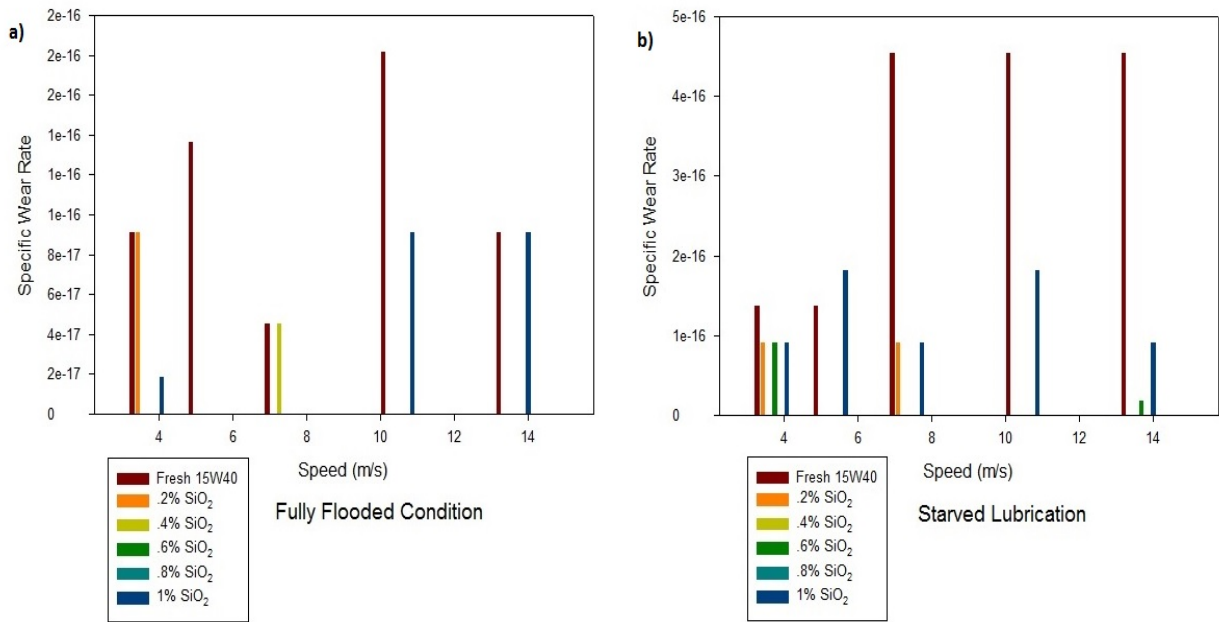
For fully flooded lubrication condition the fresh 15W40 lubricant showed higher C.O.F. then the CuO nanolubricant. At 3.663 m/s sliding speed, the average value of C.O.F.in case of fresh 15W40 lubricating oil was observed $\approx$ 0.0229. The C.O.F. in case of CuO nanofluid was observed higher than the C.O.F. in case of fresh 15W40 lower sliding speed. As the sliding speed increased the C.O.F. in case of nanolubricant was less than the fresh lubricant.

For Starved lubrication condition, the fresh 15W40 lubricant showed lower C.O.F. then the CuO nanolubricant at lower sliding speed. As the sliding speed increased the C.O.F. in case of nanolubricant was higher than the fresh lubricant.

For both fully flooded and starved lubrication conditions the C.O.F.in case of the nanolubricant was less as compared to fresh 15W40. The 0.2-0.4% w/w of CuO nanoparticles blended in fresh 15W40 showed lowest C.O.F. for almost all the sliding speed values.
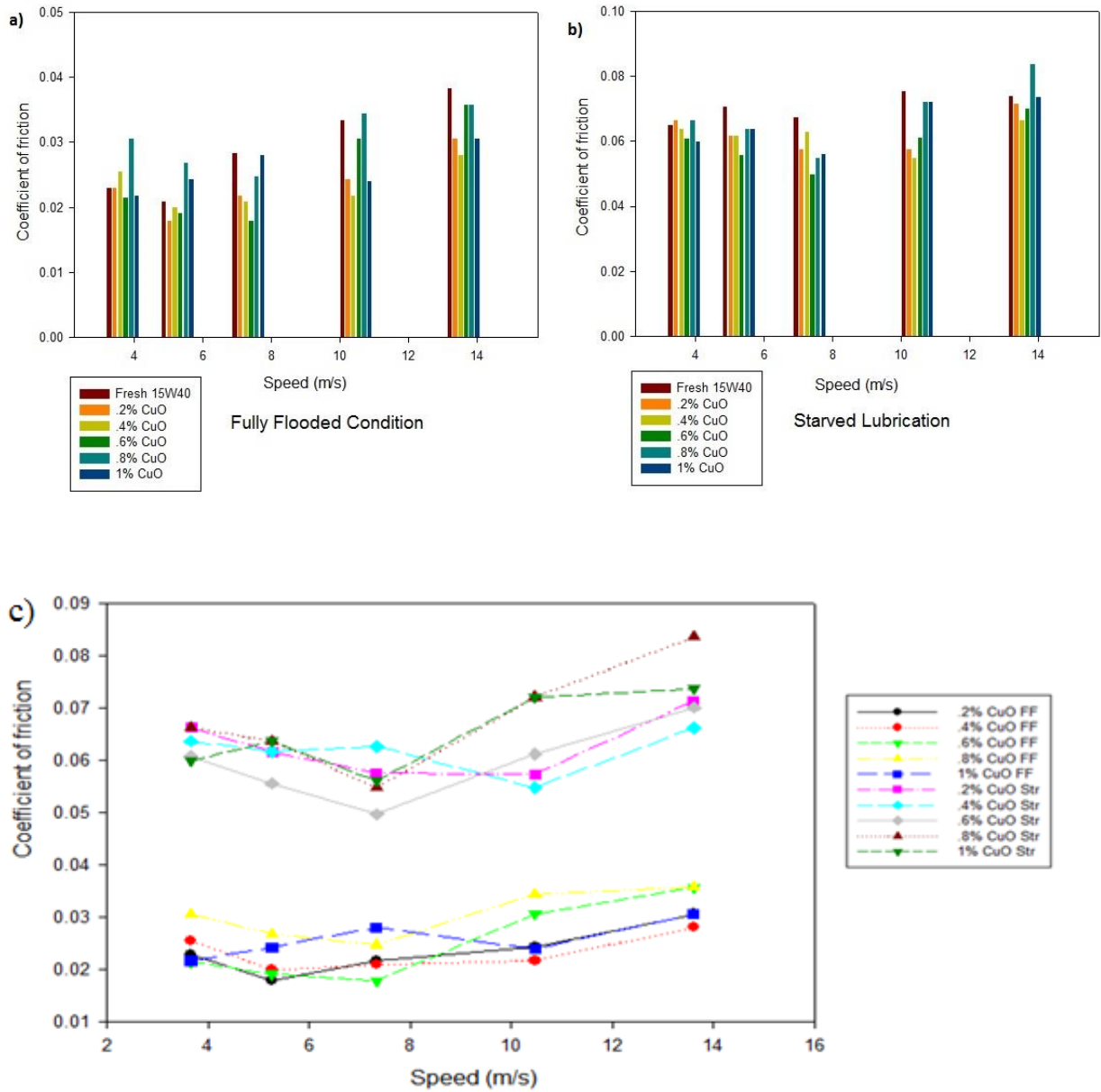
Figure 4.25: Variation of C.O.F. with sliding speed for various compositions of Nanofluid in a) fully flooded Lubrication and b) Starved Lubrication c) Comparison of COF for fully flooded and Starved Lubrication.
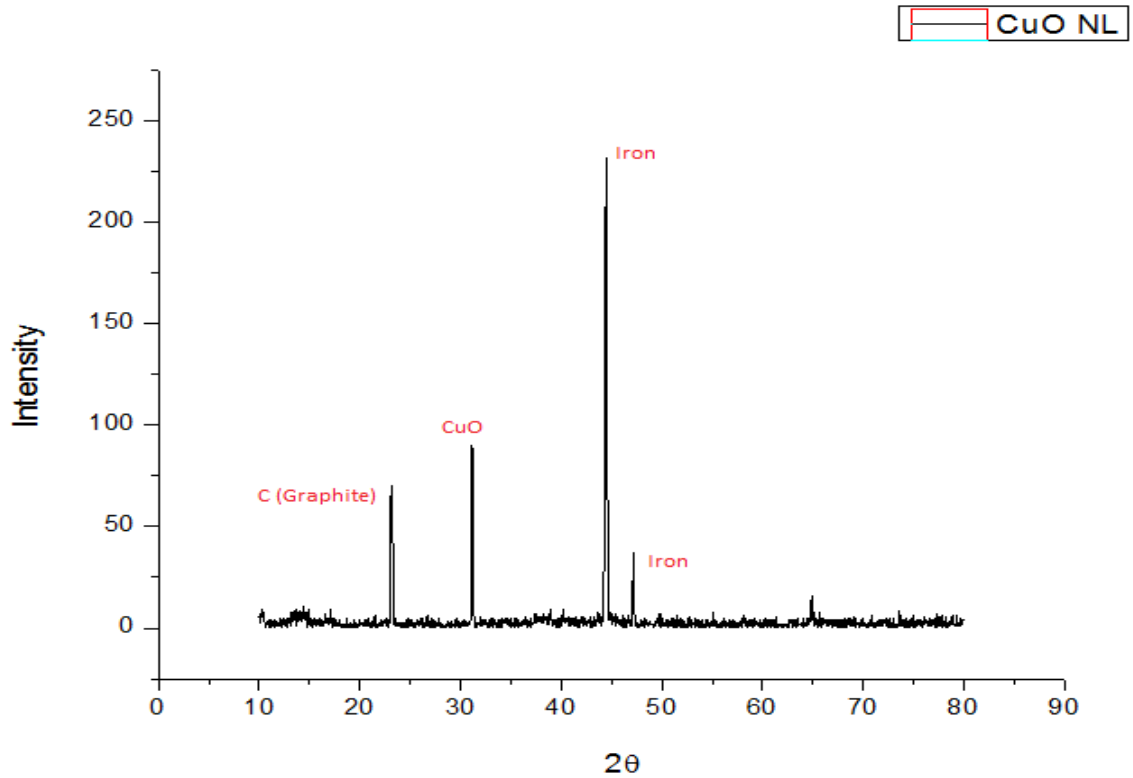
Figure 4.26: XRD analysis of tribopair in presence of CuO NL

Figure 4.26 shows the presence of CuO nanoparticles on the surface of tribopair when investigated by XRD. These nanoparticles might be responsible for mending effect of the surface of the specimen.

4.2.4.2 Effect of CuO nanoparticles on Study of Specific Wear Rate

Figure 4.27 shows the variation of Specific Wear Rate with respect to sliding speed at a constant load of 40 N for the different compositions of nanoparticles in the lubricant starting from 1%, 0.8%, 0.6%, 0.4%, 0.2% and Fresh 15W40 for fully flooded and starved lubrication.

The specific wear rate for the fully flooded condition has lower values as compared to starved lubrication due to the presence of a stable lubricating film between the tribopairs. The value specific wear rate increased with the increase in sliding speed in a fully flooded condition whereas in starved condition specific wear rate first increased than decreased. As the concentration of nanoparticles in the lubricant increased from 0.2% w/w to 1.0% w/w the specific wear rate also increased.
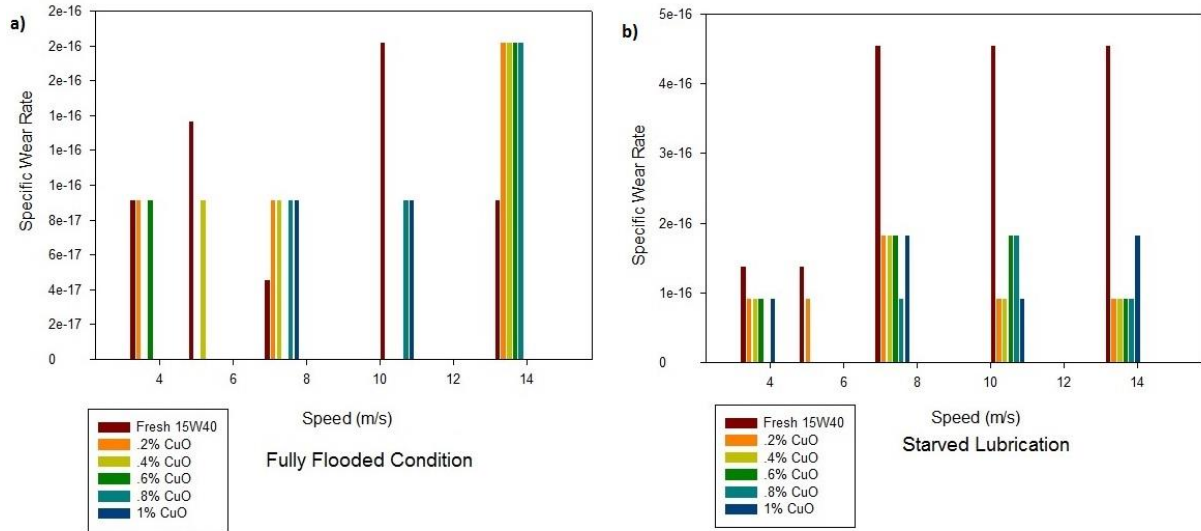
Figure 4.27: Variation of Specific wear rate with sliding speed for various compositions of nanofluid in a) Fully Flooded Lubrication and b) Starved Lubrication.

4.2.4.3 Thermal Analysis of CuO nanolubricant

The temperature of the tribopair was measured at the start and end of the experiment with the help of a thermal imaging camera. The change in average temperature or temperature rise of the tribopair was calculated and plotted against sliding speed.
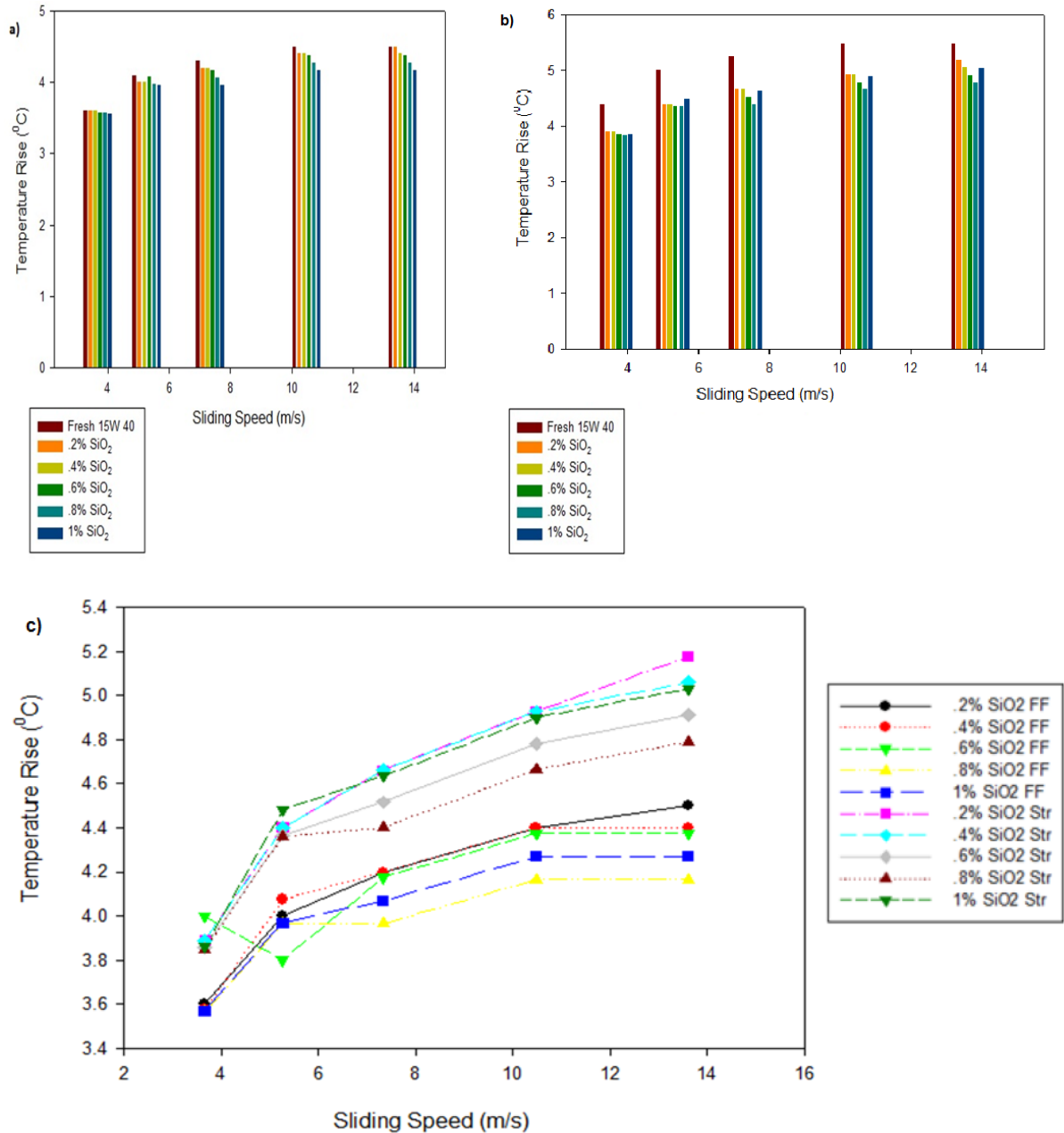
Figure 4.28 shows the temperature rise at various speeds for fully-flooded and starved lubrication condition. The temperature rise of the tribopair was less in case of CuO nanolubricant as compared to the fresh 15W40 lubricating oil. The temperature rise was less for the higher concentrations of the nanoparticles in the lubricant.

The less temperature rise was an indicator of the increased thermal conductivity and specific heat of the lubricant due to the addition of nanoparticles. The theoretical change in thermal conductivity and specific heat was calculated with the help of ESS software as shown in Figure 4.29. The blending of nanoparticles enhanced the thermal conductivity and specific heat of the nanolubricant.
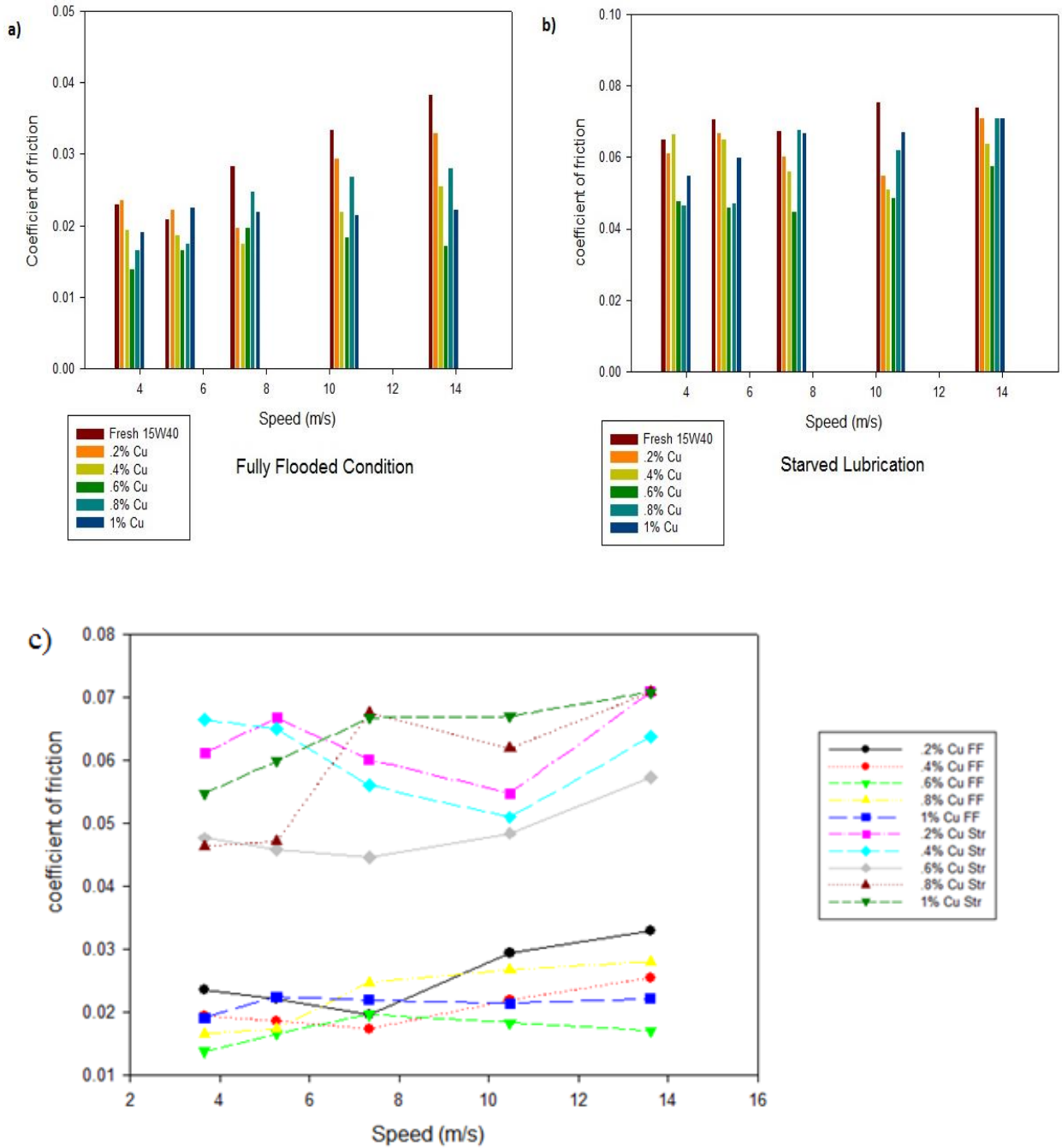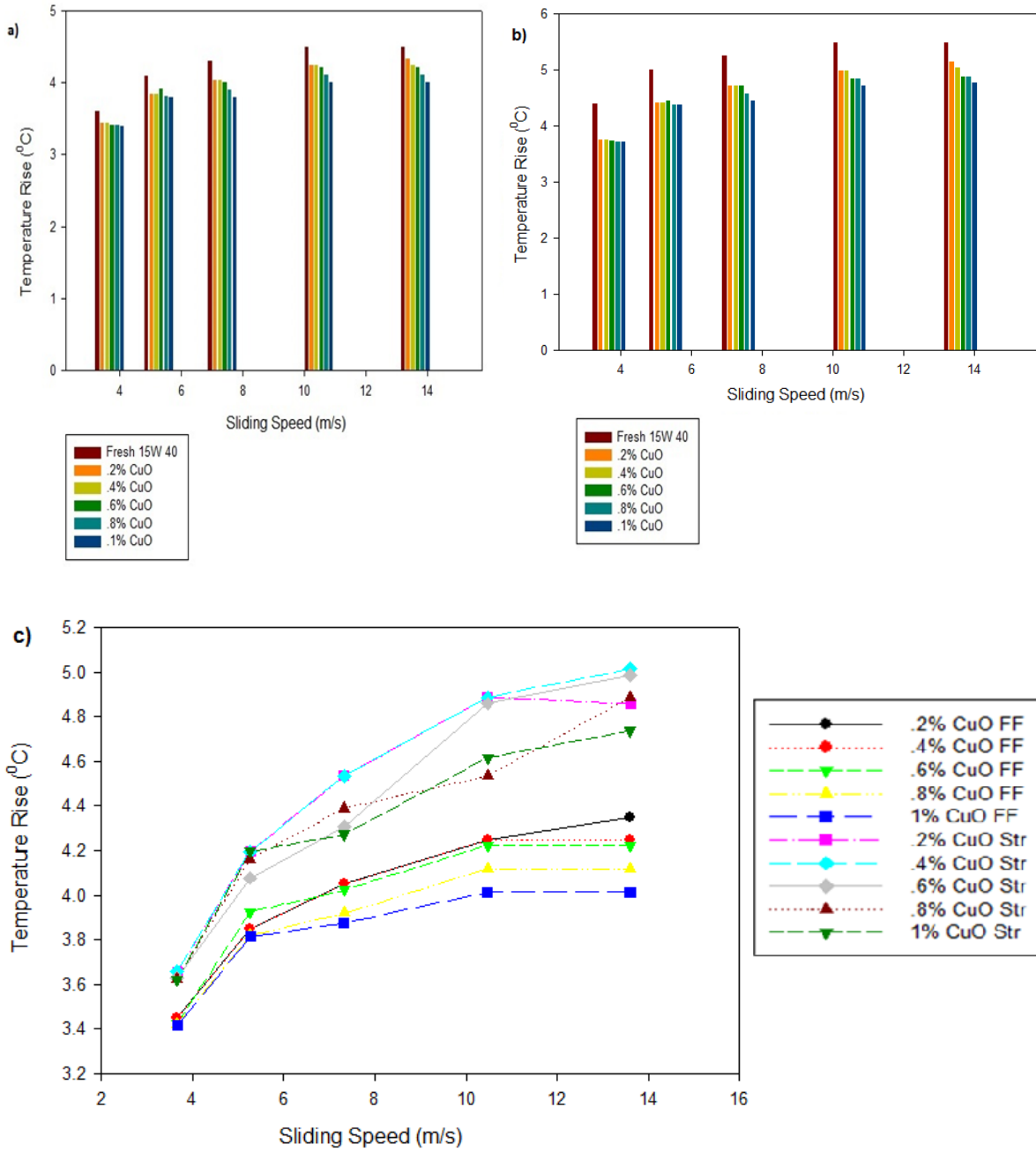
Figure 4.28: Temperature Rise with sliding speed a) fully flooded lubrication b) starved lubrication c) Comparison of Temperature Rise for fully flooded and Starved Lubrication.
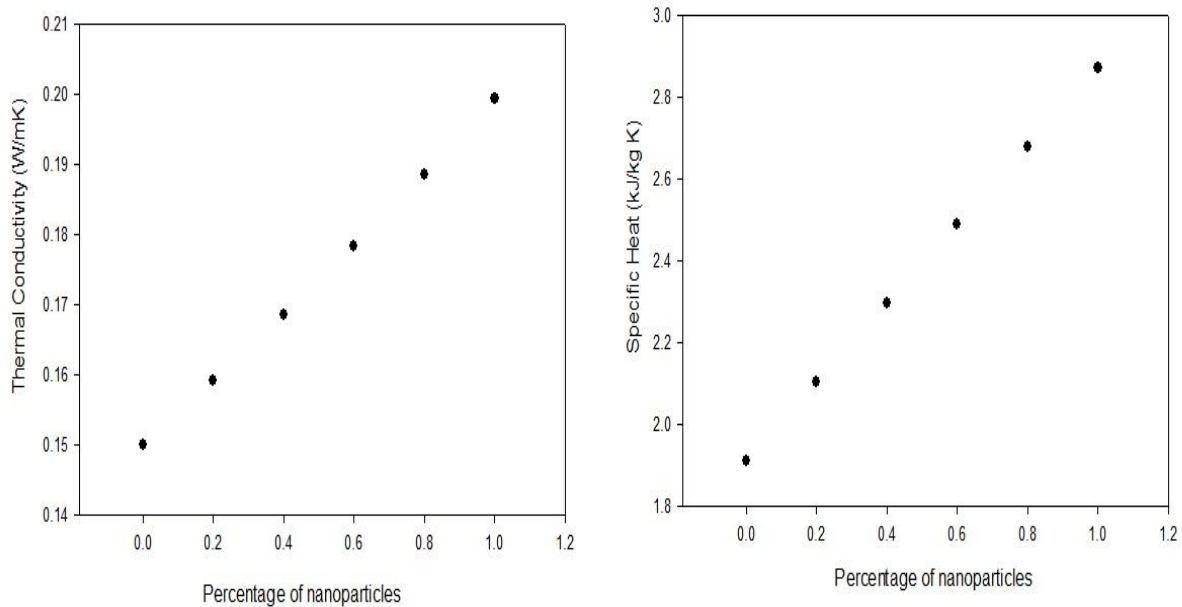
Figure 4.29: Variation in thermal conductivity and specific heat with the percentage of nanoparticles

4.2.5.1 Effect of WS₂ nanoparticles on C.O.F.

Figure 4.30 shows the variation of C.O.F. with respect to speed at a constant load of 40 N for the different compositions of nanoparticles in the lubricant starting from 1%, 0.8%, 0.6%, 0.4%, 0.2% and Fresh 15W40 for fully flooded and starved lubrication.

For fully flooded lubrication condition the fresh 15W40 lubricant showed higher C.O.F. then the WS$_2$ nanolubricant. At 3.663 m/s sliding speed the average value of C.O.F.in case of fresh 15W40 lubricating oil was observed ≈ 0.0229 which decreased as the nanoparticles were added to the lubricating oil. The minimum C.O.F. was observed in case of 0.4% w/w of WS$_2$ nanoparticles ≈ 0.0122. After 0.4% the C.O.F. again increased up to 1% w/w WS$_2$ nanoparticles ≈ 0.0189, but the value was less than the fresh 15W40. Similar trends were observed at 5.263, 7.326, 10.471 and 13.605 m/s sliding speed as shown in Figure 4.30.

79
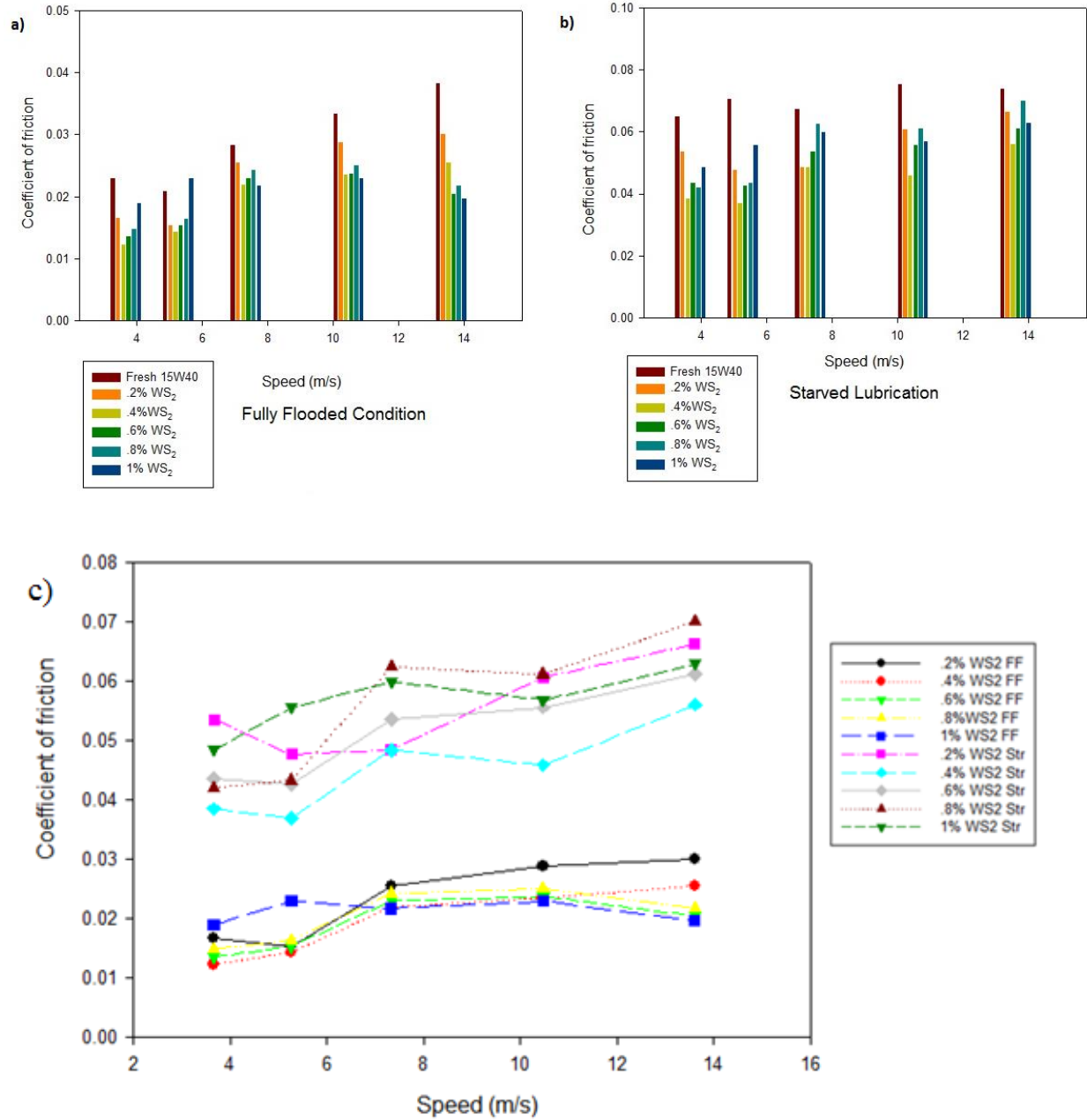
Figure 4.30: Variation of C.O.F. with sliding speed for various compositions of Nanofluid in a) fully flooded Lubrication and b) Starved Lubrication c) Comparison of COF for fully flooded and Starved Lubrication.

For Starved lubrication condition, the fresh 15W40 lubricant showed higher C.O.F. then the WS$_2$ nanolubricant. At 3.663 m/s sliding speed the average value of C.O.F.in case of fresh 15W40 lubricating oil was observed ≈ 0.0651 which decreased as the nanoparticles were added to the lubricating oil. The minimum C.O.F. was observed in case of 0.4% w/w of WS$_2$

`

nanoparticles ≈ 0.0385. After 0.4% the C.O.F. again increased up to 1% w/w WS$_2$ nanoparticles ≈ 0.0535, but the value was less than the fresh 15W40. Similar trends were observed at 5.263, 7.326, 10.471 and 13.605 m/s sliding speed as shown in Figure 4.30.

For both fully flooded and starved lubrication conditions the C.O.F.in case of the nanolubricant was less as compared to fresh 15W40. The 0.4% w/w of WS$_2$ nanoparticles blended in fresh 15W40 showed lowest C.O.F. for almost all the sliding speed values. The COF in case of WS$_2$ nanofluid first decreased but as the concentration was increased further the COF value again increased. The decrement in COF may be due to the coating action of nanoparticles on the surface of tribopair which can be observed by high intensity of nanoparticles in the XRD analysis (Figure 4.31). The COF started increasing after an optimum concentration of nanoparticles in the nanofluid, this may be due the cluster of nanoparticles not allowing the smooth gliding of the tribopair i.e. the increased concentration of nanoparticles acted as obstacle in the gliding of one tribosurface over the other.
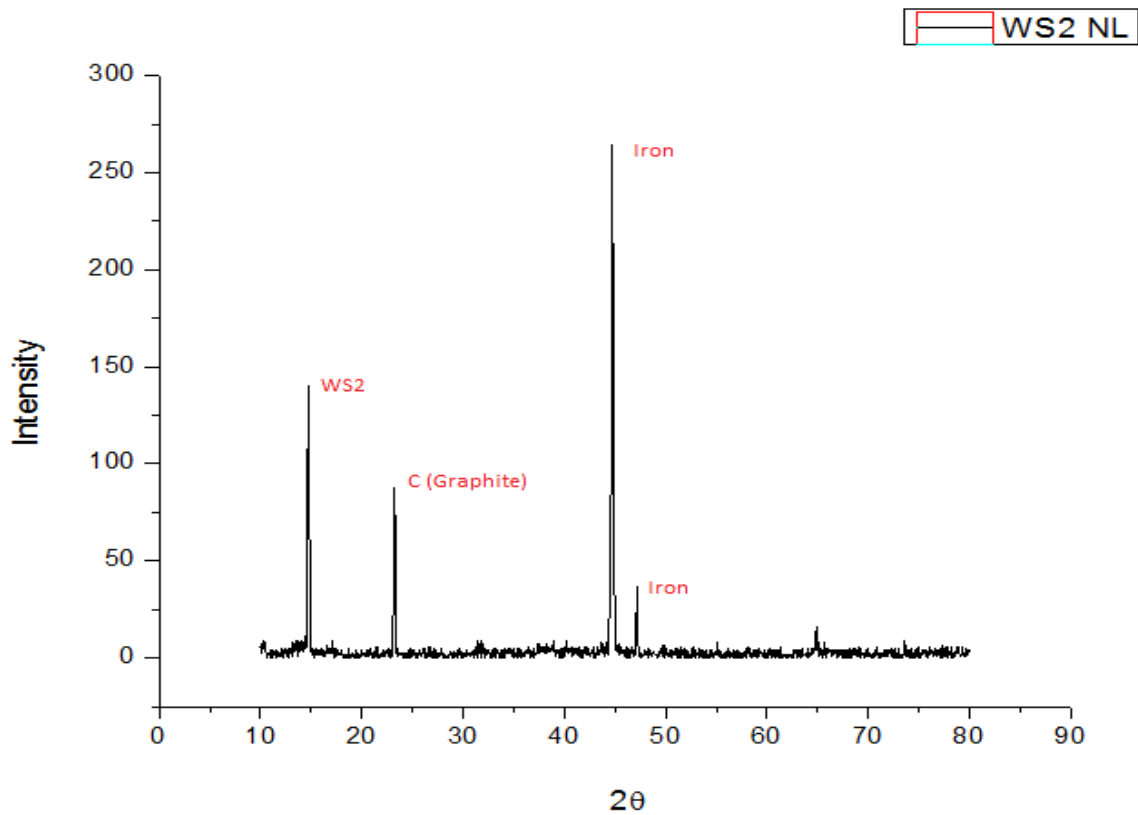
Figure 4.31: XRD analysis of tribopair in presence of WS2 NL

4.2.5.2 Effect of WS$_2$ nanoparticles on Specific Wear Rate

Figure 4.32 shows the variation of Specific Wear Rate with respect to sliding speed at a constant load of 40 N for the different compositions of nanoparticles in the lubricant starting from 1%, 0.8%, 0.6%, 0.4%, 0.2% and Fresh 15W40 for fully flooded and starved lubrication.

The specific wear rate for the fully flooded condition has lower values as compared to starved lubrication due to the presence of stable lubricating film between the tribopairs. The value specific wear rate was almost negligible in case of nanolubricant due to the no wearing of the contact surfaces.
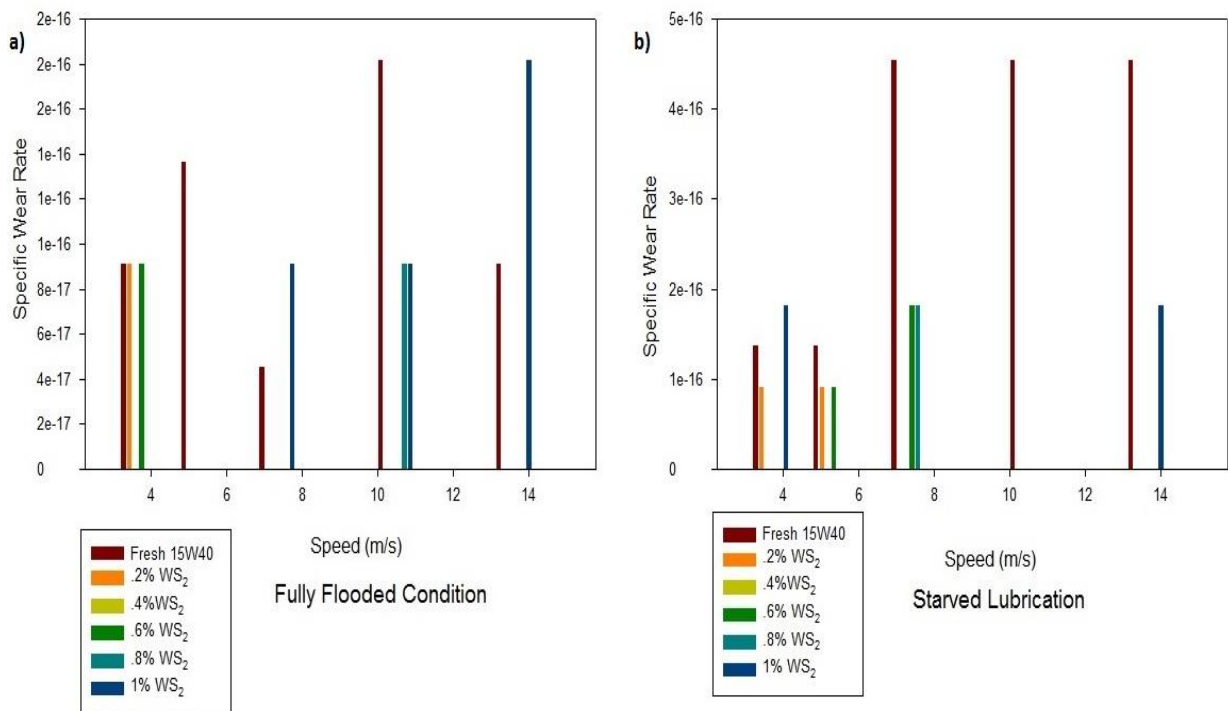
Figure 4.32: Variation of Specific wear rate with sliding speed for various compositions of nanofluid in a) Fully Flooded Lubrication and b) Starved Lubrication.

4.2.5.3 Thermal Analysis of WS$_2$ nanolubricant

The temperature of the tribopair was measured at the start and end of the experiment with the help of a thermal imaging camera. The change in average temperature or temperature rise of the tribopair was calculated and plotted against sliding speed.
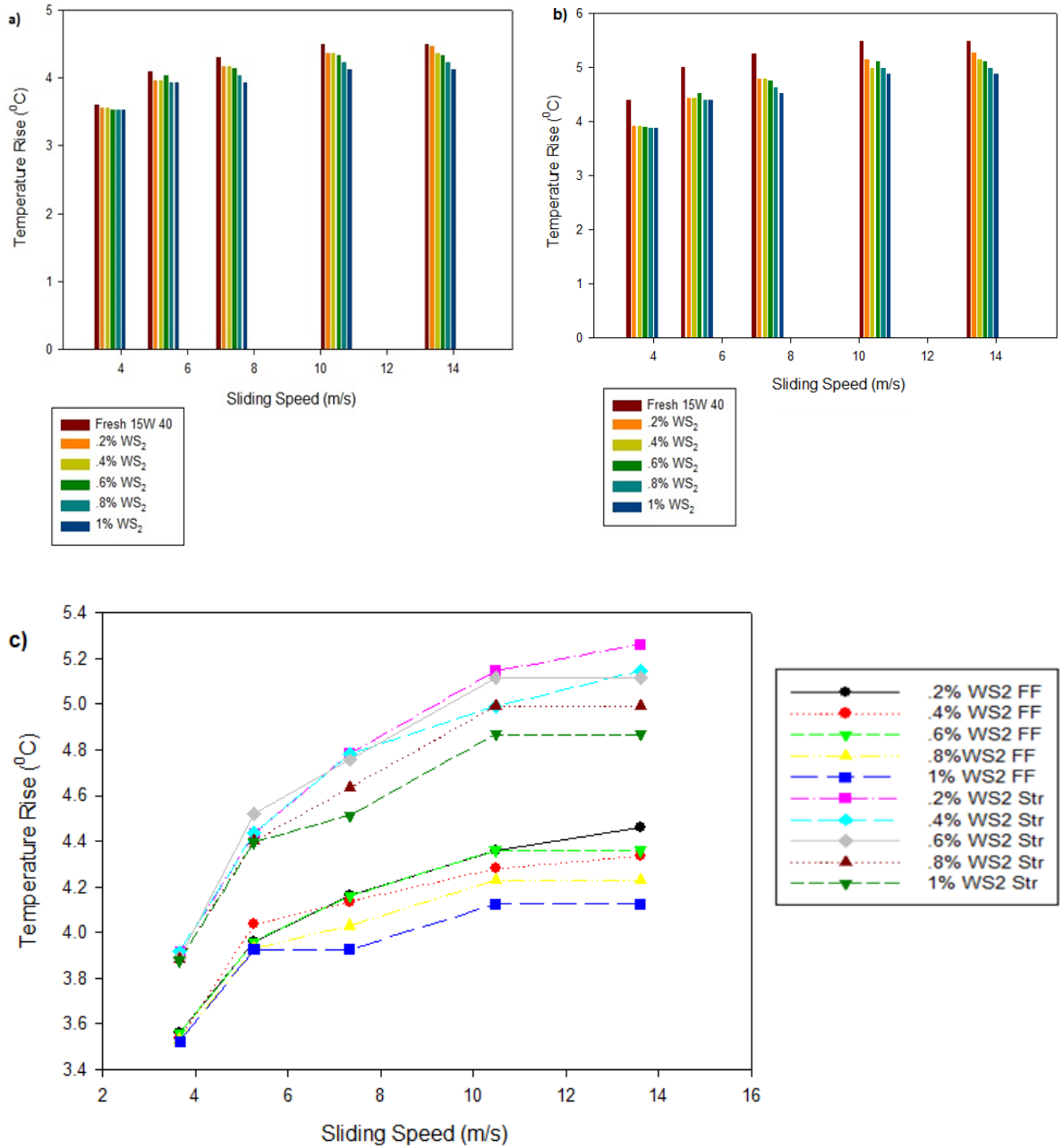
Figure 4.33: Temperature Rise with sliding speed a) fully flooded lubrication b) starved lubrication c) Comparison of Temperature Rise for fully flooded and Starved Lubrication.
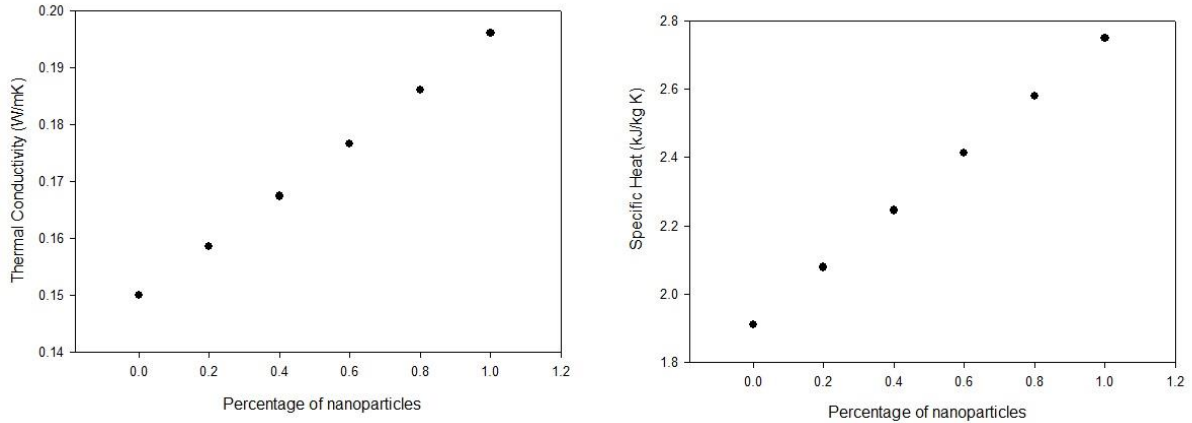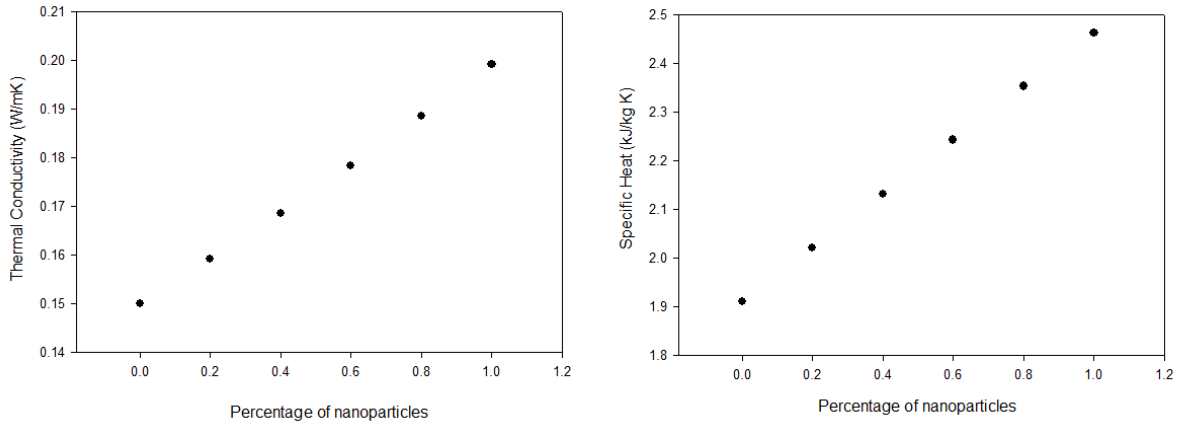
Figure 4.34: Variation in thermal conductivity and specific heat with the percentage of nanoparticles

Figure 4.33 shows the temperature rise at various speeds for fully-flooded and starved lubrication condition. The temperature rise of the tribopair was less in case of WS_2 nanolubricant as compared to the fresh 15W40 lubricating oil. The temperature rise was less for the higher concentrations of the nanoparticles in the lubricant.

The less temperature rise was an indicator of the increased thermal conductivity and specific heat of the lubricant due to the addition of nanoparticles. The theoretical change in thermal conductivity and specific heat was calculated with the help of ESS software as shown in Figure 4.34. The blending of nanoparticles enhanced the thermal conductivity and specific heat of the nanolubricant.

`

4.3 Tribological and Extreme Pressure analysis with Four Ball Tester

The tribological testing for the prepared nanolubricant had been carried out on four ball tester according to ASTM- DIN 51350 for extreme pressure and ASTM- D4172 for friction and wear characteristics of the lubricating oil.

In the four ball tester, the load is applied from vertically downwards direction. The upper ball rotates with constant rpm. The temperature of the assembly is maintained at the desired value by a temperature controlled unit. The frictional torque was measured by load displacement sensor that displays on the online monitor. The nanolubricants were tested on Four Ball Tester for their performance analysis by measuring C.O.F. and wear scar diameter and stability was analyzed by means of weld load measurement.

4.3.1 Study of Coefficient of friction

The experiment was performed on three loads 196 N, 392 N and 588 N. The C.O.F.(C.O.F.) increased with the increase of normal load. The lubricant blended with nanoparticles had lower values of C.O.F.as compared to the fresh lubricant shown in Figure 4.35. Table 4.4 and Figure 4.36 shows the percent decrease in the value of C.O.F.as compared to the fresh 15W40 lubricating oil. The nanoparticles of SiO_2 blended with 15W40 lubricating oil showed ~ 15% to 25% decrease in C.O.F. The nanoparticles of graphite showed ~ 15% - 18% decrement in C.O.F. The nanoparticles of Cu and CuO showed ~ 9% - 20% and ~ 1.5% to 17% reduction in C.O.F. respectively whereas the nanoparticle of WS_2 showed ~ 13% - 21% decrease in C.O.F.

Table 4.4: Percentage decrease in C.O.F. values in the presence of nanoparticles in the lubricant

Nano lubricant	Percent decrease in coefficient of friction		
	Load 196 N	Load 392 N	Load 588 N
SiO_2 Nano lubricant	17.46%	15.44%	25.55%
Graphite Nano lubricant	16.23%	15.4%	17.72%
Cu Nano lubricant	13.65%	9.07%	19.6%
CuO Nano lubricant	2.78%	1.48%	17%
WS_2 Nano lubricant	13.64%	15.12%	21.13%

`

Figure 4.35: Load v/s C.O.F.in presence of various lubricants a) at load 196 N, b) at load 392 N, c) at load 588 N.
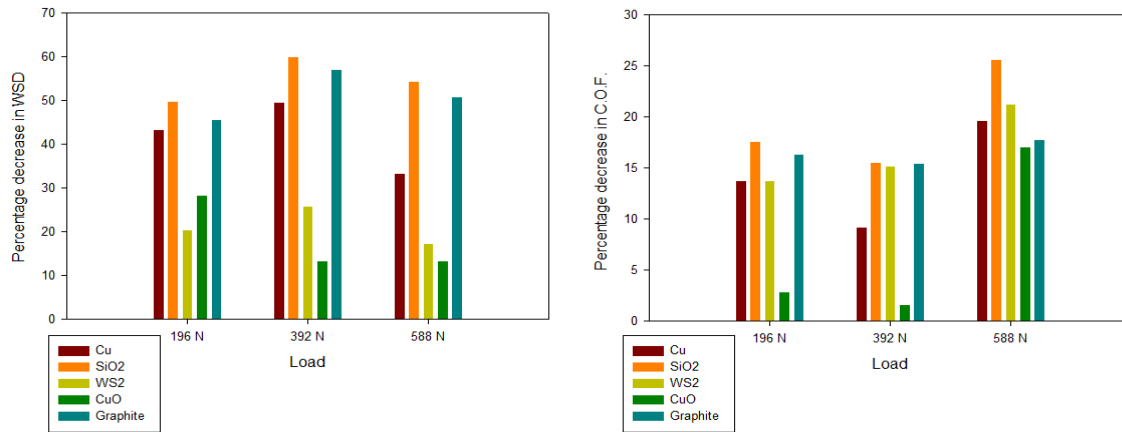
Figure 4.36: Percent decrease in WSD and COF in case of nanolubricants.

4.3.2 Study of Wear Scar Diameter

The wear scar diameter (WSD) was examined for all three loads 196 N, 392 N and 588 N. The Wear scar diameter increased as the load increased. The nanoparticles blended with the lubricant decreased the Wear scar diameter significantly. Table 4.5 and Figure 4.36 shows the percent decrease in the value of Wear scar diameter as compared to the fresh 15W40 lubricating oil. The nanoparticles of SiO_2 blended with 15W40 lubricating oil showed ~ 50% to 59% decrease in WSD. The nanoparticles of graphite showed ~ 45% - 57% decrement in WSD. The nanoparticles of Cu and CuO showed ~ 33% - 49% and ~ 13% to 28% reduction in WSD respectively whereas the nanoparticle of WS_2 showed ~ 17% - 26% decrease in WSD.

Table 4.5: Percentage decrease in WSD values in the presence of nanoparticles in the lubricant

Nano lubricant	Percent decrease in Wear Scare Diameter		
	Load 196 N	Load 392 N	Load 588 N
SiO_2 Nano lubricant	49.64%	59.91%	54.15%
Graphite Nano lubricant	45.32%	56.82%	50.73%
Cu Nano lubricant	43.16%	49.40%	33.17%
CuO Nano lubricant	28.06%	13.07%	13.17%
WS_2 Nano lubricant	20.14%	25.57%	17.07%

87
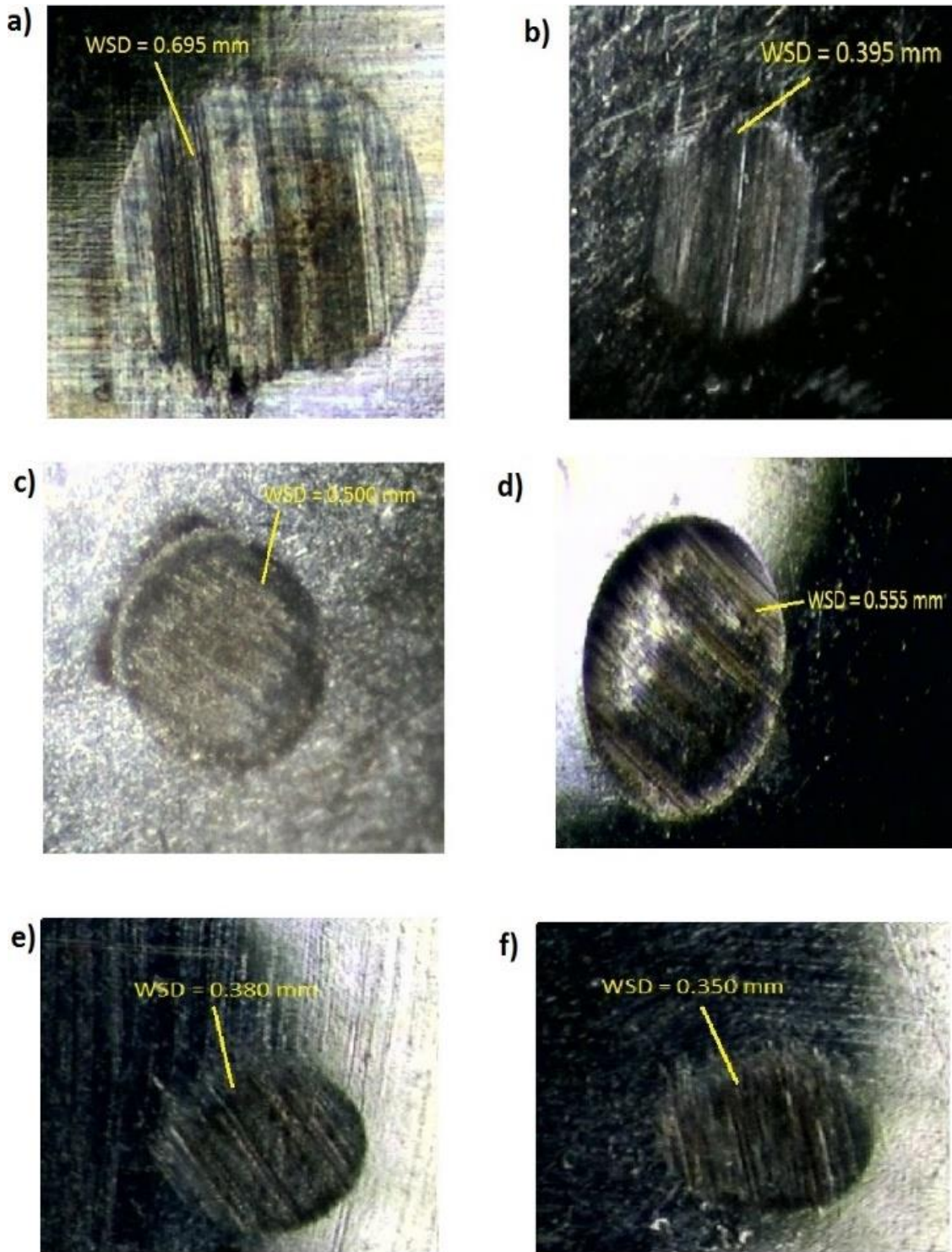
Figure 4.37: Wear Scar Diameter observed by an optical microscope at 196 N. a) 15W40 lubricant, b) Cu nanolubricant, c) CuO nanolubricant, d) WS_2 nanolubricant, e) Graphite nanolubricant, f) SiO_2 nanolubricant
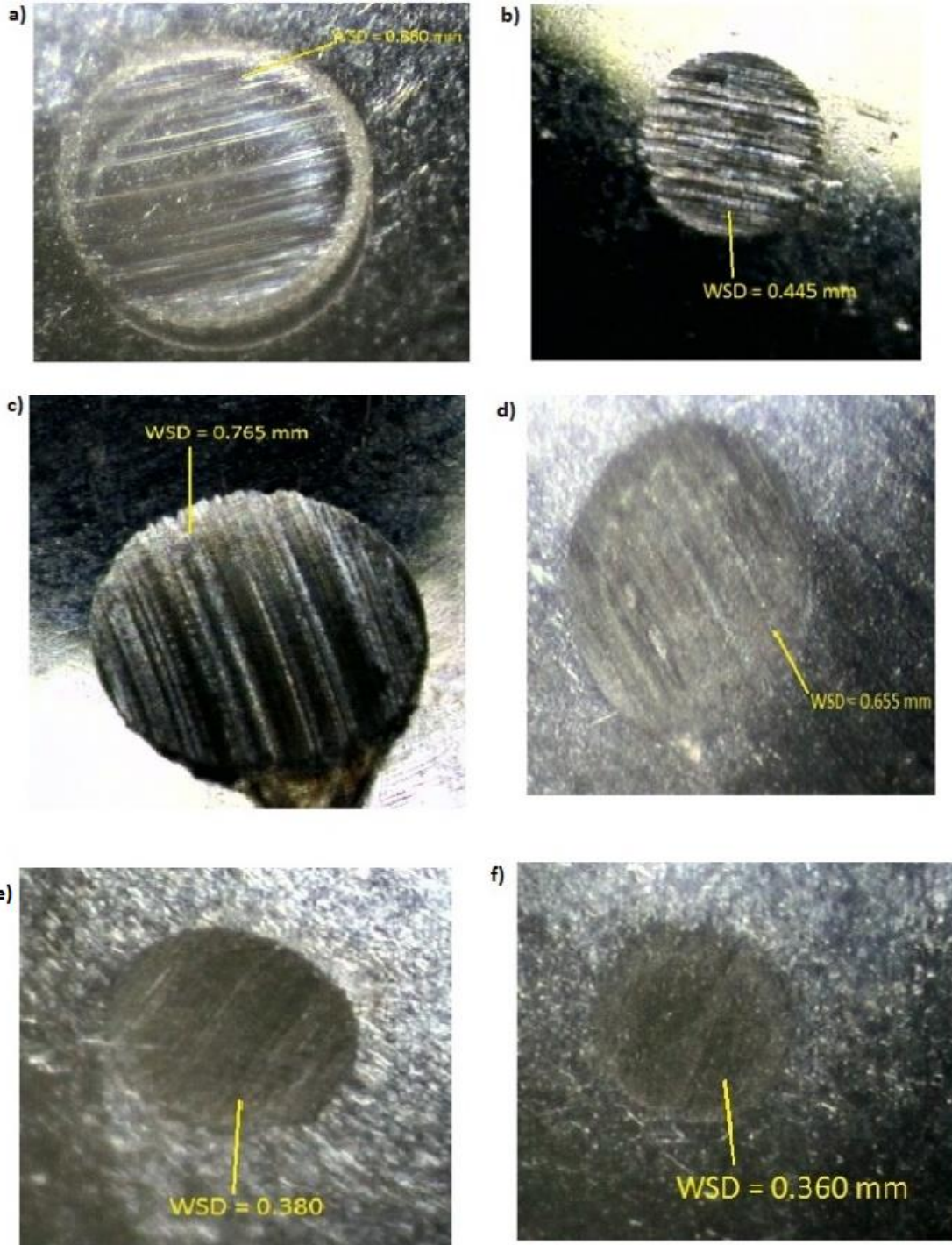
Figure 4.38: Wear Scar Diameter observed by an optical microscope at 392 N. a) 15W40 lubricant, b) Cu nanolubricant, c) CuO nanolubricant, d) WS_2 nanolubricant, e) Graphite nanolubricant, f) SiO_2 nanolubricant.
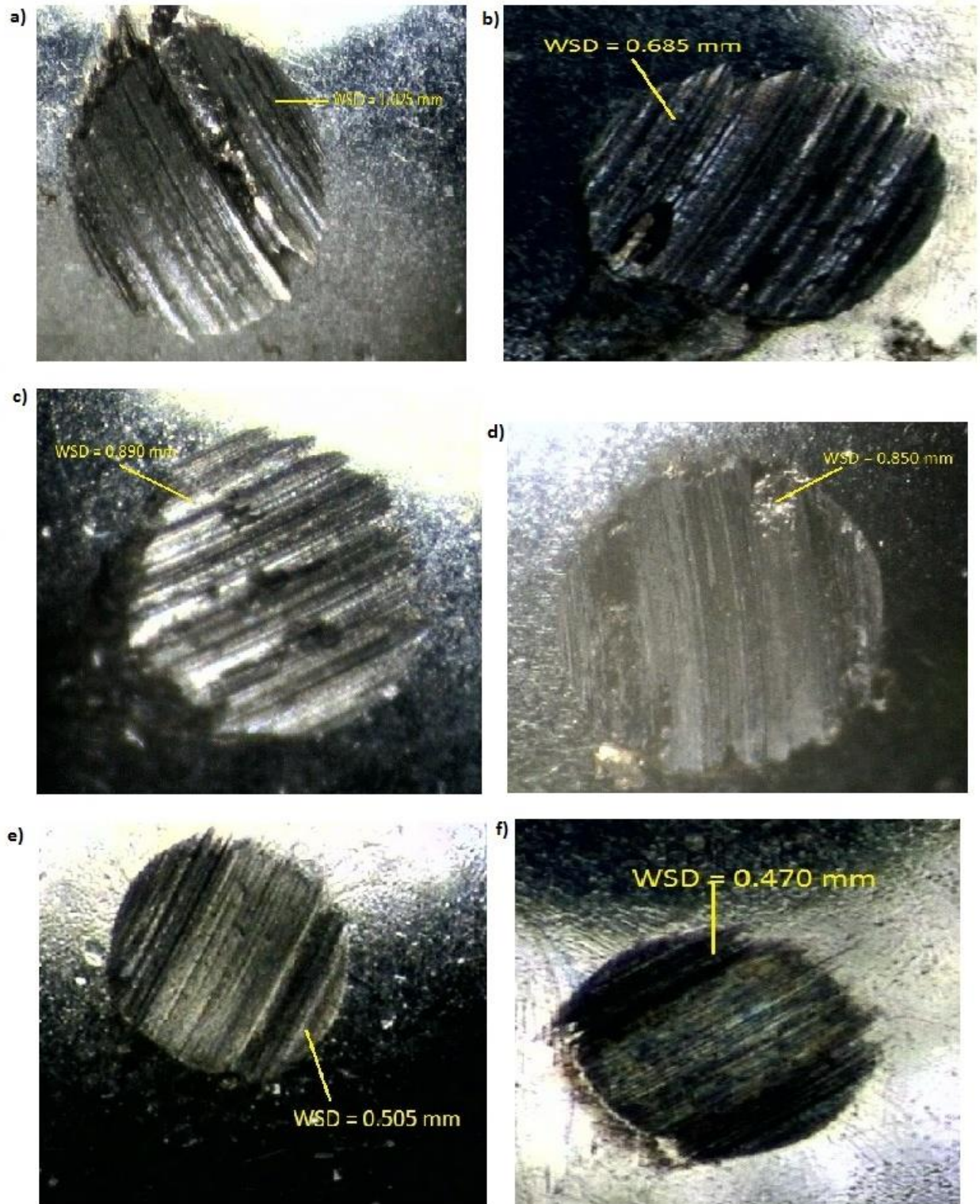
Figure 4.39: Wear Scar Diameter observed by an optical microscope at 588 N. a) 15W40 lubricant, b) Cu nanolubricant, c) CuO nanolubricant, d) WS_2 nanolubricant, e) Graphite nanolubricant, f) SiO_2 nanolubricant.

`

4.3.3 Extreme Pressure Analysis

The extreme pressure performance analysis of the prepared nanolubricant was conducted according to ASTM- DIN 51350. The weld load was calculated for each nanolubricant and compared with Fresh 15W40 lubricating oil Figure 4.40. The extreme pressure performance of the nanolubricant showed better results than the fresh 15W40 Lubricating oil. The percentage increment in weld load for Cu nanolubricant, SiO_2 nanolubricant, WS_2 nanolubricant, CuO nanolubricant, and Graphite nanolubricant obtained ~ 22%, 11%, 27%, 29%, 19% respectively.
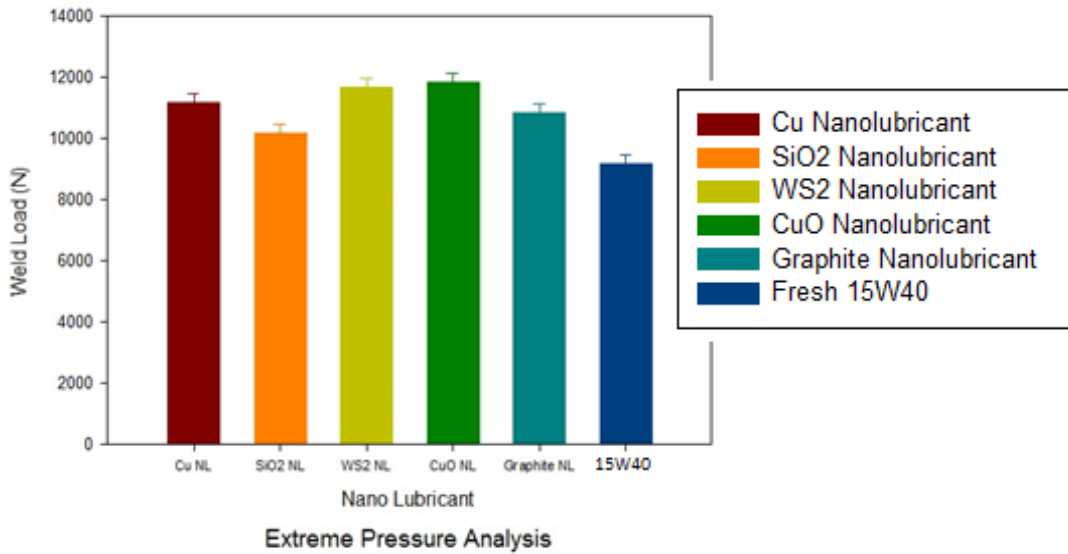
Figure 4.40: Extreme Pressure Analysis of Nanolubricants

`

4.4 Tribological analysis of optimized nanolubricant

After the tribological and extreme pressure analysis on a pin on disc and four ball tester, three nanolubricant was developed by a combination of more the one nanoparticle. The tribological, extreme pressure and thermal properties along with the stability of the nanofluid were considered for driving out the new composition. The composition of the newly developed lubricant is given in Table 4.6. The tribological behavior of the novel nanolubricants was studied on a pin on disc tribometer and four ball tester.

Table 4.6: Composition of nanolubricant developed by a combination of nanoparticles

Nanoparticle with composition	Base oil	Nanolubricant	Viscosity (mPa·s) at 40 ºC
0.6% SiO_2 + 0.2% CuO	15W40	NL1	89.846
0.6% Graphite + 0.2% CuO	15W40	NL2	88.527
0.4% WS_2 + 0.2% CuO	15W40	NL3	90.028

4.4.1 Tribological and thermal analysis on the Pin on disc tribometer

The experiment was conducted at a load of 40 N with variable sliding speed of 3.663m/s, 5.2631m/s 7.3260 m/s, 10.4712 m/s, 13.6054m/s. The atmospheric temperature at the time of testing was 28^0 C. The experiment was carried in fully flooded as well as starved lubrication condition.

4.4.1.1 Study of C.O.F.

Figure 4.41 shows the variation of C.O.F. with respect to speed at a constant load of 40 N for the various nanolubricants developed.

For fully flooded condition at lower sliding speed the nanolubricant 2 showed lowest C.O.F. followed by the nanolubricant 1. The nanolubricant 3 showed the highest C.O.F. As the higher sliding speeds were achieved the C.O.F. values for all the three nanolubricants increased but this increment was more for the nanolubricant 2 as compared to the other lubricants. At 13.663 m/s sliding speed nanolubricant 2 showed the highest C.O.F. followed by nanolubricant 1 and nanolubricant 3 showed the lowest C.O.F. values.

`

For starved lubrication condition, the C.O.F. first decreased and then increased. The C.O.F. nanolubricant 2 was lower than the nanolubricant 1 and nanolubricant 3.
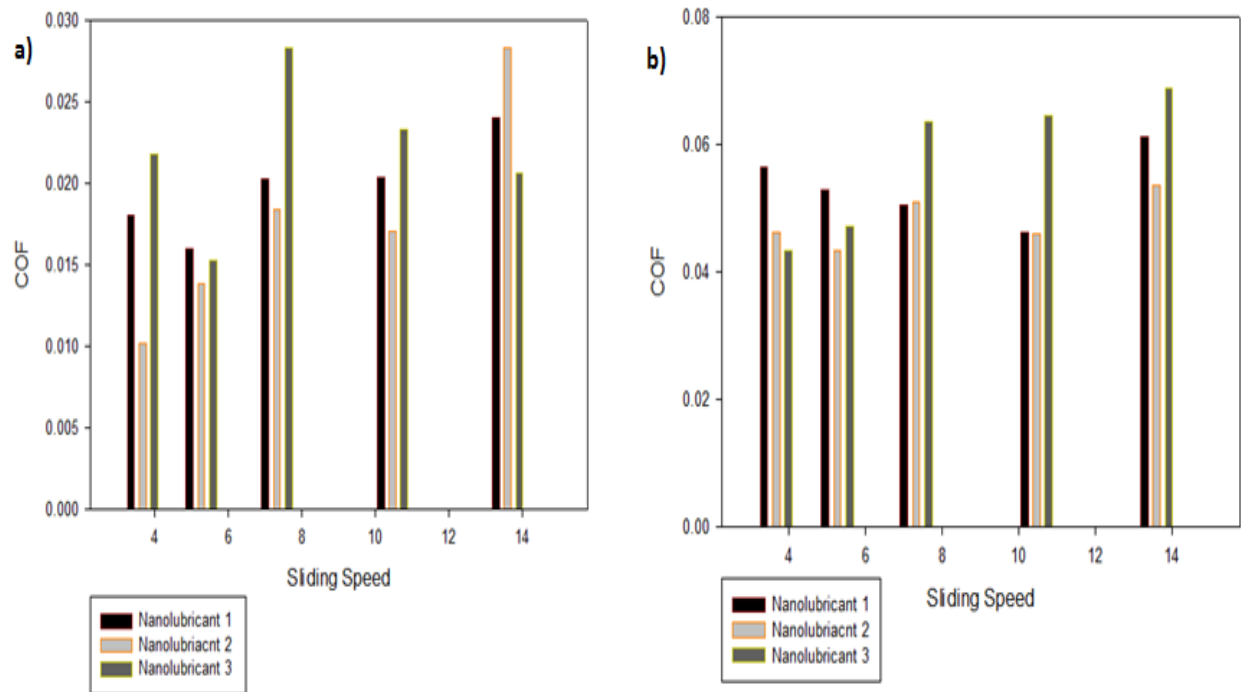
Figure 4.41: Variation of C.O.F. with sliding speed for novel Nanolubricants in a) fully flooded Lubrication and b) Starved Lubrication.

4.4.1.2 Study of Specific Wear Rate

Figure 4.42 shows the variation of Specific Wear Rate with respect to sliding speed at a constant load of 40 N for the navel nanolubricants.

The specific wear rate for the fully flooded condition has lower values as compared to starved lubrication due to the presence of stable lubricating film between the tribopairs.

For fully flooded lubrication condition the specific wear rate for nanolubricant 2 showed minimum value followed by nanolubricant 1 and nanolubricant 3.

For starved lubrication nanolubricant 3 showed lower values of C.O.F.as it acts as a solid lubricant and produces a protective coating over the surface of the tribopair. In starved condition, at higher speed, the nanolubricant 1 showed a lower value of the coefficient of friction.

93
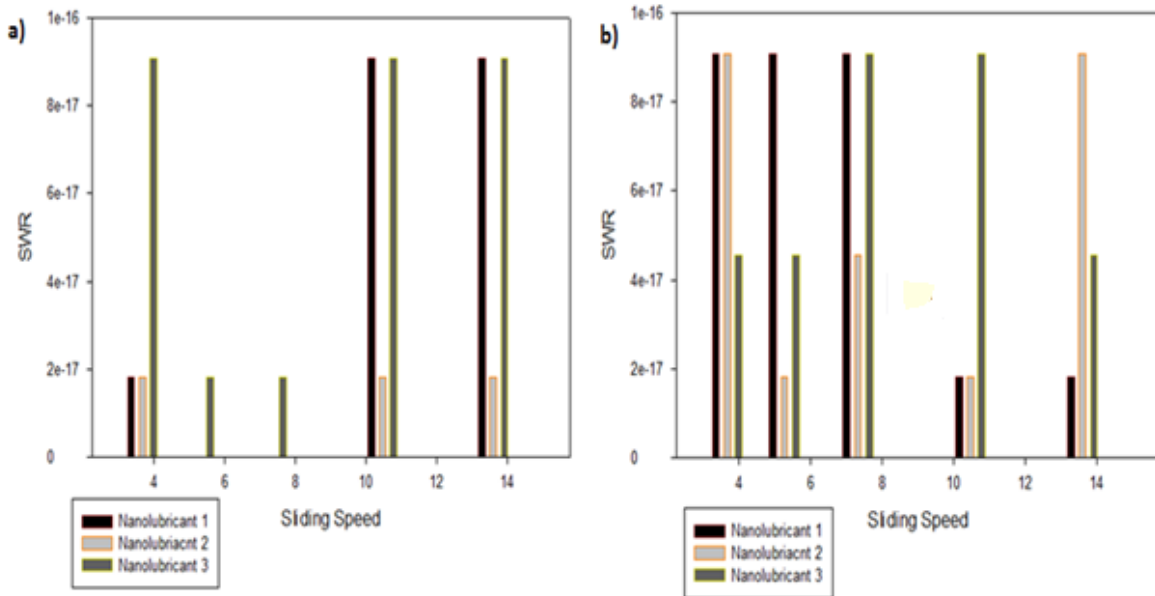
Figure 4.42: Variation of Specific wear rate with sliding speed for novel nanolubricants in a) Fully Flooded Lubrication and b) Starved Lubrication.

4.4.2 Tribological and Extreme Pressure analysis with Four Ball Tester

The tribological testing for the prepared nanolubricant had been carried out on four ball tester according to ASTM- DIN 51350 for extreme pressure and ASTM- D4172 for friction and wear characteristics of the lubricating oil, the test conditions are given in Table 3.

In the four ball tester, the load is applied from vertically downwards direction. The upper ball rotates with constant rpm. The temperature of the assembly is maintained at the desired value by a temperature controlled unit. The frictional torque was measured by load displacement sensor that displays on the online monitor.

The nanolubricants were tested on Four Ball Tester for their performance analysis by measuring C.O.F. and wear scar diameter and stability was analyzed by means of weld load measurement.

4.4.2.1 Study of C.O.F.

The experiment was performed on three loads 196 N, 392 N and 588 N. The C.O.F.(C.O.F.) increased with the increase of normal load. At lower loads, i.e. 196 N and 392 N nanolubricant 2 showed the minimum value of C.O.F. followed by nanolubricant 1. Nanolubricant 3 showed

`

a maximum value of C.O.F.at smaller load. The variation of C.O.F. with respect to load was not that much in the case of nanolubricant 3 as compared to the other two nanolubricants. At 388 N load nanolubricant 3 showed minimum C.O.F. followed whereas nanolubricant 1 showed the highest value as shown in Figure 4.43.
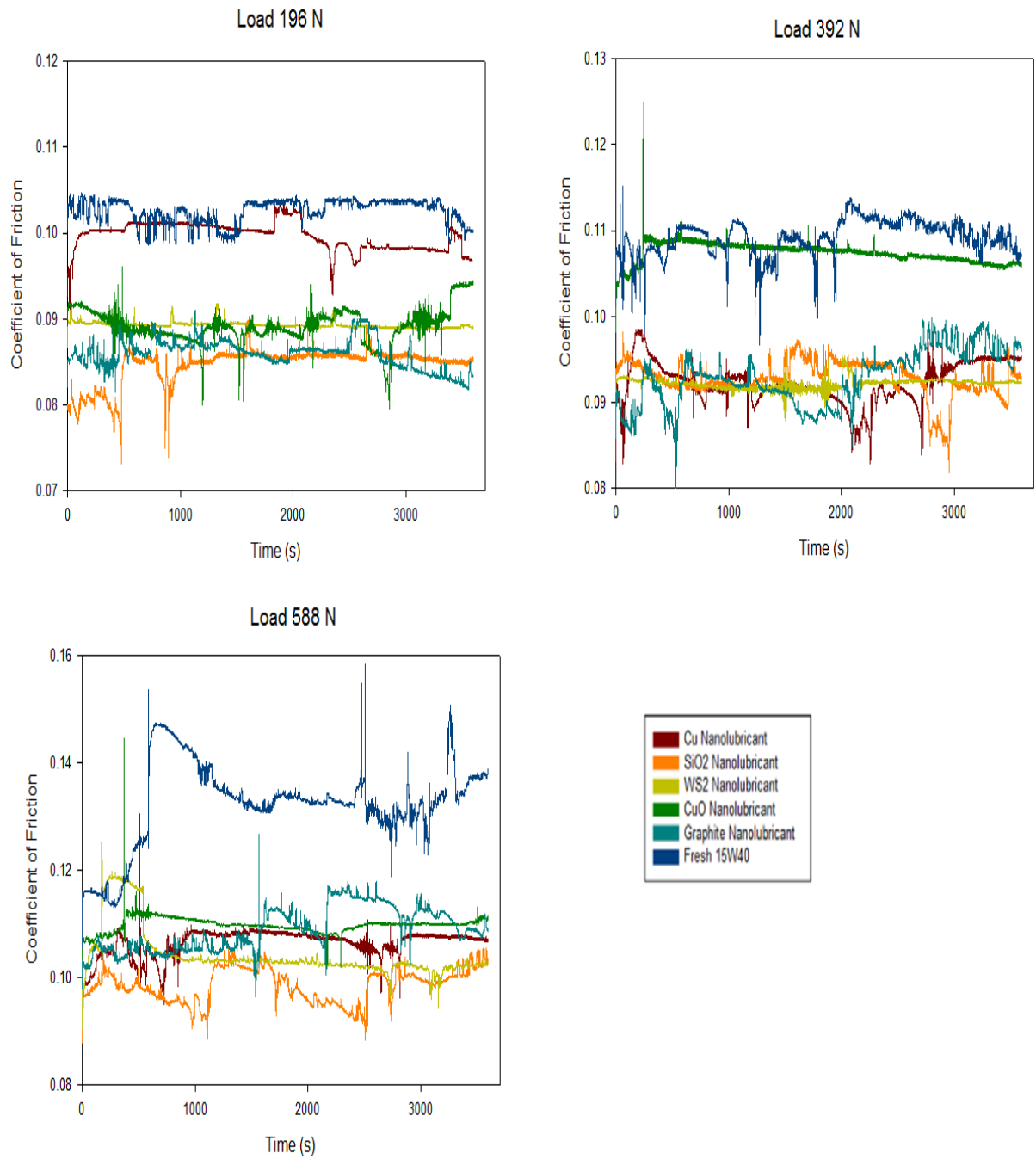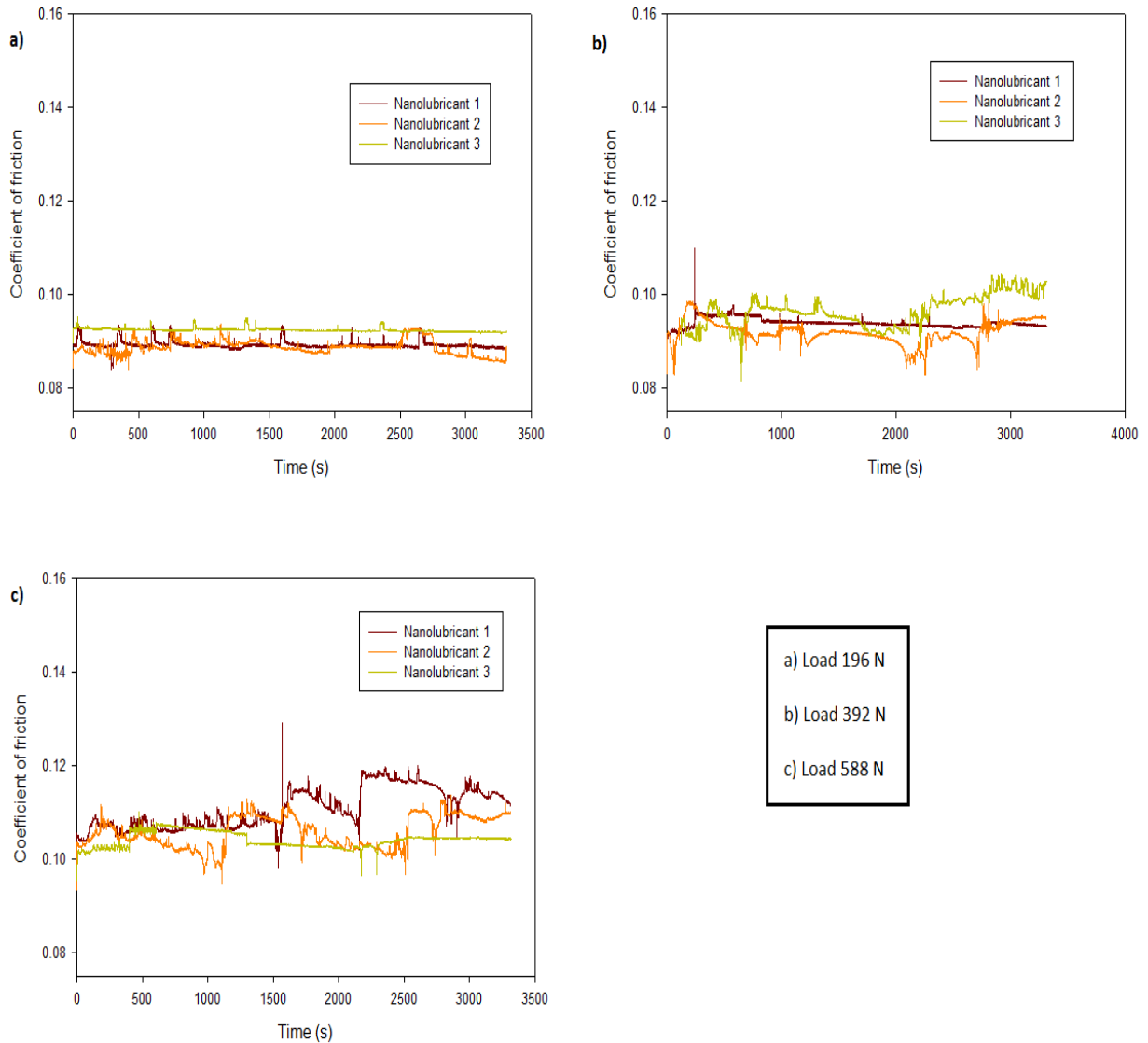

Figure 4.43: Load v/s C.O.F.in presence of various lubricants a) at load 196 N, b) at load 392 N, c) at load 588 N.

`

4.4.2.2 Study of Wear Scar Diameter

The wear scar diameter (WSD) was examined for all three loads 196 N, 392 N and 588 N. The wear scar diameter increased as the load increased. At 196 N load, the minimum WSD was observed for nanolubricant 2 followed by nanolubricant 1. For nanolubricant 3 the WSD was around 30% more than that in the case on nanolubricant 2 as shown in Figure 4.44.

a)

WSD= 0.330 mm

b)

WSD= 0.300 mm

c)

WSD=0.400 mm

a) Nanolubricant 1

b) Nanolubricant 2
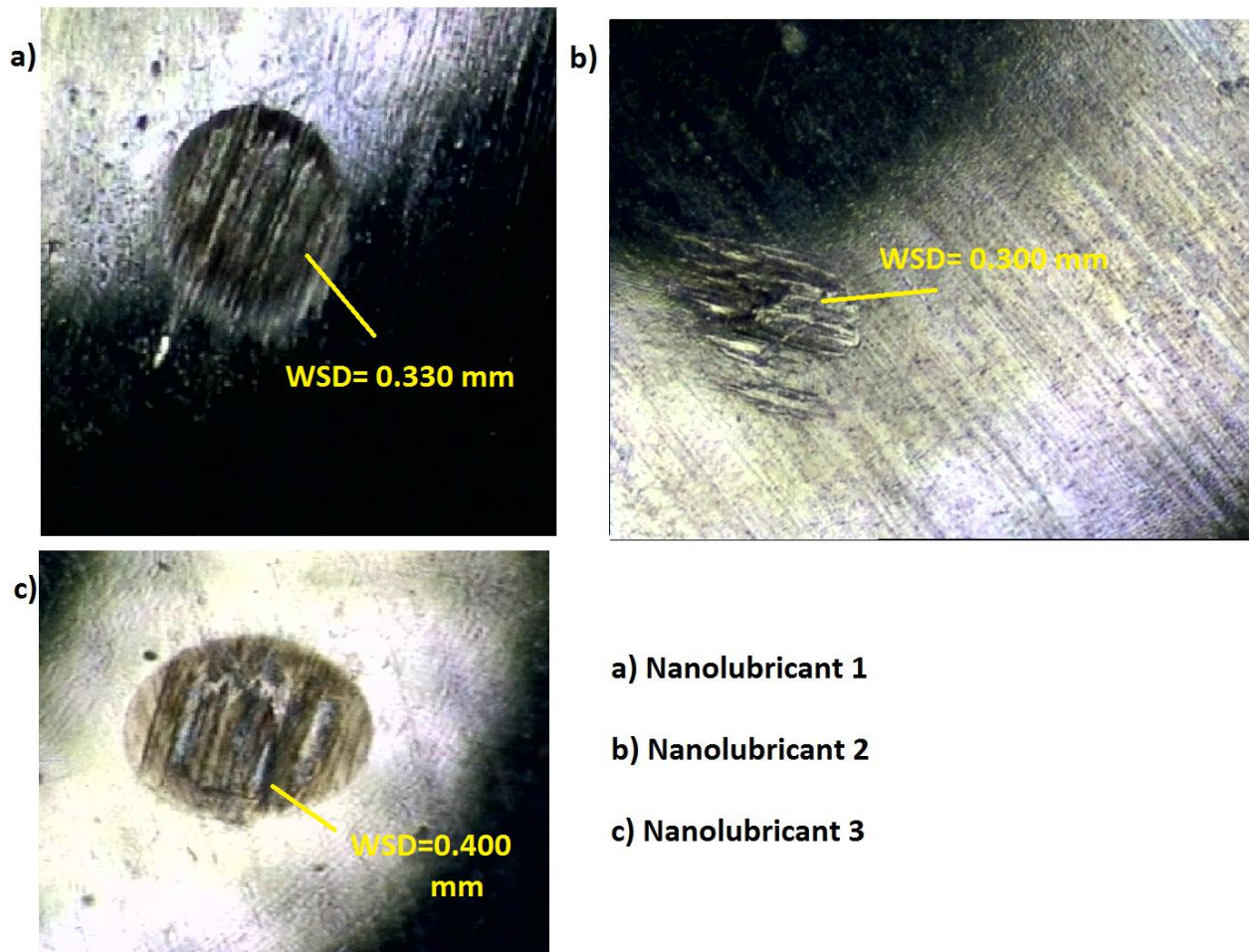
c) Nanolubricant 3

Figure 4.44: Wear Scar Diameter observed by optical microscope at 196 N. a) Nanolubricant 1, b) Nanolubricant 2, c) Nanolubricant 3.

At load 392 N minimum wear scare diameter was observed in case of nanolubricant followed by nanolubricant 3 which is having around 5% WSD than nanolubricant 1. The wear scar

diameter was highest in case of nanolubricant 2 was around 10 % more than the nanolubricant 1 as shown in Figure 4.45.
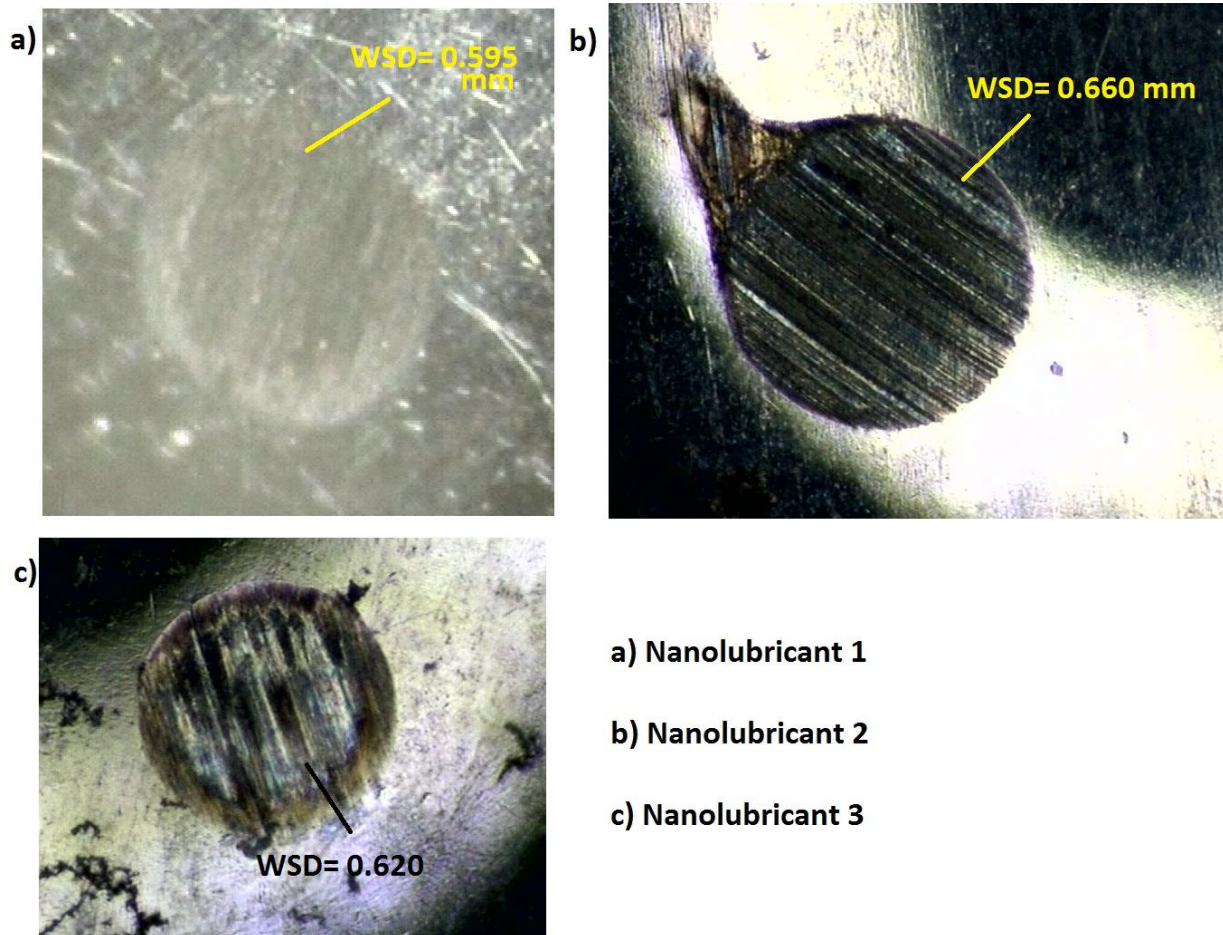
Figure 4.45: Wear Scar Diameter observed by an optical microscope at 392 N. a) Nanolubricant 1, b) Nanolubricant 2, c) Nanolubricant 3.

At 588 N load, the wear scar diameter was minimum for nanolubricant 1 followed by nanolubricant 2 which is having around 10% more WSD than nanolubricant 1. The nanolubricant 3 had maximum wear scare diameter which was around 20% more than the WSD in case of nanolubricant 1. As shown in Figure 4.46.
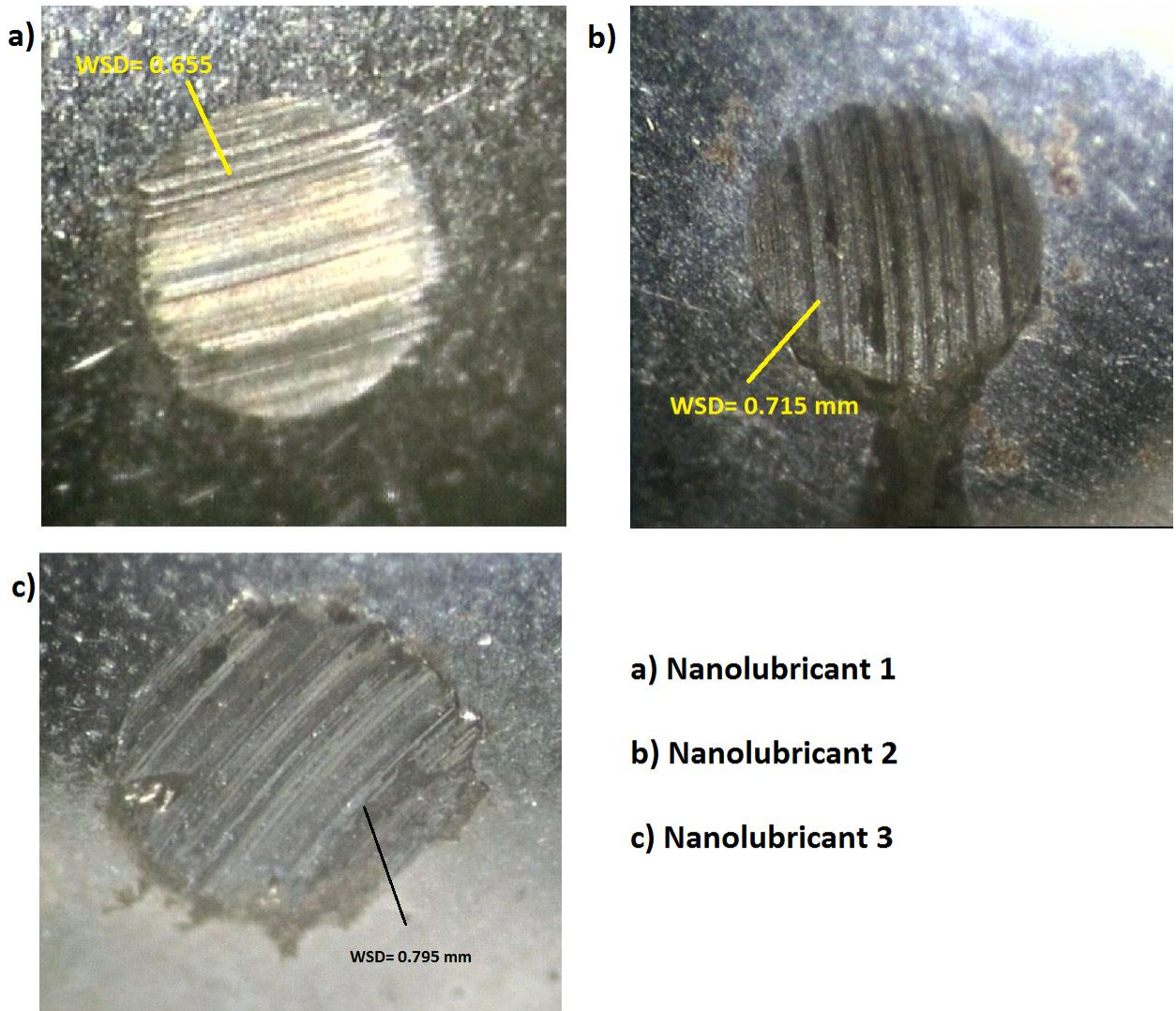
Figure 4.46: Wear Scar Diameter observed by an optical microscope at 588 N. a) Nanolubricant 1, b) Nanolubricant 2, c) Nanolubricant 3.

4.4.2.3 Extreme Pressure Analysis

The extreme pressure performance analysis of the novel nanolubricants was conducted according to ASTM- DIN 51350. The weld load was calculated for each nanolubricant. The nanolubricant 1 showed minimum weld load i.e, 10500 N followed by nanolubricant 2 11500 and nanolubricant 3 showed highest weld load of 12000 N, which makes it the better lubricant than the other two lubricants under extreme pressure conditions.

CHAPTER 5

PERFORMANCE ANALYSIS OF INTERNAL COMBUSTION ENGINE

5.1 Analysis of the Internal Combustion engine

The international combustion engine used for performance study was the Kirloskar single cylinder diesel fueled four stroke engine shown in Figure 5.1. The light duty, water cooled, vertical engine diesel engine generally used for irrigation purpose by the farmers. The engine was selected because such engines work in more adverse conditions then the automobile conditions.

Table 5.1: Specifications of the Test Engine

Parameter	Description
Make	Kirloskar
Model	AV1-5.0
Engine Type	Single cylinder
Number of strokes	Four stroke
Type of cooling	Water cooled engine
Fuel	Diesel
Lubricating oil	15W40
Bore	80 mm
Displacement	110 mm
Cubic Capacity	553 cc
Compression Ratio	16.5:1
Rated Power	3.7 kw/5 hp @ 1500 rpm

`

The long oil change intervals and dirt and dust near the operating condition make them tribological critical to study. The lubricating oil recommended for the engine is 15W40. The wet sump lubricating system is used for the engine. The specifications of the test engine are given in Table 5.1.
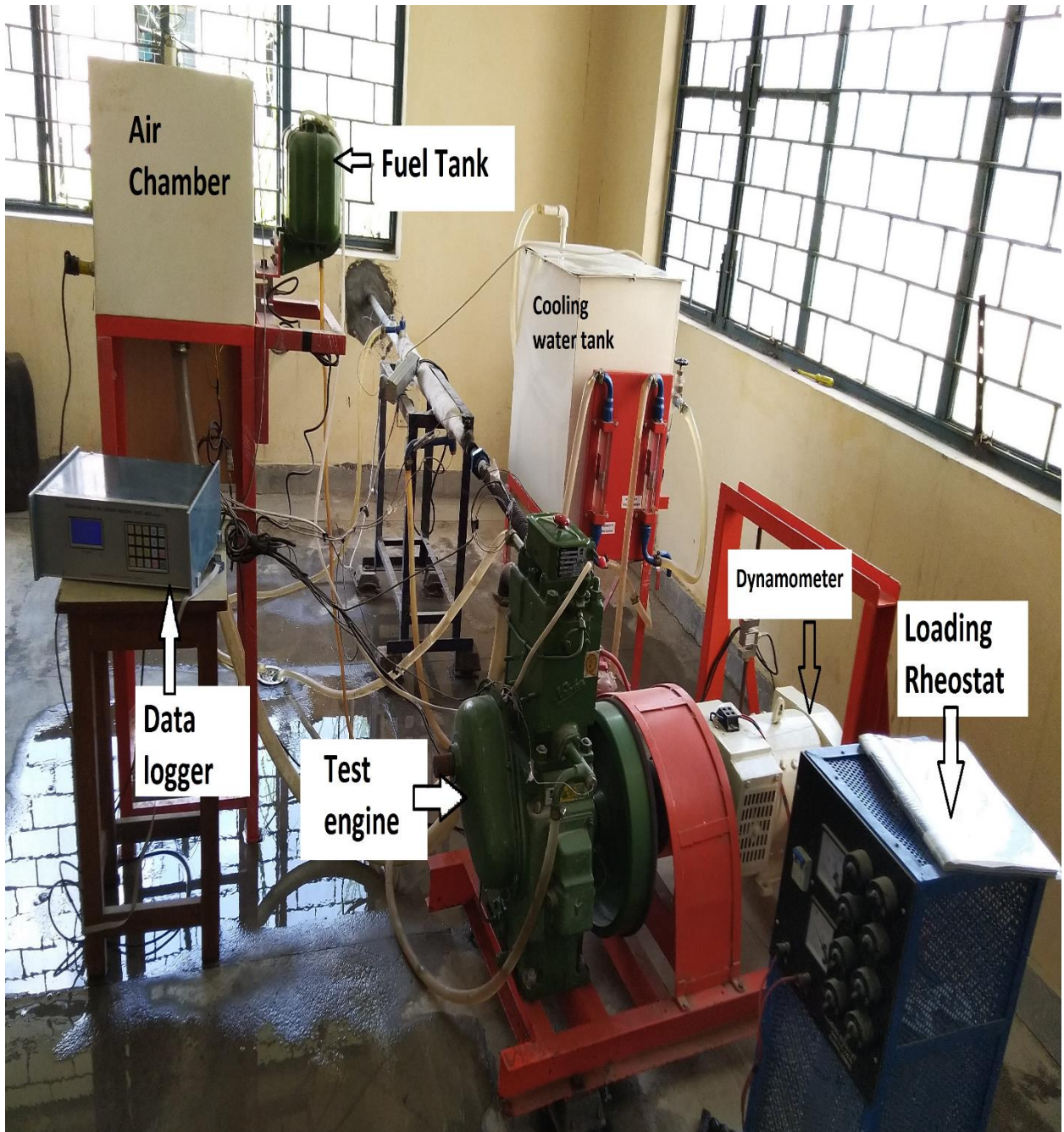
Figure 5.1: Test engine

`
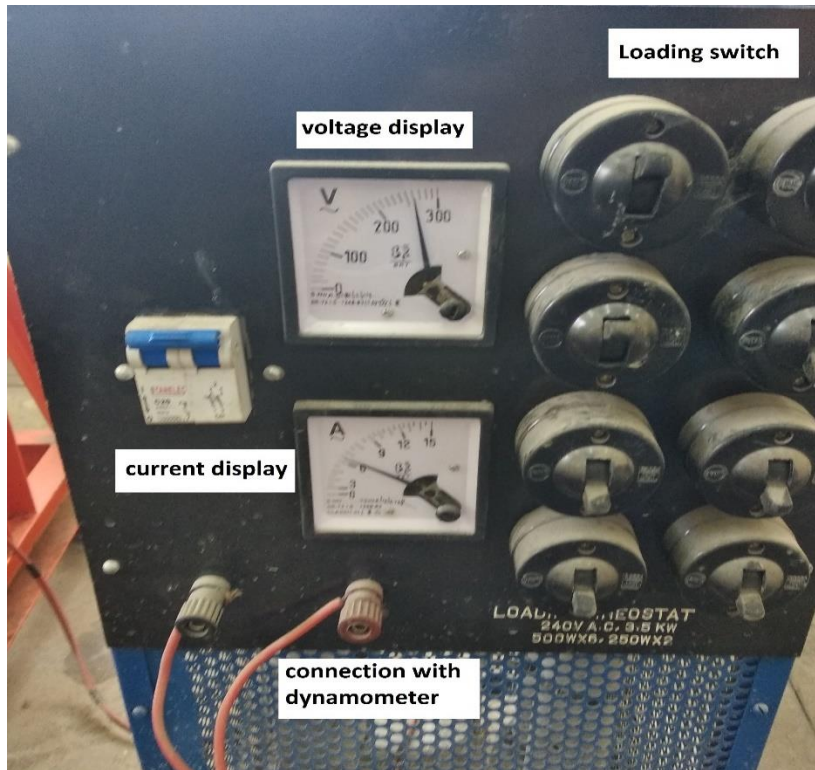
Figure 5.2 Loading Rheostat

Figure 5.3 Data logger

The test engine was connected to a data logger which displays the load, rpm, temperature at various points and the fuel consumed shown in Figure 5.3. The loading for the test engine was electrical loading for high accuracy shown in Figure 5.2. The loading rheostat was connected to the engine through a dynamometer. The rpm was measured with the help of magnetic type rpm sensor. The eddy-current dynamometer and rpm sensor were directly connected to the data logger. The fuel consumption by the engine was also measured by the sensor and displayed on the data logger. There were thermocouples provided for measurement of temperature at various points such as inlet atmospheric temperature, air temperature, inlet fuel temperature, inlet air temperature to the heat exchanger, outlet air temperature from the heat exchanger, engine exhaust temperature, inlet water cooling temperature, exhaust cooling water temperature. The schematic of the wet pump lubricating system is used in the test engine is shown in Figure 5.4. The lubricant is kept in the oil sump. The lubricant from the oil sump is pumped by a pump which receives power from the engine. The oil strainer collects and filters oil from the sump. The oil is then supplied to a secondary high pressure filter which removes the foreign particles present in the oil. The oil pressure regulator ensures the optimum oil pressure. The pressurized oil flows through the oil lines which are meant to lubricate the moving engine parts. Oil from the main oil lines flows through the holes drilled inside the crankshaft and main bearing for their lubrication. The oil sprout connected with the oil lines forces the oil upwards to lubricate the piston and its parts. The oil flows through the oil rings to lubricate and form a thin film around the cylinder walls. The second oil line having sprouts connected to help in lubricating the camshaft and the valves. After lubricating the engine parts, the oil begins to flow downwards through a separate passage and finally gets collected in the oil sump.
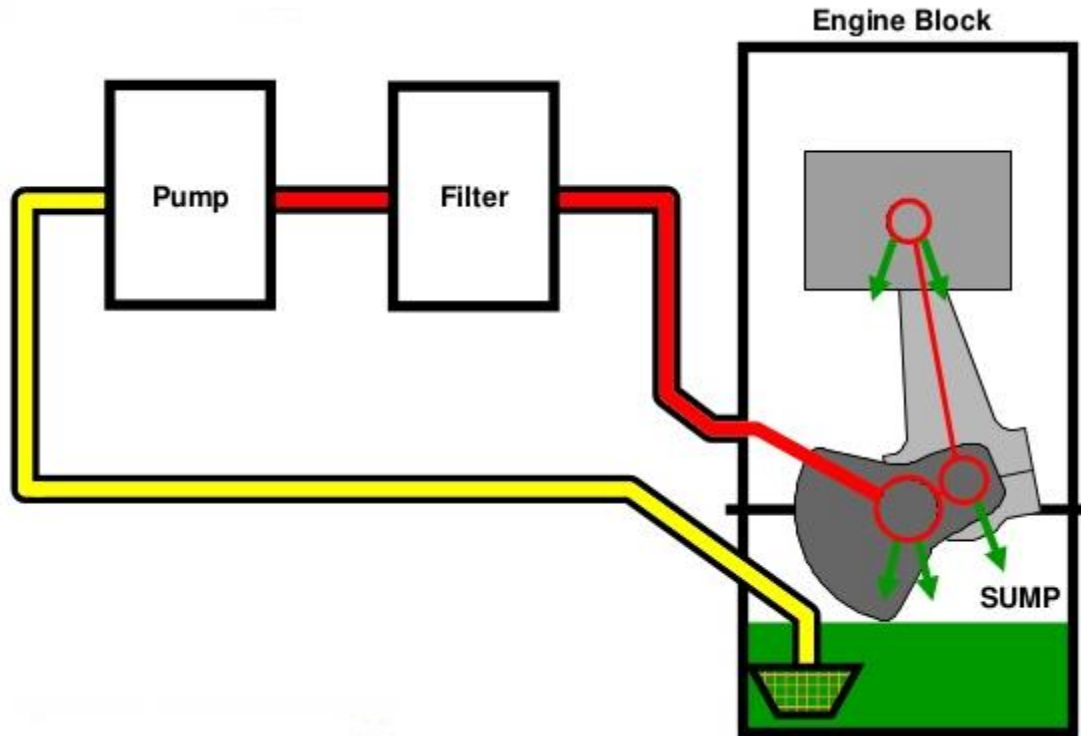
Figure 5.4: Wet sump lubricating system

5.2 Performance Analysis of the IC Engine

The performance analysis of the IC engine was studied by calculating the performance parameters like brake mean effective pressure, brake specific fuel consumption and brake thermal efficiency. The emission analysis was also performed where the exhaust gasses form the test engine were analyzed. The test was performed for fresh 15W40 and the three novel nanolubricant i.e. nanolubricant 1, nanolubricant 2 and nanolubricant 3.

The oil sump was properly cleaned; the oil filter has been changed before changing the lubricant. After the oil change the engine was started and ran for 4 hours at no load before starting the actual performance analysis. This was done just to ensure that the lubricant flows to all the parts of the engine properly.

Measurement of various engine performance parameters: The engine performance parameters like brake power, brake mean effective pressure, indicated power, brake thermal efficiency, brake mean effective fuel consumption was calculated with the help of observed parameters

from the data logger like engine load, fuel consumption, engine speed, temperature at various points, air flow rate. The equations for the measurement of the performance parameters are given bellow.

Brake power (BP): It signifies the power output of the engine or the power given by the engine to the output shaft. The brake power is measured with the help of the dynamometer. The brake power may be calculated as per equation 5.2.

$$\text{Brake Torque} = 9.81 \text{LR Nm} \quad \dots\dots\dots\dots\dots\dots\dots 5.1$$

$$\text{Brake power (BP)} = \frac{2\pi N \times 9.81 \times L \times R}{1000 \times 60} \quad \text{kW} \dots\dots\dots\dots\dots\dots 5.2$$

Where L is the Load (Kg)

R is the radius (m)

N is the rpm

Brake mean effective pressure (BMEP): It the theoretical pressure which is exerted during each power stroke. The brake mean effective pressure can be calculated as per equation 5.3.

$$\text{B. M. E. F} = \frac{60000 \times \text{brake power}}{\text{lA N} \times n} \dots\dots\dots\dots 5.3$$

Where l is the stroke length

A is the area of piston head

N is the rpm

n is the no of power stroke per cycle

n = ½ for four stroke engine

n = 1 for two stroke engine

Brake specific fuel consumption (BSFC): It is the ratio of rate of fuel consumed to the brake power. Brake specific fuel consumption is given by equation 5.4.

$$\text{BSFC} = \frac{\text{Mass of fuel consumption per unit time}}{\text{Brake power}} \ldots\ldots.5.4$$

Brake thermal efficiency: Brake thermal efficiency given in equation 5.5 is the ration of the brake power to the fuel power.

$$\text{Brake thermal efficiency} = \frac{\textit{brake power}}{\textit{mass of fuel/s}\times\textit{calorific value of fuel}}\ldots\ldots.5.5$$

5.2.1 Results of engine performance analysis

The engine performance measured for every 0.5 Kg of oil consumed. The time for the fuel consumption was recorded with the help of stop watch. The other important parameters for the test were recorded and displayed by the data logger.

5.2.1.1 Brake specific fuel consumption (BSFC)

The brake specific fuel consumption is considered to be one of the very important parameters for the performance testing as doesn't consider the calorific value so such analysis may be replicated for number of fuels used for the same engine.

`
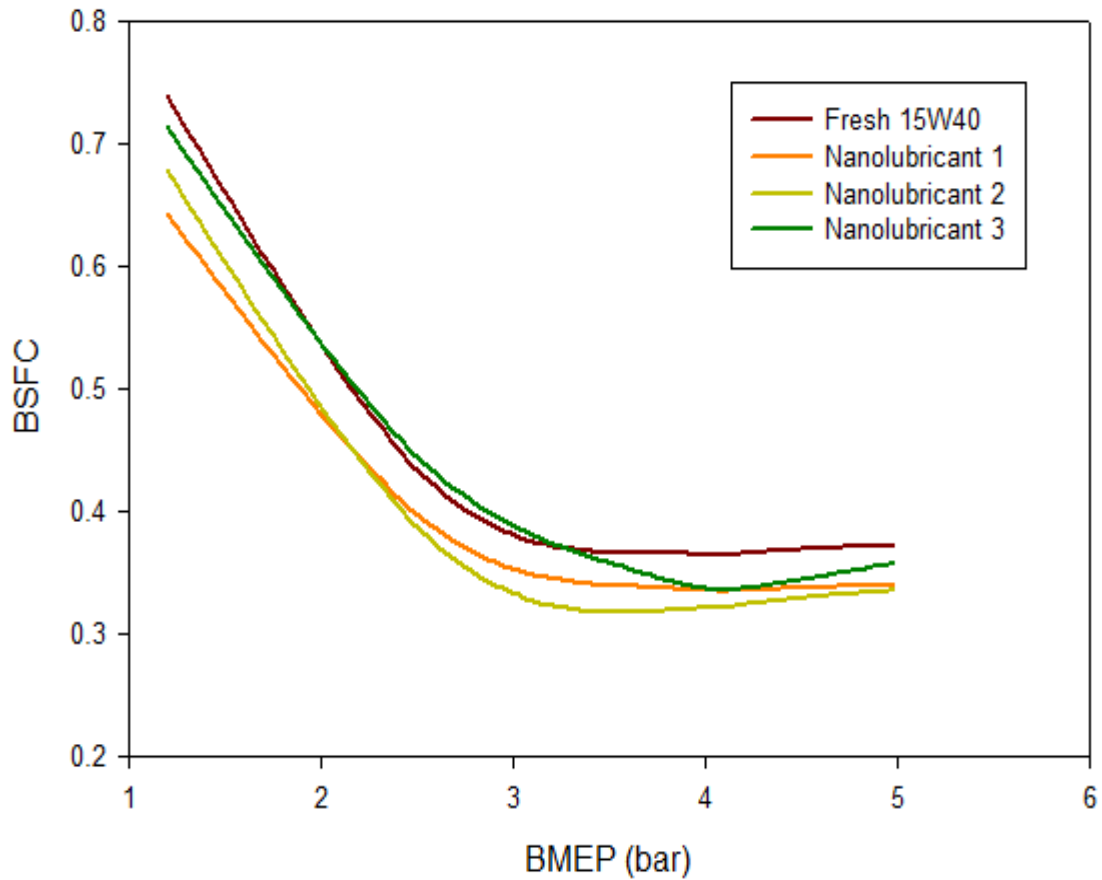
Figure 5.5: BSFC vs BMEP

The BSFC vs brake mean effective pressure (BMEP) plot shows the decrease in BSFC upto 3.2 bar BMEP after that the BSFC curve became steady as shown in Figure 13. In case of nanolubricant 1 and 2 the BSFC was minimum, in case of nanolubricant 3 BSFC was almost same as that for the fresh 15W40 but after 3.4 bar BMEP the BSFC decreased swiftly which indicates the at higher loads lubricant 3 have better properties than Fresh 15W40.

5.2.1.2 Brake thermal efficiency (BTE)

Brake thermal efficiency is a very important performance parameter for the engine as it not only considers the effectiveness of the engine to transform the chemical energy of the fuel to useful work but it also considers the tribological losses due to friction of various moving parts.

`
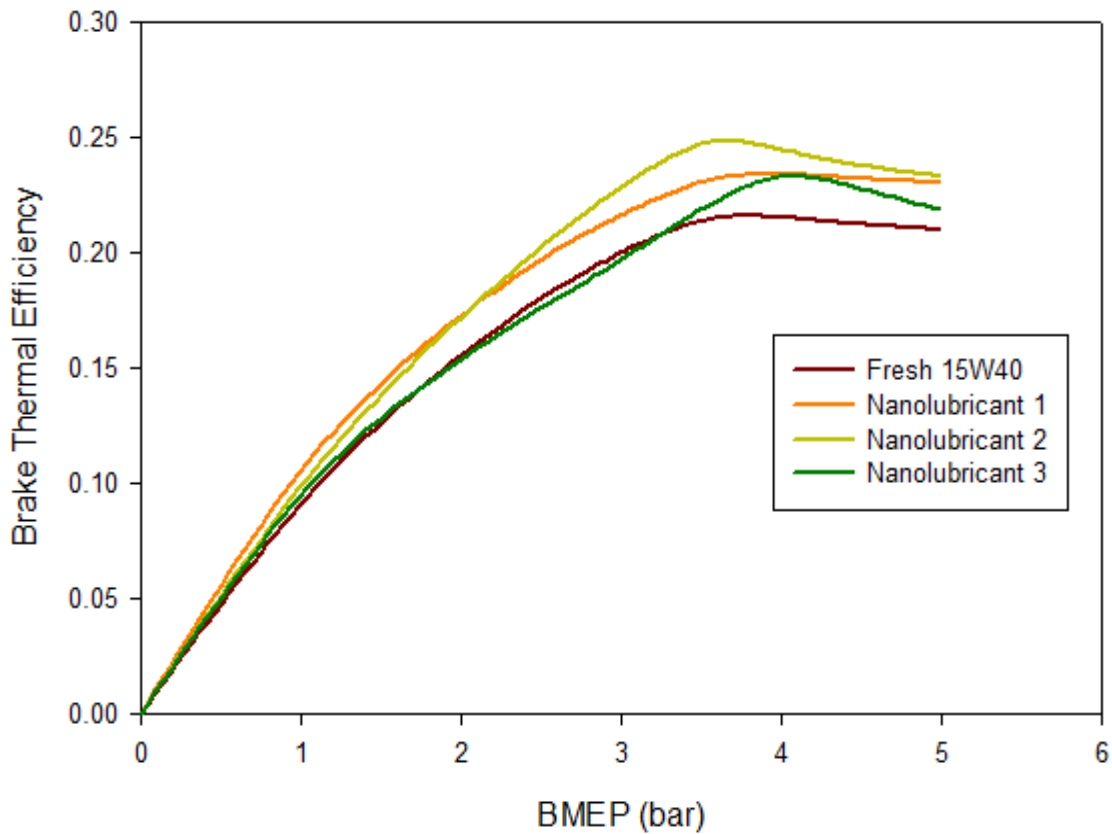
Figure 5.6: Brake Thermal Efficiency vs BMEP

The BTE vs brake mean effective pressure (BMEP) plot (Figure 5.6) shows the increase in efficiency upto 3.4 bar BMEP after that the efficiency curve started dropping with less slope. The sudden increment in brake thermal efficiency as the BMEP or engine load was increased may be due to reduction in heat losses. After achieving the maximum efficiency, the tribological and losses increases slightly as the BMEP is further increased.

In case on nanolubricant 2 the efficiency was maximum followed by nanolubricant 1, in case of nanolubricant 3 efficiency was almost same as that for the fresh 15W40 but after 4.1 bar BMEP the efficiency increased swiftly which indicates the at higher loads lubricant 3 have better properties than Fresh 15W40.

`

5.3 Emission Analysis

Engine emissions have been under critical consideration as the world eyes on the energy sources with cleaner exhaust which should not be hazardous. The exhaust form the engine was analyzed at the part as well a full load. The analysis was done to measure carbon dioxide (CO_2), carbon monoxide (CO), hydrocarbons (HC) and smoke opacity.

5.3.1 Carbon monoxide emission

Carbon monoxide is one of the major pollutant present in the diesel engine exhaust. The carbon monoxide emission increases in the engine due to incomplete burning of the fuel which may be due to engine speed, engine load, fuel injection pressure, injection timing, fuel atomization, combustion chamber design. At no load the CO emission was very large it may be due to the fact the at smaller load the engine temperature was not sufficiently large to assist the complete burning of the fuel. As the load increased the burning of fuel us proper which resulted in decrease in CO emission. However, as the load increased from 70% till full load the fuel requirement for the engine increased resulting in increased CO emission. The CO emission in case of nanolubricant 1 was least followed by nanolubricant 3 and nanolubricant 2. Fresh 15W40 showed highest CO emission as shown in Figure 5.7.
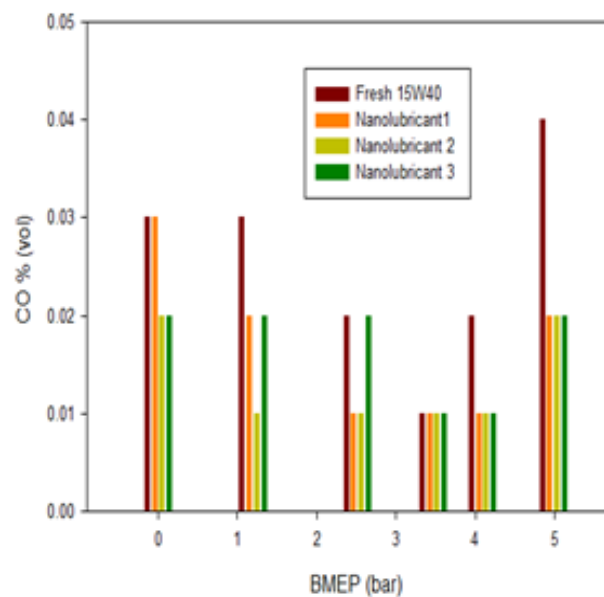
Figure 5.7: CO emission vs BMEP

5.3.2 Carbon dioxide emission

Carbon dioxide emission indicates the complete burning of the fuel; however, the emission of CO_2 is very dangerous for the environment as it not only causes serious health in the human beings but it is also responsible for the ozone depletion. The CO_2 emission increased with the increase in engine load. The CO_2 emission was minimum for 15W40 lubricating oil followed by nanolubricant 3 and nanolubricant 1. The nanolubricant 2 showed maximum CO_2 emission as shown in Figure 5.8.
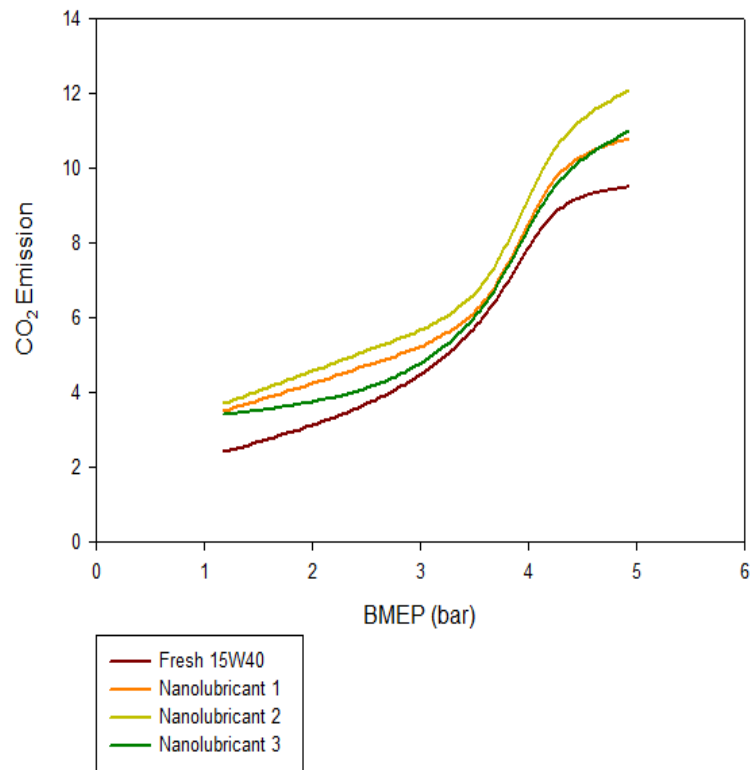
Figure 5.8: CO_2 emission vs BMEP

5.3.3 Hydrocarbon emission

The fuel used for diesel engine has its primary constituent made up of hydrogen and carbon. The emission of unburnt hydrocarbons is toxic and dangerous for the environment. The factors affecting hydrocarbon emission are the availability of oxygen, engine cylinder crevices, residence time, fuel structure, temperature etc. The HC emission was highest in case of fresh

`

15W40 lubricant followed by nanolubricant 3, nanolubricant 2 had minimum HC emission which was around 16-29% less than the HC emission of 15W40. Similarly, in case of nanolubricant 1 and 3 the HC emission reduced by 9-16% and 0- 21% respectively as shown in Figure 5.9.
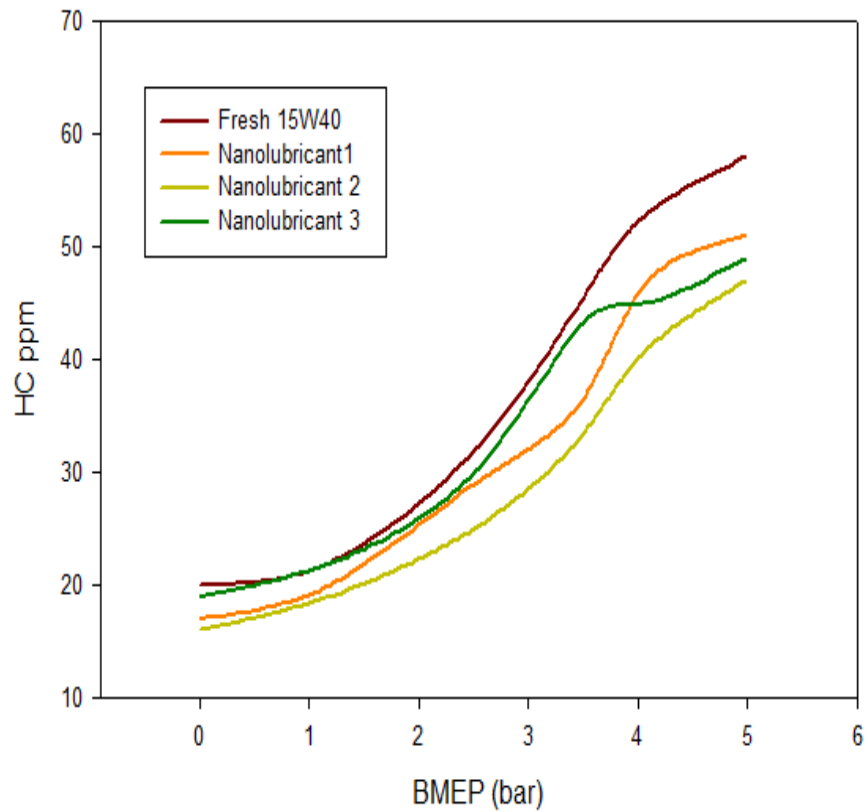
Figure 5.9: Hydrocarbon emission vs BMEP

5.3.4 Smoke opacity

Smoke opacity has been one of the very critical parameters for the emission analysis of diesel engine as it refers to the soluble organic fraction of the particulate in the emission. These particulate are micro of nano size matter comprises of soot and hydrocarbon which may be injurious if inhaled. The smoke opacity increased with the increase in BMEP it may be because as the engine load/BMEP was increased more fuel was supplied to the engine which results in

`

decreased air/fuel ration. As the air flow was less as compared to fuel, it resulted in cracking of long chain hydrocarbon of fuel resulting in soot. More is the soot formation more would be the smoke opacity.
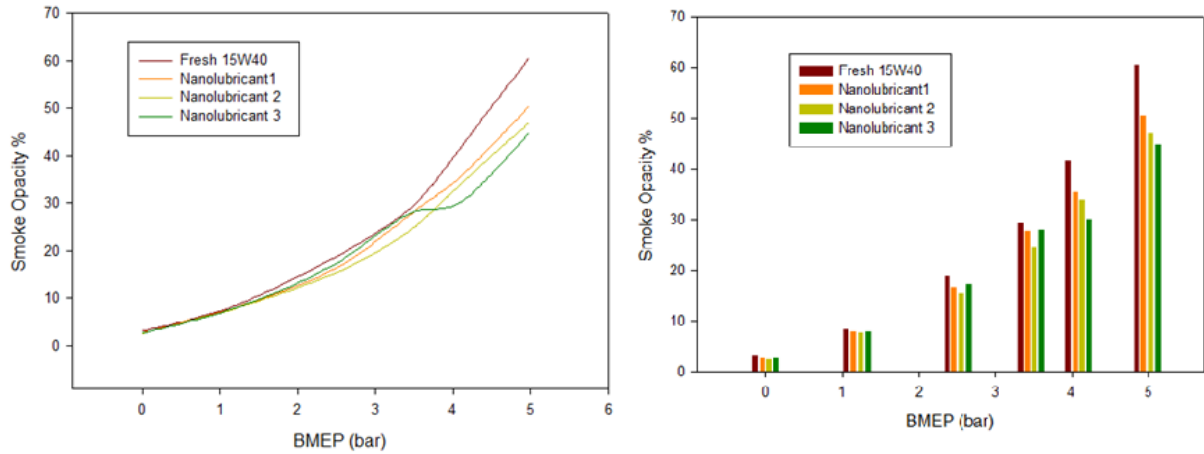
Figure 5.10: Smoke opacity vs BMEP

Till BMEP of 1.4 bar the smoke opacity was almost same for all the lubricants but as the BMEP increased further the smoke opacity in the presence of lubricant having the nanoparticles showed lesser value as compared to fresh 15W40 lubricating oil shown in Figure 5.10.

`

CHAPTER 6

CONCLUSIONS AND FUTURE SCOPE

6.1 Conclusions

Following conclusions have been made from this study:

- **Preparation of Nanolubricant**
  - SiO_2, Graphite and WS_2 nanolubricant found stable after sonication having Zeta potential $\sim$ 45 mV, 34 mV and 37 mV respectively. Cu and CuO nanolubricant sonicated in the presence of CTAB as surfactant showed enhanced zeta potential upto 24 and 28 mV respectively, which indicated improved the stability of the nanolubricant.

- **Tribological analysis on pin-on-disc tribometer**
  - The C.O.F. decreased in case of nanolubricant. The maximum drop in C.O.F. was observed in case of SiO_2 nanolubricant followed by graphite and WS_2 nanolubricant. In case of Cu and CuO nanolubricant the C.O.F. decreased but this decrement was very less as compared to the other nanolubricants.
  - For fully flooded lubrication the C.O.F. also dependent on the composition of nanoparticles in the lubricant, the amount of nanoparticles for which the C.O.F. showed minimum value was different for different nanolubricants. In starved lubrication condition; the C.O.F. was higher than the fully flooded condition, still it was less in case of nanolubricants. In starved lubrication condition also the C.O.F. depends on the type and amount of nanoparticles in the lubricant.
  - The specific wear rate for the fully flooded condition has lower values as compared to starved lubrication due to the presence of stable lubricating film between the tribopairs. The value specific wear rate was almost negligible in case of some of nanolubricant due to the no wearing of the contact surfaces or due to the mending nature of the nanoparticles.

- **Thermal Analysis**
  - The nanolubricants increased the heat transfer rate at the interface of the tribopair increasing the heat transfer coefficient, this showed the decreased temperature of the tribopair.

`

- o The maximum temperature drop was observed in case of Cu and CuO nanoparticles followed by WS_2 and graphite nanoparticles SiO_2 nanoparticles had minimum effect on the temperature of the tribopair. Moreover, as the composition of the nanoparticles in the lubricant increased the temperature drop also increased.

- o For fully flooded lubrication, the maximum decrement in temperature was observed in case of CuO nanolubricant around 7.6%, the Cu nanolunricant showed the decrease in temperature of around 7.1%, whereas the WS_2 and graphite nanolubricant showed 5.2% and 5.05% decrease in temperature but the SiO_2 nanolubricant showed only 1.8% decrease in temperature as compared to the fresh 15W40. In starved condition, the decrease in temperature for CuO, Cu, WS_2, graphite and SiO_2 nanolubricant was 9.1%, 8.8%, 7.2%, 4.5% and 2.7% respectively.

- **Tribological testing on Four ball tester**

- o The antiwear characteristics of the nanolubricant were tested on four ball tester according to ASTM- D4172 showed improved tribological performance. The C.O.F. for SiO_2 nanolubricant showed a decrease of ~ 15% to 25%. The nanoparticles of graphite showed ~ 15% - 18% decrement in C.O.F. The nanoparticles of Cu and CuO showed ~ 9% - 20% and ~ 1.5% to 17% reduction in C.O.F. respectively whereas the nanoparticle of WS_2 showed ~ 13% - 21% decrease in C.O.F.

- o There was a significant reduction in wear scar diameter recorded when measured by optical microscope. In case of SiO_2 nanolubricant WSD decreased by ~ 50% to 59%. The graphite nanolubricant showed ~ 45% - 57% decrement in WSD. Cu and CuO nanolubricant showed ~ 33% - 49% and ~ 13% to 28% reduction in WSD respectively whereas the WS_2 nanolubricant showed ~ 17% - 26% decrease in WSD.

- o The extreme pressure analysis was conducted according to ASTM- DIN 51350-02. There was a significant increase in weld load in case of nanolubricants which indicated the improved extreme pressure performance of the nanolubricant. The percentage increment in weld load for Cu nanolubricant SiO_2 nanolubricant, WS_2 nanolubricant, CuO nanolubricant and Graphite nanolubricant obtained ~ 22%, 11%, 27%, 29%, 19% respectively.

- **Performance analysis of I C engine**

- o The brake specific fuel consumption decreased and the brake thermal efficiency increased in the presence of nanolubricant which indicates the performance enhancement of the IC engine in the presence of the nanolubricants.

`

- o The HC emission was highest in case of fresh 15W40 lubricant followed by nanolubricant 3, nanolubricant 2 had minimum HC emission which was around 16-29% less than the HC emission of 15W40. Similarly, in case of nanolubricant 1 and 3 the HC emission reduced by 9-16% and 0- 21% respectively. The CO emission decrease with the increase of BMEP/engine load upto some extant and the at full load it increased again. The CO emission in case of nanolubricant 1 was least followed by nanolubricant 3 and nanolubricant 2. Fresh 15W40 showed highest CO emission. The CO_2 emission increased with the increase in engine load. The CO_2 emission was minimum for 15W40 lubricating oil followed by nanolubricant 3 and nanolubricant 1. The nanolubricant 2 showed maximum CO_2 emission.

6.2 Scope for future study:

- The nanoparticles can be used as lubricant additive for other grades of lubricating oil.
- The one step technique can be implemented for the preparation of nanolubricant.
- The bio surfactants can be used as surfactants.
- The nanolubricant can be developed for commercial use.

`

References

1. K. Holmberg, P. Andersson, N. Nylund, K. Mäkelä, A. Erdemir, "Global energy consumption due to friction in trucks and buses," Tribology International., vol. 78, (2014), 94–114.

2. V. Linden, L. Herman, "A fuel consumption model for off-road use of mobile machinery in agriculture" Energy vol. 77, (2014), 880-889.

3. F. Rastegar, D.E. Richardson, "Alternative to chrome: HVOF cermet coatings for high horsepower diesel engines", Surface Coatings Technology. vol. 90 (1997), 156–163.

4. A. Fischer, K. Bobzin, Friction, "wear and wear protection" International Symposium on Friction, (2008), Aachen, Germany, Wiley-VCH, 2009.

5. R.C.D.Richardson, "The maximum hardness of strained surfaces and the abrasive wear of metals and alloys", Wear. vol. 10 (1967), 353–382.

6. T. Sasada, S. Norose, H. Mishina, "The behavior of adhered fragments interposed between sliding surfaces and the formation process of wear particles" J. Tribology vol. 103, (1981), 195-201.

7. J. Sato, M. Shima, T. Sugawara, A. Tahara, "Effect of lubricants on fretting wear of steel" Wear. vol. 125, (1988), 83–95.

8. A.Karimi F.Avellan, "Comparison of erosion mechanisms in different types of cavitation" Wear. 113 (1986), 305–322.

9. K.R. Trethewey, T.J. Haley, C.C. Clark, "Effect of ultrasonically induced cavitation on corrosion behaviour of a copper–manganese–aluminium alloy" Br. Corros. J. vol. 23 (1988), 55–60.

10. C. N. Rowe "Specific Film Thickness—A Closer Examination of the Effects of EHL Film Thickness and Surface Roughness on Bearing Fatigue" A S L E Transactions vol. 24, (1981), 423-430.

11. Stachowiak G W & Batchelor A W, Engineering Tribology, Third Edition, Elsevier Inc., 2005.

12. A. Cameron, Principles of Lubrication, Longmans, London, (1966), 305-340.

13. C. Barus, "Isotherms, Isopiestics and Isometrics Relative to Viscosity" American Journal of Science vol. 45, (1893), 87-96.

14. E.W. Dean and G.H.B. Davis, "Viscosity Variations of Oils with Temperature", Chem. and Met. Eng. vol. 36, (1929), 618-619.

15. L.B. Sargent Jr, "Pressure-Viscosity Coefficients of Liquid Lubricants", ASLE Transactions vol. 26, (1983) 1-10.

16. P.S.Y. Chu and A. Cameron, "Pressure Viscosity Characteristics of Lubricating Oils", Journal of the Institute of Petroleum vol. 48 (1962),147-155.

17. H.H. Zuidema, "The Performance of Lubricating Oils" Reinhold Publ., New York, (1952), 26-28.

18. A.N. Smith, "Turbine Lubricant Oxidation: Testing, Experience and Prediction" ASTM Technical Publication 916, 1983.

19. SAE Standard, Engine Viscosity Classification, SAE J300, 1989.

20. M. J. Neale The Tribology Handbook, Second edition, Butterworth Heinemann 2001.

21. M. K. Dubey, J Bijwe, SSV Ramakumar "PTFE based nano-lubricants" Wear, vol. 306 (2013), 80-88.

22. S.M. Alves, B.S. Barros, M.F. Trajano, K.S.B. Ribeiro, E. Moura "Tribological behavior of vegetable oil-based lubricants with nanoparticles of oxides in boundary lubrication conditions" Tribology International, vol. 65, (2013) 28-36.

23. Z. Tang, S. Li "A review of recent developments of friction modifiers for liquid lubricants (2007-present)". Curr Opin Solid State Mater Sci. vol. 18, (2014), 119-139.

24. A. B. Hernández, R. González, D. Felgueroso "Wear prevention behaviour of nanoparticle suspension under extreme pressure conditions" Wear vol. 263 (7-12 SPEC. ISS.) (2007), 1568-1574.

25. J. Padgurskas, R. Rukuiza, I. Prosyčevas, R. Kreivaitis "Tribological properties of lubricant additives of Fe, Cu and Co nanoparticles" Tribology International. vol. 60 (2013), 224-232.

26. W. Dai, B. Kheireddin, H. Gao, H. Liang "Roles of nanoparticles in oil lubrication" Tribology International, vol.102, (2016) 88-98.

27. S. Tarasov, A. Kolubaev, S. Belyaev, M. Lerner, F. Tepper "Study of friction reduction by nanocopper additives to motor oil" Wear. vol. 252(1-2) (2002)6 3-69.

28. S. Wang, S. Han, G. Xin "High-quality graphene directly grown on Cu nanoparticles for Cu-graphene nanocomposites" Mater Des. vol. 139 (2018)181-187.

29. H.L. Yu, Y. Xu, P.J. Shi "Characterization and nano-mechanical properties of tribofilms using Cu nanoparticles as additives" Surf Coatings Technol.vol. 203 (2008), 28-34.

30. H.D. Huang, J.P. Tu, L.P. Gan, C.Z. Li "An investigation on tribological properties of graphite nanosheets as oil additive" Wear vol. 261 (2006), 140-144.

31. S. Chaudhary, R.C. Singh RC, R. Chaudhary "Experimental Investigation of Influence of SiO_2 Nanoparticles on the Tribological and Rheological properties of 15W40 Lubricating Oil" Int J Eng Technol.vol 9 (2017), 4307-4314.

32. Y. Li, J.E. Zhou, S. Tung, E. Schneider, S. Xi, "A review on development of nanofluid preparation and characterization" Powder Technology vol. 196.2 (2009) 89–101.

33. P. K. Namburu, D. K. Das, K. M. Tanguturi, R. S. Vajjha, "Numerical study of turbulent flow and heat transfer characteristics of nanofluids considering variable properties" International Journal of Thermal Science vol. 48, (2009) 290–302.

34. T. Yousefi, F. Veysia, E. Shojaeizadeha, S. Zinadinib, "An experimental investigation on the effect of Al_2O_3-H_2O nanofluid on the efficiency of flat-plate solar collectors" Renewable. Energy, vol. 39 (2012) 293-298.

35. W. Williams, J. Buongiorno, L.W. Hu., "Experimental investigation of turbulent convective heat transfer and pressure loss of alumina/water and zirconia/water nanoparticle colloids (nanofluids) in horizontal tubes", Journal of Heat Transfer vol. 130, (2008) 040301.1–044503.4.

36. C. Tao, B. Wang, G.C. Barber, J.D. Schall, H. Lan "Tribological behaviour of SnO_2 nanoparticles as an oil additive on brass" Lubr Sci., (2018), 1-9.

37. J. Guo, G.C Barber, D.J Schall, Q. Zou, S.B. Jacob SB "Tribological properties of ZnO and WS_2nanofluids using different surfactants" Wear, vol. 382, (2017), 8-14.

38. L. Peña-Parás, J. Taha-Tijerina, L. Garza, D. M. Cortés, R. Michalczewski, C. Lapray "Effect of CuO and Al_2O_3 nanoparticle additives on the tribological behavior of fully formulated oils" Wear. 2015;332-333:1256-1261.

39. Hernández Battez A, Viesca JL, González R, Blanco D, Asedegbega E, Osorio A. Friction reduction properties of a CuO nanolubricant used as lubricant for a NiCrBSi coating. Wear vol. 268, (2010), 325-328.

40. P.C. Hiemenz, M. Dekker, Principles of colloid and surface chemistry, Second Edition, Dekker, New York, 1986.

41. D. Wu, H. Zhu, L. Wang, L. Liua, "Critical issues in nanofluids preparation, characterization and thermal conductivity", Current Nanoscience vol. 5, (2009), 103–112.

42. H. Chang, C. Jwo, P. Fan, S. Pai, "Process optimization and material properties for nanofluid manufacturing" International Journal of Advance Manufacturing Technology vol. 34, (2007), 300–306.

43. Y. Li, J.E. Zhou, S. Tung, E. Schneider, S. Xi, "A review on development of nanofluid preparation and characterization" Powder Technology vol. 196, (2009). 89–101.

44. S.K. Das, S.U.S. Choi, W.H. Yu, T. Pradeep, "Nanofluid: Science and Technology" Jhon Wiley & sons, (2008), 397.

45. E.J. Swanson, J. Tavares, S. Coulombe, "Improved dual-plasma process for the synthesis of coated or functionalized metal nanoparticles", IEEE Transactions on Plasma Science vol. 36, (2008), 886–887.

46. M. Zafarani, M. Taghi R. M., "Effect of temperature on volumetric and transport properties of nanofluids containing ZnO nanoparticles poly (ethylene glycol) and water", Journal of Chemical Thermodynamics vol. 54, (2012), 55–67.

47. M. Moosavi, K. Elaheh. Goharshadi, A. Youssefi, "Fabrication, characterization, and measurement of some physicochemical properties of ZnO nanofluids", International Journal of Heat Fluid Flow, vol. 31, (2010), 599-605.

48. V. S. Raykar, A. K. Singh, "Thermal and rheological behavior of acetylacetone stabilized ZnO nanofluids", Thermochimica Acta, vol. 502, (2010), 60–65.

49. Y. Wei, H. Xie, L. Chen, Y. Li, "Investigation of thermal conductivity and viscosity of ethylene glycol based ZnO nanofluid", Thermochimica Acta, vol. 491, (2009) 92–96.

50. S.J. Chung, J.P. Leonard, I. Nettleship, J.K. Lee, Y. Soong, D.V. Martello, M.K. Chyu, "Characterization of ZnO nanoparticle suspension in water: effectiveness of ultrasonic dispersion", Powder Technology, vol. 194, (2009), 75-80.

51. G. J. Lee, C. K. Kim, M. K. Lee, C. K. Rhee, S. Kim, C. Kim, "Thermal conductivity enhancement of ZnO nanofluid using a one-step physical method", Thermochimica Acta, vol. 542, (2012), 24-27.

52. M. Kole, T.K. Dey, "Thermophysical and pool boiling characteristics of ZnO-ethylene glycol nanofluids", International Journal of Thermal Science, vol. 62, (2012), 61–70.

53. K.S. Suganthi, K.S. Rajan, "Temperature induced changes in ZnO–water nanofluid: zeta potential, size distribution and viscosity profiles", International Journal of Heat Mass Transfer vol. 55, (2012), 7969–7980.

54. X. F. Yang, Z. H. Liu, "Pool boiling heat transfer of functionalized nanofluid under sub-atmospheric pressures", International Journal of Thermal Science vol. 50, (2011), 2402–2412.

55. V. E. Timofeeva, M. R. Moravek, D. Singh, "Improving the heat transfer efficiency of synthetic oil with silica nanoparticles", Journal of Colloid Interface Science, vol. 364, (2011), 71–79.

56. P. D. Kulkarni, D. K. Das, R. S. Vajjha, "Application of nanofluids in heating buildings and reducing pollution", Applied Energy, vol. 86, (2009), 2566–2573.

57. A. Kanjirakat, S. Reza, J. Yu, K. Seokwon, J. Saeil, D.Banerjee, "Experimental study of forced convective heat transfer of nanofluids in a microchannel", International Communications in Heat Mass Transfer, vol. 39, (2012). 1325–1330.

58. A.A.R. Darzi, M. Farhadi, K. Sedighi, R. Shafaghat, K. Zabihi, "Experimental investigation of turbulent heat transfer and flow characteristics of SiO_2/water nanofluid within helically corrugated tubes", International Communications in Heat Mass Transfer, vol. 39, (2012), 1425-1434.

59. S. A. Fazeli, S. M. Hashemi, H. Zirakzadeh, M. Ashjaee, "Experimental and numerical investigation of heat transfer in a miniature heat sink utilizing silica nanofluid", Superlattices and Microstructures, vol. 51, (2012), 247–264.

60. M. D. Byrne, R.A. Hart, A.K. da Silva, "Experimental thermalehydraulic evaluation of CuO nanofluids in microchannels at various concentrations with and without suspension enhancers", International Journal of Heat Mass Transfer, vol. 55, (2012), 2684-2691.

61. S. W. Lee, S. D. Park, I. C. Bang, "Critical heat flux for CuO nanofluid fabricated by pulsed laser ablation differentiating deposition characteristics", International Journal of Heat Mass Transfer. vol. 55. (2012), 6908–6915.

62. K. R. Priya, K.S. Suganthi, K.S. Rajan, "Transport properties of ultra-low concentration CuO–water nanofluids containing non-spherical nanoparticles", International Journal of Heat Mass Transfer, vol. 55, (2012). 4734–4743.

63. S. Harikrishnan, S. Kalaiselvam, "Preparation and thermal characteristics of CuO–oleic acid nanofluids as a phase change material", Thermochimica Acta, vol. 533 (2012), 46–55.

64. S. Suresh, M. Chandrasekar, S. C. Sekhar, "Experimental studies on heat transfer and friction factor characteristics of CuO/water nanofluid under turbulent flow in a helically dimpled tube", Experimental Thermal and Fluid Science, vol. 35, (2011), 542-549.

65. N. Kannadasan, K. Ramanathan, S. Suresh, "Comparison of heat transfer and pressure drop in horizontal and vertical helically coiled heat exchanger with CuO/water based nano fluids", Experimental Thermal and Fluid Science, vol. 42, (2012), 64–70.

66. M. Saeedinia, M.A. Akhavan-Behabadi, M. Nasr, "Experimental study on heat transfer and pressure drop of nanofluid flow in a horizontal coiled wire inserted tube under constant heat flux", Experimental Thermal and Fluid Science, vol. 36, (2012), 158-168.

67. M. H. Chang, H. S. Liu, C. Y. Tai, "Preparation of copper oxide nanoparticles and its application in nanofluid", Powder Technology, vol. 207, (2011), 378-386.

68. Z. H. Liu, Y. Y. Li, R. Bao, "Thermal performance of inclined grooved heat pipes using nanofluids", International Journal of Thermal Science, vol. 49, (2010), 1680-1687.

69. S. K. Sonawane, K. Patankar, A. Fogla, B. Puranik, U. Bhandarkar, S. S. Kumar, "An experimental investigation of thermo-physical properties and heat transfer performance of Al_2O_3-aviation turbine fuel nanofluids", Applied Thermal Engineering, vol. 31, (2011), 2841-2849.

70. P. E. Gharagozloo, K. E. Goodson, "Temperature-dependent aggregation and diffusion in nanofluids, International Journal of Heat Mass Transfer, vol. 54, (2011), 797-806.

71. Y. H. Hung, T. Teng, B. Lin, "Evaluation of the thermal performance of a heat pipe using alumina nanofluids", International Communications in Heat Mass Transfer, vol. 44, (2013), 504–511.

72. S. Suresh, P. Selvakumar, M. Chandrasekar, V. S. Raman, "Experimental studies on heat transfer and friction factor characteristics of Al_2O_3/water nanofluid under turbulent flow with spiraled rod inserts", Chemical Engineering and Processing: Process Intensification, vol. 53, (2012), 24–30.

73. M. P. Beck, T. Sun, A.S. Teja, "The thermal conductivity of alumina nanoparticles dispersed in ethylene glycol", Fluid Phase Equilibria, vol. 260, (2007). 275–278.

74. S. Soltani, S. Etemad, J. Thibault, "Pool boiling heat transfer of non-Newtonian nanofluids", International Communications in Heat Mass Transfer, vol. 37, (2010), 29–33.

75. Q. Jian, W. Hui-ying, P. Cheng, "Thermal performance of an oscillating heat pipe with Al_2O_3–water nanofluids", International Communications in Heat Mass Transfer. vol. 37, (2010), 111–115.

76. P. K. Singh, P.V. Harikrishna, T. Sundararajan, S. K. Das, "Experimental and numerical investigation into the hydrodynamics of nanofluids in microchannels", Experimental Thermal and Fluid Science, vol. 42, (2012), 174-186.

77. C.J. Ho, W.K. Liu, Y.S. Chang, C.C. Lin, "Natural convection heat transfer of alumina-water nanofluid in vertical square enclosures: an experimental study", International Journal of Thermal Science, vol. 49, (2010). 1345-1353.

78. T. Teng, H. Hsu, H. Mo, C. Chen, "Thermal efficiency of heat pipe with alumina nanofluid", Journal of Alloys Compounds, vol. 504, (2010), 380-S384.

79. T. Yousefi, F. Veysia, E. Shojaeizadeha, S. Zinadinib, "An experimental investigation on the effect of Al_2O_3-H_2O nanofluid on the efficiency of flat-plate solar collectors", Renewable Energy, 39, (2012), 293-298.

80. M.M. Heyhat, F. Kowsary, A.M. Rashidi, M.H. Momenpour, A. Amrollahi, "Experimental investigation of laminar convective heat transfer and pressure drop of water-based Al_2O_3 nanofluids in fully developed flow regime", Experimental Thermal and Fluid Science, vol. 44, (2013), 483-489.

81. J. Lee, K. S. Hwang, S. P. Jang, B. H. Lee, J. H. Kim, Choi, C. J. Choi, "Effective viscosities and thermal conductivities of aqueous nanofluids containing low volume concentrations of Al_2O_3 nanoparticles", International Journal of Heat Mass Transfer, vol. 51, (2008), 2651-2656.

82. S. D. Pandey, V.K. Nema, "Experimental analysis of heat transfer and friction factor of nanofluid as a coolant in a corrugated plate heat exchanger", Experimental Thermal and Fluid Science, vol. 38, (2012), 248-256.

83. R. N. Hegde, S. S. Rao, R.P. Reddy, "Studies on nanoparticle coating due to boiling induced precipitation and its effect on heat transfer enhancement on a vertical cylindrical surface", Experimental Thermal and Fluid Science, vol. 38, (2012), 229-236.

84. E. Esmaeilzadeh, H. Almohammadi, Sh. Nasiri Vatan, A.N. Omrani, "Experimental investigation of hydrodynamics and heat transfer characteristics of Al_2O_3/water under laminar flow inside a horizontal tube", International Journal of Thermal Science, vol. 63, (2013), 31-37.

85. R. Jacob, T. Basak, S.K. Das, "Experimental and numerical study on microwave heating of nanofluids", International Journal of Thermal Science, vol. 59, (2012), 45-57.

86. S. Mo, Y. Chen, L. J.ia, X. Luo, "Investigation on crystallization of TiO2ewater nanofluids and deionized water", Applied Energy, vol. 93, (2012), 65-70.

87. L. Fedele, L. Colla, S. Bobbo, "Viscosity and thermal conductivity measurements of water-based nanofluids containing titanium oxide nanoparticles", International Journal of Refrigeration, vol. 35, (2012), 1359-1366.

88. M.H. Kayhani, H. Soltanzadeh, M.M. Heyhat, M. Nazari, F. Kowsary, "Experimental study of convective heat transfer and pressure drop of TiO_2/water nanofluid", International Communications in Heat Mass Transfer, vol. 39, (2012), 456–462.

89. W. Duangthongsuk, S. Wongwises, "An experimental study on the heat transfer performance and pressure drop of TiO_2–water nanofluids flowing under a turbulent flow regime", International Journal of Heat Mass Transfer, vol. 53, (2010), 334–344.

90. Y. He, Y. Jin, H. Chen, Y. Ding, D. Cang, H. Lu, "Heat transfer and flow behaviour of aqueous suspensions of TiO_2 nanoparticles (nanofluids) flowing upward through a vertical pipe", International Journal of Heat Mass Transfer, vol. 50, (2007), 2272-2281.

91. S.M.S. Murshed, K.C. Leong, C. Yang, "Enhanced thermal conductivity of TiO_2–water based nanofluids", International Journal of Thermal Science, vol. 44, (2005), 367–373.

92. A.R. Sajadi, M.H. Kazemi, Investigation of turbulent convective heat transfer and pressure drop of TiO_2/water nanofluid in circular tube, International Communications in Heat Mass Transfer 38 (10) (2011) 1474–1478.

93. A.A. Arani, J. Amani, "Experimental study on the effect of TiO_2-water nanofluid on heat transfer and pressure drop", Experimental Thermal and Fluid Science, vol. 42, (2012), 107-115.

94. H. Chen, Y. Ding, A. Lapkin, "Rheological behavior of nanofluids containing tube/rod-like nanoparticles", Powder Technology, vol. 194, (2009), 132-141.

95. M. Abareshi, E. K. Goharshadi, S. M. Zebarjad, H. K. Fadafan, A. Youssefi, "Fabrication, characterization and measurement of thermal conductivity of Fe3O4 nanofluids", Journal of Magnatism and Magnetic Materials, vol. 322, (2010), 3895-3901.

96. Q. Li, Y. Xuan, J. Wang, "Experimental investigations on transport properties of magnetic fluids", Experimental Thermal and Fluid Science, vol. 30, (2005), 109-116.

97. W. Yu, H. Xie, L. Chen, Y. Li, "Enhancement of thermal conductivity of kerosene-based Fe_3O_4 nanofluids prepared via phase-transfer method", Colloids and Surfaces: A Physicochemical and Engineering Aspects, vol. 355, (2010), 109-113.

98. L. S. Sundar, M.T. Naik, K.V. Sharma, M.K. Singh, T. S. Reddy, "Experimental investigation of forced convection heat transfer and friction factor in a tube with Fe_3O_4 magnetic nanofluid", Experimental Thermal and Fluid Science, vol. 37, (2012), 65-71.

99. M. Sheikhbahai, M. N. Esfahany, N. Etesami, "Experimental investigation of pool boiling of Fe_3O_4/ethylene glycol water nanofluid in electric field", International Journal of Thermal Science, vol. 62, (2012), 149-153.

100. L. S. Sundar, E. V. Ramana, M.K. Singh, A.C.M. De Sousa, "Viscosity of low volume concentrations of magnetic Fe_3O_4 nanoparticles dispersed in ethylene glycol and water mixture", Chemical Physics Letters, vol. 554, (2012), 236-242.

101. F. Asadzadeh, M. Nasr Esfahany, N. Etesami, "Natural convective heat transfer of Fe_3O_4/ethylene glycol nanofluid in electric field", International Journal of Thermal Science vol. 62, (2012), 114-119

102. T. X. Phuoc, M. Massoudi, "Experimental observations of the effects of shear rates and particle concentration on the viscosity of Fe_2O_3-deionized water nanofluids", International Journal of Thermal Science, vol. 48, (2009), 1294-1301.

103. M. Abareshi, S. H. Sajjadi, S. M. Zebarjad, E. K. Goharshadi, "Fabrication, characterization, and measurement of viscosity of α-Fe_2O_3-glycerol nanofluids", Journal of Molecular Liquids, vol. 163, (2011), 27-32.

104. S. Guo, Y. Li, J. Jiang, H. Xie, "Nanofluids containing α-Fe2O3 nanoparticles and their heat transfer enhancements", Nanoscale Research Letters, vol. 5, (2010), 1222-1227.

105. W. Yu., H. Xie, Y. Li, L. Chen, "Experimental investigation on thermal conductivity and viscosity of aluminum nitride nanofluid", Particuology, vol. 9, (2011), 187–191.

106. M. Wozniak, A. Danelska, D. Kata, M. Szafran, "New anhydrous aluminum nitride dispersions as potential heat-transferring media", Powder Technology, vol. 235, (2012), 717–722.

107. P. Hu, W. Shan, F. Yu, Z. Chen, "Thermal conductivity of AlN-ethanol nanofluids", International Journal of Thermophysics, vol. 29, (2008), 1968-1973.

108. Y. Xuan, Q. Li, "Heat transfer enhancement of nanofluids", International Journal of Heat Fluid Flow vol. 21, (2000), 58–64.

109. X.F. Li, D.S. Zhu, X.J. Wang, N. Wang, J.W. Gao, H. Li, "Thermal conductivity enhancement dependent pH and chemical surfactant for Cu-H2O nanofluids", Thermochimica Acta, vol. 469, (2008), 98-103.

110. X. F. Li, D.S. Zhu, X. J. Wang, "Evaluation on dispersion behavior of the aqueous copper nano-suspensions", Journal of Colloid Interface Science, vol. 310, (2007), 456-463.

111. H. Peng, G. Ding, H. Haitao, "Effect of surfactant additives on nucleate pool boiling heat transfer of refrigerant-based nanofluid", Experimental Thermal and Fluid Science vol. 35, (2011), 960–970.

112. R. Kathiravan, R. Kumar, A. Gupta, R. Chandra, "Preparation and pool boiling characteristics of copper nanofluids over a flat plate heater", International Journal of Heat Mass Transfer, vol. 53, (2010), 1673-1681.

113. M. Kole, T.K. Dey, "Thermal performance of screen mesh wick heat pipes using water based copper nanofluids", Applied Thermal Engineering, vol. 50, (2013), 763–770.

114. H. E. Patel, S. K. Das, T. Sundararajan, A. S Nair, B. George, T. Pradeep, "Thermal conductivities of naked and monolayer protected metal nanoparticle based nanofluids: manifestation of anomalous enhancement and chemical effects", Appllied Physics Letters, vol. 83, (2003), 2931–2933.

115. L. G. Asirvatham, B. Raja, D. M. Lal, S. Wongwises, "Convective heat transfer of nanofluids with correlations", Particuology, vol. 9, (2011), 626-631.

116. T. Parametthanuwat, S. Rittidech, A. Pattiya, "A correlation to predict heat-transfer rates of a two-phase closed thermosyphon (TPCT) using silver nanofluid at normal operating conditions", International Journal of Heat Mass Transfer vol. 53, (2010), 4960–4965.

117. E. Tamjid, B. H. Guenther, "Rheology and colloidal structure of silver nanoparticles dispersed in diethylene glycol", Powder Technology, vol. 197, (2010), 49–53.

118. P. Sharma, H. Baek, T. Cho, S. Park, K. B. Lee, "Enhancement of thermal conductivity of ethylene glycol based silver nanofluids", Powder Technology, vol. 208, (2011), 7-19.

119. R. Hajian, M. Layeghi, K. A. Sani, "Experimental study of nanofluid effects on the thermal performance with response time of heat pipe", Energy Conversion Management. vol. 56, (2012). 63–68.

120. T. Parametthanuwat, S. Rittidech, A. Pattiya, "A correlation to predict heat transfer rates of a two-phase closed thermosyphon (TPCT) using silver nanofluid at normal operating conditions", International Journal of Heat Mass Transfer, vol. 53, (2010), 4960-4965.

121. G. Paul, S. Sarkar, T. Pal, P.K. Das, I. Manna, "Concentration and size dependence of nano-silver dispersed water based nanofluids", Journal of Colloid Interface Science, vol. 371, (2012), 20-27.

122. G. Paul, T. Pal, I. Manna, Thermo-physical property measurement of nanogold dispersed water based nanofluids prepared by chemical precipitation technique, Journal of Colloid Interface Science 349 (2010) 434-437

123. S. chaudhary, Sonia, R.C.Singh, R. Chaudhary "Analysis and Synthesis of Gold Nano Particles International journal of advanced production and industrial engineering" vol. 1, 2016, 45-50

124. C. Choi, H.S. Yoo, J.M. Oh, "Preparation and heat transfer properties of nanoparticle-in-transformer oil dispersions as advanced energy-efficient coolants", Current Applied Physics vol. 8, (2008), 710-712.

125. S.H. Kim, S.R. Choi, D. Kim, "Thermal conductivity of metal-oxide nanofluids: particle size dependence and effect of laser irradiation", Journal of Heat Transfer, vol. 129, (2007) 298-307.

126. A. T. Utomo, H. Poth, P.T. Robbins, A. W. Pacek, "Experimental and theoretical studies of thermal conductivity, viscosity and heat transfer coefficient of titania and alumina nanofluids", International Journal of Heat Mass Transfer, vol. 55, (2012), 7772-7781.

127. G. A. Longo, C. Zilio, "Experimental measurement of thermophysical properties of oxideewater nano-fluids down to ice-point", Experimental Thermal and Fluid Science, vol. 35, (2011), 1313-1324.

128. J. Qu, H Wu, "Thermal performance comparison of oscillating heat pipes with SiO2/water and Al2O3/water nanofluids", International Journal of Thermal Science, vol. 50, (2011) 1954-1962.

129. P. Zhang, W. Lu, X. Liu, W, Zhai, M. Zhou, X. Jiang, "A comparative study on torsional fretting and torsional sliding wear of CuNiAl under different lubricated conditions", Tribology International, vol. 117, (2018), 78–86.

130. O. A. Alawi, N. A. C. Sidik, M. Beriache, "Applications of nanorefrigerant and nanolubricants in refrigeration, air-conditioning and heat pump systems: A review", International Communications in Heat and Mass Transfer, vol. 68. (2015). 91–97.

131. H. Wu, L. Qin, G. Dong, M. Hua, S. Yang, J. Zhang, "An investigation on the lubrication mechanism of MoS2 nano sheet in point contact: The manner of particle entering the contact area", Tribology International, vol. 107, (2017), 48–55.

132. W. Z. Xia, J. Zhao, H. Wu, S. Jiao, X. Zhao, X. Zhang, J. Xu, Z. Jiang, "Analysis of oil-in-water based nano lubricants with varying mass fractions of oil and TiO2 nanoparticles", Wear, vol. 280, (2013), 458-467

133. N. Salah, A. Alshahrie, M. Sh. A. Wahab, N. D. Alharbi, Z. H. Khan, "Carbon nanotubes of oil fly ash integrated with ultrathin CuO nanosheets as effective lubricant additives", Diamond & Related Materials, vol. 78, (2017), 97–104.

134. M. Asnidaa, S. Hishama, N.W. Awanga, A.K. Amirruddina, M.M. Noora,□, K. Kadirgamaa, D. Ramasamya,b,□, G. Najafic, F. Tarlochan, Copper (II) oxide nanoparticles as additve in engine oil to increase the durability of piston-liner contact, Fuel 212 (2018) 656–667.

135. M. N. A. W. M. Yazid, N. A. C.heSidik, R. Mamat, G. Najafi, "A review of the impact of preparation on stability of carbon nanotube nanofluids", International Communications in Heat and Mass Transfer, vol. 78(2016), 253–263.

136. N. Bena, Q. Zhanga, D. Menga, M. Lee, "Analysis of real contact area and re-lubrication in oscillating bulk forming process by corrosion method", Journal of Materials Processing Tech., vol. 253, (2018), 178–194.

137. Y. Hu, X. Meng, Y. Xie, "A new efficient flow continuity lubrication model for the piston ring-pack with consideration of oil storage of the cross-hatched texture", Tribology International, vol. 119, (2018), 443–463.

138. A.A.M. Redhwan, W.H Azmi, M.Z. Sharif, R. Mamat, N.N.M. Zawawi, "Comparative study of thermo-physical properties of SiO_2 and Al_2O_3 nanoparticles dispersed in PAG lubricant", Applied Thermal Engineering, vol. 116, (2017), 823–832.

139. N. A. C. Sidik, M. N. A. Witri M. Yazid, S. Samion, "A review on the use of carbon nanotubes nanofluid for energy harvesting system", International Journal of Heat and Mass Transfer, vol. 111, (2017), 782–794.

140. W. Zhang, M. Yi, G. Xiao, J. Ma, G. Wu, C. Xu, "Al2O3-coated h-BN composite powders and as-prepared Si3N4-based self lubricating ceramic cutting tool material", International Journal of Refractory Metals & Hard Materials, vol. 71, (2018), 1–7.

141. W. Dai, B. Kheireddin, H. Gao, H. Liang, "Roles of nanoparticles in oil lubrication", Tribology International, vol. 102, (2016), 88–98.

142. N.N.M. Zawawi, W.H. Azmi, A.A.M. Redhwan, M.Z. Sharif, K.V. Sharma, "Thermo-physical properties of Al2O3-SiO2/PAG composite nanolubricant for refrigeration system, international journal of refrigeration, vol.80, (2017), 1–10.

143. A. I. EL-Seesy, A. K. A. Rahman, M. Bady, S. Ookawar, "The Influence of Multi-Walled Carbon Nanotubes Additives into Non-Edible Biodiesel-Diesel Fuel Blend on Diesel Engine Performance and Emissions", Energy Procedia, vol.100, (2016),166 – 172.

144. S. P. Darminesh, N. A. C. Sidik, G. Najafi, R. Mamat, T. L. Ken, Y. Asako, "Recent development on biodegradable nanolubricant: A review", International Communications in Heat and Mass Transfer, vol. 86, (2017), 159–165.

145. A. Alasli, T. Evgin, A. Turgut, "Re-dispersion ability of multi wall carbon nanotubes within low viscous mineral oil", Colloids and Surfaces A, vol. 538, (2018), 219–228.

146. J. Diabb, C.A.Rodríguez, N. Mamidi, J.A. Sandoval, J.T. Tijerin, O. Martínez-Romero, A.E. Zúñiga, "Study of lubrication and wear in single point incremental sheet forming (SPIF) process using vegetable oil nanolubricants", Wear, vol.376-377, (2017), 777–785.

147. M.A. Kedzierski, R. Brignoli, K.T. Quine, J.S. Brown, "Viscosity, density, and thermal conductivity of aluminum oxide and zinc oxide nanolubricants", international journal of refrigeration, vol.74, (2017), 3–11.

148. M. Laad, V. K. S. Jatti, "Titanium oxide nanoparticles as additives in engine oil", Journal of King Saud University – Engineering Sciences (2016).

149. R. Greenberg., G. Halperin, I. Etsion, R. Tenne. "The effect of WS 2 nanoparticles on friction reduction in various lubrication regimes" Tribology Letters, vol. 17, (2004) 179–186.

150. Z. Tang, S. Li. "A review of recent developments of friction modifiers for liquid lubricants (2007-present)" Curr. Opin. Solid State Mater. Sci., vol. 18, (2014) 119–139

151. P. Ussa, F. Dassenoy, B. Vacher, T. Le "Tribology International WS$_2$ nanoparticles anti-wear and friction reducing properties on rough surfaces in the presence of ZDDP additive" Tribiology Int. vol. 102, (2016), 213–221.

152. L. Rapoport, L., Leshchinsky V., Lapsker I., Volovik Y., Nepomnyashchy O., Lvovsky M., Popovitz-Biro R., Feldman Y, Tenne R., "Tribological properties of WS$_2$ nanoparticles under mixed lubrication" Wear, vol. 255, pp: 785–793 (2003).

153. I. Lahouij, J. Dassenoy, L. Knoop, J. Martin, B. Vacher "In Situ TEM Observation of the Behavior of an Individual Fullerene-Like MoS$_2$ Nanoparticle in a Dynamic Contact" Tribology Letter, vol. 42, (2011), 133–140,

154. Y. Xu, E. Hu, K. Hu, Y. Xu, X. Hu, "Tribology International Formation of an adsorption fi lm of MoS 2 nanoparticles and dioctyl sebacate on a steel surface for alleviating friction and wear" Tribiology Int. vol. 92, (2015), 172–183.

155. I. Lahouij, "Real time TEM imaging of compression and shear of single fullerene-like MoS2 nanoparticle" Tribology Letter, vol. 45, (2012), 131–141.

156. V.N. Bakunin, A. Yu, G.N. Kuzmina, O.P. Parenago, "Synthesis and application of inorganic nanoparticles as lubricant components – a review" Journal of Nanoparticle Research, vol. 6, (2004), 273–284.

157. Y. long, X. Yi., "Tribological properties and lubricating mechanisms of Cu nanoparticles in lubricant" Transactions of Nonferrous Metals Society of China, vol. 18, (2008) 636-641.

158. Vivek, W. Khond, V. Kriplani "Effect of nanofluid additives on performances and emission of emulsified diesel and biodiesel fueled stationary CI engine: a comprehensive review" Renewable and sustainable energy reviews, vol. 59, (2016) 1338-1348.

159. C. Castillo, A. Spikes, "Mechanism of action of colloidal solid dispersions" Journal of Tribology, vol. 125, (2001) 552–557.

160. E. SongfenG, S. Lei., Z. Guo, "Tribological properties of self-assembled gold nanoparticles on silicon with polydopamine as the adhesion layer" Applied Surface Science; vol. 292, (2014) 750– 755.

161. S. Nie, R. Emory, "Probing single molecules and single nanoparticles by surface-enhanced Raman scattering," Science, vol. 275, (1997), 1102–1106.

162. Y. Chen, Y. Zhang, S. Zhang, L. Yu, P. Zhang, Z. Zhang, "Preparation of nickel- based nanolubricants via a facile in situ one-step route and investigation of their tribological properties." Tribology international, vol. 51, (2013) 73–83.

163. A. Battez, R. Gonz´alez, J. Viesca., J. Fern´andez, A. Machadoc, R. Choud, J. Riba., "CuO, ZrO2 and ZnO nanoparticles as antiwear additive in oil lubricants", Wear, vol. 265, (2008), 422–428.

164. H. Ghaednia, L. Robert, J. Khodadadi," Experimental analysis of stable CuO nanoparticle enhanced lubricants", Journal of Experimental Nanoscience, vol. 10, (2011), 1–18.

165. Lin C., Wu M., "Continuous production of CuO nanoparticles in a rotating packed bed" Ceramics International, vol. 42, (2016), 2133–2139.

166. P. Parás, J. Tijerina, L. Garza, M. Cortés, R. Michalczewski, C. Lapray, "Effect of CuO and Al$_2$O$_3$ nanoparticle additives on the tribological behavior of fully formulated oils." Wear, vol. 333, (2015), 1256–1261.

167. R. Dinesh, M. Prasad, R. Kumar, N. Santharaj, J. Santhip, A. Raaj., "Investigation of Tribological and Thermophysical Properties of Engine Oil Containing Nano additives" Materials Today: Proceedings, vol. 3, (2016), 45 – 53.

168. S. Radice, S. Mischler, "Effect of electrochemical and mechanical parameters on the lubrication behaviour of Al$_2$O$_3$ nanoparticles in aqueous suspensions", Wear, vol. 261, (2006), 1032–1041.

`

169. T. Luo, X. Wei, H. Zhao, G. Cai, X. Zheng, "Tribology properties of Al2O$_3$/TiO$_2$ nanocomposites as lubricant additives". Ceramics International, vol. 40, (2014) 10103–10109.

170. H. Chu, W. Hsu, J. Lin, "The anti-scuffing performance of diamond nano-particles as an oil additive", Wear, vol. 268, (2010) 960–967.

171. M. Shen, B. Luo, S. Wen, "The tribological properties of oils added with diamond nano-particles" Tribology Transactions, vol. 44, (2008) 494–498.

172. C. Lee, Y. Hwang., Y. Choi, J. Lee, C. Choi, J. Oh, "A Study on the tribological characteristics of graphite nanolubricants", International journal of precision engineering and manufacturing, vol. 10, (2009) 85-90 (2009).

173. J. Cornelio, P. Cuervo, L.Palacio, J. Romero, A. Toro, "Tribological properties of carbon nanotubes as lubricant additive in oil and water for a wheel–rail system" journal of material research and technology, vol. 5, (2016) 68–76.

174. J. Yang, H. Yao, Y. Liu, Y. Zhang, "Synthesis and Tribological properties of WSe$_2$ Nanorods" Nanoscale Res Lett, vol. 3, (2008), 481–485.

175. D. Guo, G. Xie , J. Luo, "Mechanical properties of nanoparticles: basics and applications". Journal of Physics, vol. 47, (2014) 1-25.

176. X. Xu, J. Luo, X. Lu, C. Zhang, "Effect of Nanoparticle Impact on Material Removal", Tribology Transactions, vol. 51, (2008), 718-722.

177. H. Xie, B. Jiang, J. He, X. Xia, F. Pan, "Lubrication performance of MoS2 and SiO2 nanoparticles as lubricant additives in magnesium alloy-steel contacts" Tribology International, vol. 93, (2016), 63-70.

178. J. Panda, J. Bijwe, R Pandey, "Role of micro and nanoparticles of hBN as secondary solid lubricant for improving tribo-potential of PAEK composite" Tribology International, vol. 130, (2019) 400-412.

179. E. Rico, I. Minondo, D. Cuervo, "The effectiveness of PTFE nanoparticle powder as an EP additive to mineral base oils" Wear, vol. 262, (2007), 1399-1406.

180. E. Rico, I. Minondo, D. Cuervo, "Rolling contact fatigue life of AISI 52100 steel balls with mineral and synthetic polyester lubricants with PTFE nanoparticle powder as an additive" Wear, vol. 266, (2009), 671-677.

181. N. Xu, M. Zhang, W. Li, G. Zhao, X. Wang, W. Liu., "Study on the selectivity of calcium carbonate nanoparticles under the boundary lubrication condition" Wear, vol 307, (2013) 35–43.

182. P. Rabaso, F. Ville, F. Dassenoy, M. Diaby, P. Afanasiev, J. Cavoret, "Boundary lubrication: influence of the size and structure of inorganic fullerene-like MoS2 nanoparticles on friction and wear reduction" Wear, vol. 320, (2014), 161–178.

183. J. Pottuz, J. Martin, F. Dassenoy, M. Belin, G. Montagnac, B. Reynard, "Pressure-induced exfoliation of inorganic fullerene-like WS_2 particles in a Hertzian contact". Applied Physics, vol. 99, (2006) 3524-3529.

184. W. Dai, B. Kheireddin, H. Gao, H. Liang, "Roles of nanoparticles in oil lubrication", Tribology International, vol.102, (2016), 88–98.

`

Appendix 1: Type of lubricant additives

Main Type	*Function and sub-types*
Acid neutralizers	Neutralise contaminating strong acids formed, for example, by combustion of high Sulphur fuels or, less often, by decomposition of active EP additives
Anti-foam	Reduces surface foam
Anti-oxidants	Reduce oxidation, Various types are: oxidation inhibitors, retarders; anti-catalyst metal deactivators, metal passivators
Anti-rust	Reduces rusting of ferrous surfaces swept by oil
Anti-wear agents	Reduce wear and prevent scuffing of agents rubbing surfaces under steady load operating conditions; the nature of the film is uncertain
Corrosion inhibition	Type (a) reduces corrosion of lead; type (b) reduces corrosion of cuprous metals
Detergents	Reduce or prevent deposits formed at high temperatures, e.g. in ic engines
Dispersants	Prevent deposition of sludge by dispersing a finely divided suspension of the insoluble material formed at low temperature
Emulsifier	Forms emulsions; either water-in-oil or oil-in-water according to type
Extreme Pressure	Prevents scuffing of rubbing surfaces under severe operating conditions, e.g. heavy shock load, by formation of a mainly inorganic surface film
Oiliness	Reduces friction under boundary lubrication conditions; increases load-carrying capacity
Pour point depressant	Reduces pour point of paraffinic oils

`

Tackiness	Reduces loss of oil by gravity, e.g. from vertical sliding surfaces, or by centrifugal forces
Viscosity index improvers	Reduce the decrease in viscosity due to increase of temperature

Appendix 2: Type of additives for different machinery

Type of machinery	Usual base oil type	Usual additives	Special Requirements
Food processing	Medicinal white oil	None	Safety in case of ingestion
Oil hydraulic	Paraffinic down to about -20°C, naphthenic below	Anti-oxidant, Anti-rust, Anti-wear, Anti-foam, Pour point depressant	Minimum viscosity changes with temperature; minimum wear of steel/steel
Steam and gas turbines	Paraffinic or naphthenic distillates	Anti-oxidants, Anti-rust	Ready separation from water, good oxidation stability
Steam engine cylinders	Unrefined or refined residual or high-viscosity distillates	None or fatty oil	Maintenance of oil film no hot surfaces; resistance to washing away by wet steam
Air compressor cylinders	Paraffinic or naphthenic distillates	Anti-oxidants, Anti-rust	Low deposit formation tendency

`

Gears (steel/steel)	Paraffinic or naphthenic	Anti-oxidant, Anti-wear, EP, Anti-foam, Pour point depressant	Protections against abrasion and scuffing
Gears (steel/bronze)	Paraffinic	Oiliness, Anti-oxidants	Reduce friction, temperature rise, wear and oxidation
Machine tool slideways	Paraffinic or naphthenic	Oiliness, tackiness	Maintains smooth sliding at very low speed. Keeps film on vertical surfaces
Hermetically sealed refrigerators	Naphthenic	None	Good thermal stability, miscibility with refrigerant, low flow point
Diesel Engines	Paraffinic or naphthenic	Detergent, Dispersant, Anti-oxidant, Acid-neutralizer Anti-foam, Anti-wear, Corrosion inhibitor	Vary with type of engine thus affecting additive combination

Appendix 3: Results of thermal Imaging camera

Effect of Graphite nanoparticles on Temperature of tribopair

Lubricant	Temperature (^{0}C)	Test Condition	Sliding Speed (m/s)				
			3.663	5.2631	7.3260	10.4712	13.6054
Fresh 15W 40	Minimum	Start	32.0	31.8	32.1	31.9	32.3
		End	32.8	32.9	33.5	33.6	34.0
	Average	Start	32.8	32.7	32.8	33.0	32.9
		End	36.4	36.8	37.1	37.5	37.6
	Maximum	Start	34.2	35.4	35.0	34.0	34.5
		End	37.4	38.9	39.1	39.2	40.8
0.2 % Graphite nanoparticles	Minimum	Start	32.2	32.0	31.9	32.1	32.2
		End	32.8	32.9	32.8	33.6	33.8
	Average	Start	32.9	32.5	32.8	32.7	32.7
		End	36.4	36.2	37.0	36.9	37.2
	Maximum	Start	34.7	35.0	35.2	34.9	34.4
		End	37.5	37.9	38.7	40.2	40.4
0.4 % Graphite nanoparticles	Minimum	Start	32.0	31.8	32.1	31.9	32.3
		End	32.8	32.9	33.5	33.6	34.0
	Average	Start	32.8	32.7	32.8	33.0	32.9
		End	36.4	36.8	37.1	37.5	37.6
	Maximum	Start	34.2	35.4	35.0	34.0	34.5
		End	37.4	38.9	39.1	39.2	40.8
0.6 % Graphite nanoparticles	Minimum	Start	31.0	31.6	31.1	31.9	31.8
		End	31.8	32.6	32.2	33.4	33.4
	Average	Start	31.4	31.5	32.0	32.6	32.9
		End	35.4	35.6	35.9	37.0	37.4

Lubricant	Temperature (°C)	Test Condition					
	Maximum	Start	33.9	34.2	34.5	34.0	34.3
		End	36.4	36.9	37.1	38.5	39.9
0.8 % Graphite nanoparticles	Minimum	Start	31.2	31.9	32.0	32.7	32.2
		End	31.9	32.6	32.9	33.7	33.1
	Average	Start	32.4	32.8	32.9	33.3	33.1
		End	35.5	35.9	36.1	37.4	37.0
	Maximum	Start	34.0	35.1	35.0	34.8	34.7
		End	36.8	38.9	39.0	38.9	39.4
1.0 % Graphite nanoparticles	Minimum	Start	32.3	31.8	32.2	32.4	32.0
		End	32.9	32.4	33.1	33.3	33.0
	Average	Start	32.9	33.0	32.4	32.8	33.0
		End	35.8	36.0	35.2	35.4	36.7
	Maximum	Start	34.2	34.5	34.0	34.6	34.5
		End	36.7	37.9	38.2	38.8	39.0

Effect of SiO_2 nanoparticles on Temperature of tribopair

Lubricant	Temperature (°C)	Test Condition	Sliding Speed (m/s)				
			3.663	5.2631	7.3260	10.4712	13.6054
Fresh 15W 40	Minimum	Start	32.0	31.8	32.1	31.9	32.3
		End	32.8	32.9	33.5	33.6	34.0
	Average	Start	32.8	32.7	32.8	33.0	32.9
		End	36.4	36.8	37.1	37.5	37.6
	Maximum	Start	34.2	35.4	35.0	34.0	34.5
		End	37.4	38.9	39.1	39.2	40.8
0.2 % SiO_2 nanoparticles	Minimum	Start	31.6	31.4	31.5	31.6	31.7
		End	32.3	32.4	32.8	33.1	33.5
		Start	32.4	32.3	32.4	32.6	32.5

	Average	End	35.9	36.2	36.9	36.8	36.2
	Maximum	Start	35	35.3	35.2	34.6	34.5
		End	38.2	38.4	39.2	40.7	40.9
0.4 % SiO$_2$ nanoparticles	Minimum	Start	31.4	31.2	31.7	31.4	31.7
		End	32.3	32.4	33.0	33.1	33.5
	Average	Start	32.3	32.5	32.4	32.9	32.7
		End	35.9	36.8	37.0	37.4	37.6
	Maximum	Start	34.5	35.7	35	33.7	34.7
		End	37.9	39.4	39.6	39.7	41.2
0.6 % SiO$_2$ nanoparticles	Minimum	Start	30.4	31	30.7	31.4	31.2
		End	31.3	32.1	31.7	32.9	32.8
	Average	Start	30.9	31.3	31.6	32.5	32.7
		End	34.9	35.6	35.8	36.9	37.4
	Maximum	Start	34.2	34.5	34.5	33.7	34.5
		End	36.9	37.4	37.6	39.0	40.4
0.8 % SiO$_2$ nanoparticles	Minimum	Start	30.6	31.3	31.6	32.2	31.6
		End	31.4	32.1	32.4	33.2	33.3
	Average	Start	31.9	32.6	32.5	33.2	32.9
		End	35.0	35.9	36.2	37.3	37.1
	Maximum	Start	34.3	35.4	35	34.5	34.9
		End	37.3	39.4	39.5	39.4	39.9
1.0 % SiO$_2$ nanoparticles	Minimum	Start	31.7	31.2	31.8	31.9	31.4
		End	32.4	31.9	32.6	32.8	32.5
	Average	Start	32.4	32.8	32	32.7	32.8
		End	35.3	36.0	35.1	35.3	34.7
	Maximum	Start	34.5	34.8	34	34.3	34.7
		End	37.2	38.4	38.7	39.3	39.5

Effect of WS₂ nanoparticles on Temperature of tribopair

Lubricant	Temperature (⁰C)	Test Condition	Sliding Speed (m/s)				
			3.663	5.2631	7.3260	10.4712	13.6054
Fresh 15W 40	Minimum	Start	32.0	31.8	32.1	31.9	32.3
		End	32.8	32.9	33.5	33.6	34.0
	Average	Start	32.8	32.7	32.8	33.0	32.9
		End	36.4	36.8	37.1	37.5	37.6
	Maximum	Start	34.2	35.4	35.0	34.0	34.5
		End	37.4	38.9	39.1	39.2	40.8
0.2 % WS₂ nanoparticles	Minimum	Start	32	31.8	31.9	32	32.2
		End	32.7	32.8	33.1	33.5	33.8
	Average	Start	32.6	32.5	32.6	32.8	32.7
		End	36.1	36.4	37.1	37.4	37.4
	Maximum	Start	35.1	35.4	35.3	34.7	34.7
		End	38.1	38.5	39.3	40.8	41
0.4 % WS₂ nanoparticles	Minimum	Start	31.8	31.6	32.1	31.8	32.1
		End	32.7	32.8	33.4	33.5	33.9
	Average	Start	32.5	32.7	32.6	33.1	32.9
		End	36.1	37.0	37.2	37.6	37.6
	Maximum	Start	34.6	35.8	35.1	33.8	34.8
		End	37.9	39.5	39.6	39.8	41.4
0.6 % WS₂ nanoparticles	Minimum	Start	30.8	31.4	31.1	31.8	31.6
		End	31.8	32.5	32.2	33.4	33.3
	Average	Start	31.1	31.5	31.8	32.7	32.9
		End	35.1	35.8	36.0	37.1	37.6
	Maximum	Start	34.3	34.6	34.6	33.8	34.6
		End	36.9	37.4	37.7	39.1	40.5
0.8 % WS₂ nanoparticles	Minimum	Start	31	31.7	32	32.6	32
		End	31.8	32.6	32.8	33.6	34.8

Lubricant	Temperature	Test Condition					
	Average	Start	32.1	32.8	32.7	33.4	33.1
		End	35.2	36.1	36.2	37.5	35.2
	Maximum	Start	34.4	35.5	35.1	34.6	35
		End	37.3	39.4	39.5	39.4	39.9
1.0 % WS$_2$ nanoparticles	Minimum	Start	32.1	31.6	32.2	32.3	31.8
		End	32.8	32.3	33.1	33.2	32.8
	Average	Start	32.6	33	32.2	32.9	33
		End	35.5	36.2	35.3	35.5	35.9
	Maximum	Start	34.6	34.9	34.1	34.4	34.8
		End	37.2	38.4	38.7	39.2	39.5

Effect of Cu nanoparticles on Temperature of tribopair

Lubricant	Temperature (^{0}C)	Test Condition	Sliding Speed (m/s)				
			3.663	5.2631	7.3260	10.4712	13.6054
Fresh 15W 40	Minimum	Start	32.0	31.8	32.1	31.9	32.3
		End	32.8	32.9	33.5	33.6	34.0
	Average	Start	32.8	32.7	32.8	33.0	32.9
		End	36.4	36.8	37.1	37.5	37.6
	Maximum	Start	34.2	35.4	35.0	34.0	34.5
		End	37.4	38.9	39.1	39.2	40.8
0.2 % Cu nanoparticles	Minimum	Start	32.4	32.2	32.3	32.4	32.4
		End	33.2	33.3	33.2	34.0	34.2
	Average	Start	32.8	32.7	32.8	33	32.9
		End	36.4	36.7	37.4	37.3	37.7
	Maximum	Start	35.2	35.5	35.4	34.8	34.8
		End	38.1	38.4	39.3	40.8	41.0
0.4 % Cu nanoparticles	Minimum	Start	32.2	32	32.5	32.2	32.5
		End	33.2	33.3	33.9	34.0	34.4

	Average	Start	32.7	32.9	32.8	33.3	33.1
		End	36.4	37.3	37.5	37.9	38.1
	Maximum	Start	34.7	35.9	35.2	33.9	34.9
		End	38.0	39.5	39.7	39.8	41.4
0.6 % Cu nanoparticles	Minimum	Start	31.2	31.8	31.5	32.2	32
		End	32.2	33.0	32.6	33.8	33.8
	Average	Start	31.3	31.7	32	32.9	33.1
		End	35.4	36.1	36.3	37.4	37.9
	Maximum	Start	34.4	34.7	34.7	33.9	34.7
		End	37.0	37.5	37.7	39.1	40.5
0.8 % Cu nanoparticles	Minimum	Start	31.4	32.1	32.4	33	32.4
		End	32.3	33.0	33.3	34.1	33.5
	Average	Start	32.3	33	32.9	33.6	33.3
		End	35.5	36.4	36.5	37.8	37.5
	Maximum	Start	34.5	35.6	35.2	34.7	35.1
		End	37.4	39.5	39.6	39.5	40.0
1.0 % Cu nanoparticles	Minimum	Start	32.5	32	32.6	32.7	32.2
		End	33.3	32.8	33.5	33.7	33.4
	Average	Start	32.8	33.2	32.4	33.1	33.2
		End	35.8	36.5	35.6	35.8	36.2
	Maximum	Start	34.7	35	34.2	34.5	34.9
		End	37.3	38.5	38.8	39.4	39.6

Effect of CuO nanoparticles on Temperature of tribopair

Lubricant	Temperature (⁰C)	Test Condition	Sliding Speed (m/s)				
			3.663	5.2631	7.3260	10.4712	13.6054
Fresh 15W 40	Minimum	Start	32.0	31.8	32.1	31.9	32.3
		End	32.8	32.9	33.5	33.6	34.0
	Average	Start	32.8	32.7	32.8	33.0	32.9
		End	36.4	36.8	37.1	37.5	37.6
	Maximum	Start	34.2	35.4	35.0	34.0	34.5
		End	37.4	38.9	39.1	39.2	40.8
0.2 % CuO nanoparticles	Minimum	Start	32.8	32.6	32.7	32.8	32.8
		End	33.6	33.7	33.6	34.4	34.6
	Average	Start	33	32.9	33	33.2	33.1
		End	36.6	36.9	37.6	37.5	37.9
	Maximum	Start	35.3	35.6	35.5	34.9	34.9
		End	38.2	38.6	39.4	40.9	41.1
0.4 % CuO nanoparticles	Minimum	Start	32.6	32.4	32.9	32.6	32.9
		End	33.6	33.7	34.3	34.4	34.8
	Average	Start	32.9	33.1	33	33.5	33.3
		End	36.7	37.5	37.7	38.1	38.0
	Maximum	Start	34.8	36	35.3	34	35
		End	38.1	39.6	39.8	39.9	41.5
0.6 % CuO nanoparticles	Minimum	Start	31.6	32.2	31.9	32.6	32.4
		End	32.6	33.4	33.0	34.2	34.2
	Average	Start	31.5	31.9	32.2	33.1	33.3
		End	35.6	36.3	36.5	37.6	38.0
	Maximum	Start	34.5	34.8	34.8	34	34.8
		End	37.1	37.6	37.8	39.2	40.6
0.8 % CuO nanoparticles	Minimum	Start	31.8	32.5	32.8	33.4	32.8
		End	32.7	33.4	33.7	34.5	33.9

	Average	Start	32.5	33.2	33.1	33.8	33.5
		End	35.7	36.6	36.7	38.0	38.7
	Maximum	Start	34.6	35.7	35.3	34.8	35.2
		End	37.5	39.6	39.7	39.6	40.1
1.0 % CuO nanoparticles	Minimum	Start	32.9	32.4	33	33.1	32.6
		End	33.7	33.2	33.9	34.1	33.8
	Average	Start	33	33.4	32.6	33.3	33.4
		End	36.1	36.7	35.8	36.0	35.4
	Maximum	Start	34.8	35.1	34.3	34.6	35
		End	37.4	38.6	38.9	39.5	39.7

Curriculum Vitae

Personal Information:

Name	:	Sumit Chaudhary
Full correspondence address	:	House No.: 415, Amravati Enclave, Panchkula – 134107, Haryana, India.
Date of Birth	:	02, September, 1987
Nationality	:	Indian
email	:	sumit.chaudhary2@gmail.com
Contact No.	:	+91-9212343458

Education:

S. No.	Examination	Univeristy/ Board	Year	Percentage/ CGPA
1	Ph.D.	Delhi Technological University	2015 onwards	9.0 (course work)
2	M.Tech	Delhi Technological University	2010-12	80.6
3	B.Tech	Kurukshetra University Kurukshetra	2004-2008	71.8
4	XII	C.B.S.E.	2003-04	66.4
5	X	H.B.S.E.	2001-02	69.7

Work/Research Experience:

- Worked as Assistant Professor at Maharaja Agrasen Institute of Technology, Rohini, Delhi, (affiliated to GGSIP University Delhi), From 23rd July 2012 to 3rd August 2015.

- Worked as Jonior Research Fellow (CSIR) at Delhi Technological University, Delhi form 4th August 2015 to 31 July 2015.

- Working as Senior Research Fellow (CSIR) at Delhi Technological University, Delhi form 1st August 2015.

Scholastic Achievements:

- Six times GATE qualified in Mechanical Engineering with highest percentile 98.7.
- Two times CSIR NET qualified in Engineering Sciences.

Professional Activities:

- Reviewer for Case Studies in Thermal Engineering, Elsevier Publication.

List of Publications during Ph.D

Journal Publications:

a) **Sumit Chaudhary**, Ramesh Chandra Singh & Rajiv Chaudhary "An Experimental Investigation of the impact of Nanoparticles on the Tribological properties of 15W40 Lubricating Oil" International Journal of Mechanical and Production Engineering Research and Development (IJMPERD), Vol. 8 (5), 2018, 185-194. **(SCOPUS Indexed)**

b) **Sumit Chaudhary**, Ramesh Chandra Singh & Rajiv Chaudhary "Experimental Investigation of Influence of SiO_2 Nanoparticles on the Tribological and Rheological properties of SAE 40 Lubricating Oil" International Journal of Engineering and Technology (IJET), Vol 9 (6), 2017, 4307-4314. **(SCOPUS Indexed)**

c) **Sumit Chaudhary**, R. C. Singh & Rajiv Chaudhary "The study of Blending Techniques used for making Nanofluids and their Characterizations- A Review" International journal of advanced production and industrial engineering IJAPIE-2018-07-328, Vol 3 (3), ISSN 2455-8419.

d) **Sumit Chaudhary,** Sonia, R. C. Singh & Rajiv Chaudhary "Analysis and Synthesis of Gold Nano Particles" International journal of advanced production and industrial engineering IJAPIE-2018-07-328, Vol 1 (2), ISSN 2455-8419.

e) **Sumit Chaudhary,** R. C. Singh & Rajiv Chaudhary "Evaluation of high temperature Tribological behaviour of Nickel coating using LRT" Lecture Notes in Mechanical Engineering. (Accepted) **(SCOPUS Indexed)**

`

Conference Papers:

a) **Sumit Chaudhary, Ramesh Singh and Rajiv Chaudhary** "Stability analysis of nanolubricant prepared by two-step technique" ICAPIE 2018. (presented)

b) **Sumit Chaudhary, Ramesh Chandra Singh and Rajiv Chaudhary** "Tribological and thermal analysis of tribopair under dry, starved and fully flooded lubricating conditions" 34th NCME 2018.

c) Vinod, Bakir, **Sumit Chaudhary, R. C. Singh & Rajiv Chaudhary** "Mechanism of crack Generation and propagation in metals. NFEST 2018.

d) **Sumit Chaudhary, R. C. Singh & Rajiv Chaudhary** "Automatic gear shifting in manual transmission using electromagnetic clutch and embedded system" ICAPIE 2017.

e) **Sumit Chaudhary, Ramesh Chandra Singh and Rajiv Chaudhary** "Synthesis and Characterization of ZnO Nanoparticles" ICAPIE 2016.

f) Anshul Kumar, **Sumit Chaudhary, R.C. Singh** "Comparison of finite difference method, analytical integration method and hybrid approach for determining pressure profile at the interface of sliding surface using Reynolds equation" ICAPIE 2016.

g) **Sumit Chaudhary,** Vipin Kumar Sharma, **R. C. Singh & Rajiv Chaudhary** "Experimental Investigation of the Temperature Variation and Vibrations at Different Loads at the Periphery of Single Cylinder Diesel Engine" ISFT 2016.